NBS TECHNICAL NOTE 1231

U.S. DEPARTMENT OF COMMERCE/National Bureau of Standards

NBS Reactor: Summary of Activities July 1985 Through June 1986

The National Bureau of Standards[1] was established by an act of Congress on March 3, 1901. The Bureau's overall goal is to strengthen and advance the nation's science and technology and facilitate their effective application for public benefit. To this end, the Bureau conducts research and provides: (1) a basis for the nation's physical measurement system, (2) scientific and technological services for industry and government, (3) a technical basis for equity in trade, and (4) technical services to promote public safety. The Bureau's technical work is performed by the National Measurement Laboratory, the National Engineering Laboratory, the Institute for Computer Sciences and Technology, and the Institute for Materials Science and Engineering.

The National Measurement Laboratory

Provides the national system of physical and chemical measurement; coordinates the system with measurement systems of other nations and furnishes essential services leading to accurate and uniform physical and chemical measurement throughout the Nation's scientific community, industry, and commerce; provides advisory and research services to other Government agencies; conducts physical and chemical research; develops, produces, and distributes Standard Reference Materials; and provides calibration services. The Laboratory consists of the following centers:

- Basic Standards[2]
- Radiation Research
- Chemical Physics
- Analytical Chemistry

The National Engineering Laboratory

Provides technology and technical services to the public and private sectors to address national needs and to solve national problems; conducts research in engineering and applied science in support of these efforts; builds and maintains competence in the necessary disciplines required to carry out this research and technical service; develops engineering data and measurement capabilities; provides engineering measurement traceability services; develops test methods and proposes engineering standards and code changes; develops and proposes new engineering practices; and develops and improves mechanisms to transfer results of its research to the ultimate user. The Laboratory consists of the following centers:

- Applied Mathematics
- Electronics and Electrical Engineering[2]
- Manufacturing Engineering
- Building Technology
- Fire Research
- Chemical Engineering[2]

The Institute for Computer Sciences and Technology

Conducts research and provides scientific and technical services to aid Federal agencies in the selection, acquisition, application, and use of computer technology to improve effectiveness and economy in Government operations in accordance with Public Law 89-306 (40 U.S.C. 759), relevant Executive Orders, and other directives; carries out this mission by managing the Federal Information Processing Standards Program, developing Federal ADP standards guidelines, and managing Federal participation in ADP voluntary standardization activities; provides scientific and technological advisory services and assistance to Federal agencies; and provides the technical foundation for computer-related policies of the Federal Government. The Institute consists of the following centers:

- Programming Science and Technology
- Computer Systems Engineering

The Institute for Materials Science and Engineering

Conducts research and provides measurements, data, standards, reference materials, quantitative understanding and other technical information fundamental to the processing, structure, properties and performance of materials; addresses the scientific basis for new advanced materials technologies; plans research around cross-country scientific themes such as nondestructive evaluation and phase diagram development; oversees Bureau-wide technical programs in nuclear reactor radiation research and nondestructive evaluation; and broadly disseminates generic technical information resulting from its programs. The Institute consists of the following Divisions:

- Ceramics
- Fracture and Deformation[3]
- Polymers
- Metallurgy
- Reactor Radiation

---

[1] Headquarters and Laboratories at Gaithersburg, MD, unless otherwise noted; mailing address Gaithersburg, MD 20899.

[2] Some divisions within the center are located at Boulder, CO 80303.

[3] Located at Boulder, CO, with some elements at Gaithersburg, MD.

NBS Technical Note 1231

NBS Reactor: Summary of Activities July 1985 Through June 1986

Frederick J. Shorten, Editor

Reactor Radiation Division
Institute for Materials Science and Engineering
National Bureau of Standards
Gaithersburg, Md 20899

December 1986

U.S. Department of Commerce
Malcolm Baldrige, Secretary

National Bureau of Standards
Ernest Ambler, Director

National Bureau of Standards Technical Note 1231
Natl. Bur. Stand. (U.S.), Tech. Note 1231, 161 pages (Dec. 1986)
CODEN: NBTNAE

U.S. GOVERNMENT PRINTING OFFICE
WASHINGTON: 1986

For sale by the Superintendent of Documents, U.S. Government Printing Office, Washington DC 20402

FOREWORD

The National Bureau of Standards Reactor was built not only to serve the needs of the NBS but also those of other government agencies as a National Center for the application of neutron methods to problems of national interest. The Reactor Radiation Division was established to operate the reactor and to foster its scientific and technological use. Toward this end, the Division has a small nucleus of scientists experienced in the use of reactors for a wide range of scientific and technical problems. In addition to pursuing their own research and developing sophisticated experimental facilities, they actively seek out and encourage collaboration with other scientists engaged in challenging programs whose work can benefit from use of the reactor, but who as yet do not have the reactor experience necessary to take full advantage of the facilities available. The Division also provides irradiation services to a wide variety of users as well as engineering and other technical services.

The reactor power has recently been increased from 10 to 20 MW. The increased power combined with its 25 experimental facilities ranging from intense neutron beams to extensive irradiation facilities, makes it one of the most versatile high performance research reactors in the country. Thus, it is able to serve a large number of scientists and engineers in a broad range of activities both within and outside the NBS.

This report attempts to summarize all the work done which is dependent on the reactor including a large number of programs outside the Division. The first section summarizes the programs carried out by scientists in the Reactor Radiation Division and their collaborators. The second section summarizes NBS work originating outside NBS for which the Division provides reactor facilities and irradiation services. The remaining sections are self-explanatory.

Appreciation is extended to F. J. Shorten of the Reactor Radiation Division for his extensive contributions to the editing, organization, and preparation of this report, and K. E. Ferrel for efforts in typing manuscripts.

R. S. Carter

R. S. Carter
Chief, Reactor Radiation Division
National Bureau of Standards

ABSTRACT

This report summarizes all those programs which use the NBS reactor. It covers the period for July 1985 through June 1986. The programs range from the use of neutron beams to study the structure and dynamics of materials through nuclear physics and neutron standards to sample irradiations for activation analysis, isotope production, neutron radiography, and nondestructive evaluation.

Key words: Activation analysis; crystal structure; diffraction; isotopes; molecular dynamics; neutron; neutron radiography; nondestructive evaluation; nuclear reactor; radiation.

DISCLAIMER

TABLE OF CONTENTS

TABLE OF CONTENTS

A. REACTOR RADIATION DIVISION AND COLLABORATIVE PROGRAMS

TRANSLATION-ROTATION COUPLING - $(KCN)_x(KBr)_{1-x}$

J. M. Rowe and J. J. Rush

and

J. Bouillot
(Institut Universitaire de Technologie, Annecy, France)

and

K. H. Michel
(University of Antwerp (UIA), Wilrijk, Belgium)

and

F. Luty
(University of Utah, Salt Lake City, UT)

We have extended our neutron powder diffraction studies of $(KCN)_x(KBr)_{1-x}$ samples to $x = 0.7$, a range which has been shown to transform to a rhombohedral structure in which the quadrupoles are ordered, by a nearly continuous transition. This work had two goals - first, to quantify the anomalous temperature dependence of mean square displacements observed in the high temperature cubic phase as the transition temperature is approached from above, and second, to refine the structure of the low temperature rhombohedral phase by the Rietveld method. The results obtained in the cubic phase show that the mean square displacements decrease with decreasing temperature in the range 200-150 K, as expected, then increase as temperature is decreased from 150-115 K, exactly as would be predicted for a soft mode driven second order transition in which the soft mode is the elastic constant c_{44}. Although we were unable to approach T_c closely enough to fully test the predictions of non-classical critical behavior, we have confirmed the anomalous temperature dependence of the mean square displacements. Below the transition temperature, we observe a mixed phase in which a portion of the sample has a monoclinic structure, and the rest has a rhombohedral structure. We were unable to produce a single phase sample at low temperature, in contrast to the results of Ref. 1, a result which we attribute to the different states of strain in our powder samples and the single crystal used for the x-ray measurements. As a result, we are forced to analyse the data using a mixed structure refinement program, and have not yet been able to obtain satisfactory results at temperatures just below the transition. However, we have achieved a satisfactory refinement at 8 K, from which we conclude that the trigonal axis has contracted at the transition, and the $(CN)^-$ ions are oriented perpendicular to this axis, a somewhat surprising result. From our refinement, it appears that the ions are disordered in this plane, although one might expect to find an ordered "pinwheel" structure based on the nature of the quadrupolar forces that dominate the interactions between $(CN)^-$ ions. Attempts to properly refine the structures at higher temperatures are continuing.

We have also continued to refine the theoretical description of translation-rotation coupling, and to relate this to the many observations on mixed cyanide crystals. At the present time, we are concentrating on two aspects - first, the random fields created by the substitution of either halide ions or different alkali metals, and second, to explain the unusual diffraction lineshapes observed in single crystal diffraction peaks. These calculations are quite complex, requiring extensive analytical and numerical analysis, but the results to date are encouraging.

Current ongoing efforts in this program include structural measurements of other mixed systems and neutron and Brillouin scattering measurements (in collaboration with S. Satija, University of Delaware) on $(RbCN)_x(RbBr)_{1-x}$ single crystals.

NEUTRON SCATTERING STUDY OF THE VIBRATIONAL DENSITY OF STATES IN ICOSAHEDRAL AND CRYSTALLINE $Al_{0.80}Mn_{0.20}$

P. F. Miceli, S. E. Youngquist, D. A. Neumann and H. Zabel
(University of Illinois, Champaign, IL)

and

J. J. Rush and J. M. Rowe

The discovery at NBS of "quasicrystals" with long range bond orientational order displaying five-fold symmetry has led to intense current research interest. While most of the present activity has concentrated on this striking icosahedral symmetry, the effects that this new type of order has on the physical properties are also of fundamental significance. Recent calculations of the electron and phonon density of states of "quasiperiodic" structures have predicted characteristic difference from the density of states of crystalline systems.

NBS scientists, in collaboration with researchers from the University of Illinois, have performed the first measurement of the vibrational density of states in a quasicrystal, Al_4Mn, using the BT-4 spectrometer at the NBSR. Neutron spectra were measured under a variety of different conditions of wavevector and energy transfer in order to assure that the resulting weighted density of vibrational states represented as thorough an averaging as possible over reciprocal space. In order to determine the role of structure, vibration spectra were also measured on a sample of the same composition displaying long range translational order. A summary of the weighted density-of-states results is shown in figure 1.

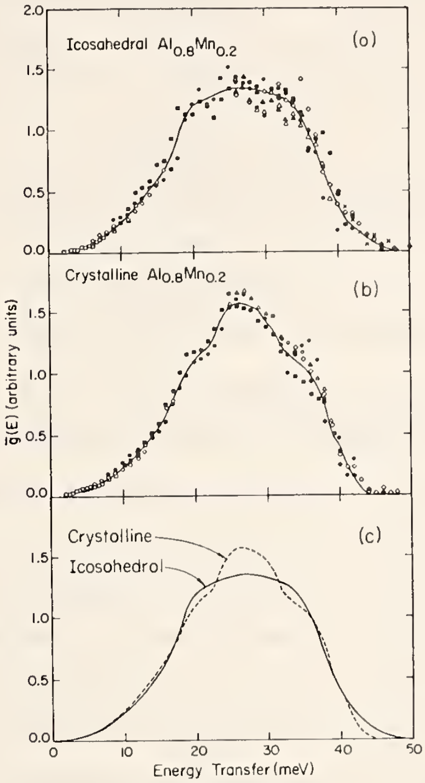

Figure 1. Weighted vibrational density of states $\bar{g}(E)$ measured for the (a) icosahedral (quasicrystal) and (b) crystalline phases of $Al_{0.08}Mn_{0.20}$ under various conditions of momentum transfer and fixed final energy.

Contrary to some theoretical predictions, the measured density of states do not show the existence of localized states and demonstrate that the quasicrystal and crystalline materials as elastically similar. At high vibrational energies, however, the quasicrystal shows a relative excess of phonon density. These neutron scattering results thus provide a direct test for models of the interatomic forces and dynamics of the icosahedral phase.

ISOTOPE EFFECTS IN THE PDH SYSTEM-LATTICE DYNAMICS OF $PDT_{0.71}$

J. M. Rowe and J. J. Rush

and

J. E. Schirber
(Sandia National Laboratory, Albuquerque, NM)

and

J. M. Mintz
(Sandia National Laboratory, Livermore, CA)

The origin of the reverse isotope effect in PdH and PdD (T_c = 8, 10 K respectively) has been attributed to the existence of strongly anharmonic optic modes, which lead to a change in λ, the electron-phonon coupling constant which appears in an exponential, that overcomes the change in the mean phonon energy, which appears as a factor, in the McMillan theory of superconductivity. This conclusion was based on a comparison of the coherent neutron scattering data for $PdD_{0.63}$ (which determines the phonon dispersion relation), to incoherent neutron scattering data for $PdH_{0.6}$. This comparison led to the conclusion that the effective force constant determining optic mode energies in PdH was 1.2 times that for PdD. Recently, T_c was also measured for PdT, and found to be 12 K, once again displaying a reverse isotope effect. We have prepared a single crystal of $PdT_{0.71}$ with a volume of 0.4 cc, and measured the phonon dispersion relation, thus allowing for a much more accurate comparison of the phonon terms appearing in the McMillan theory. Analysis of these

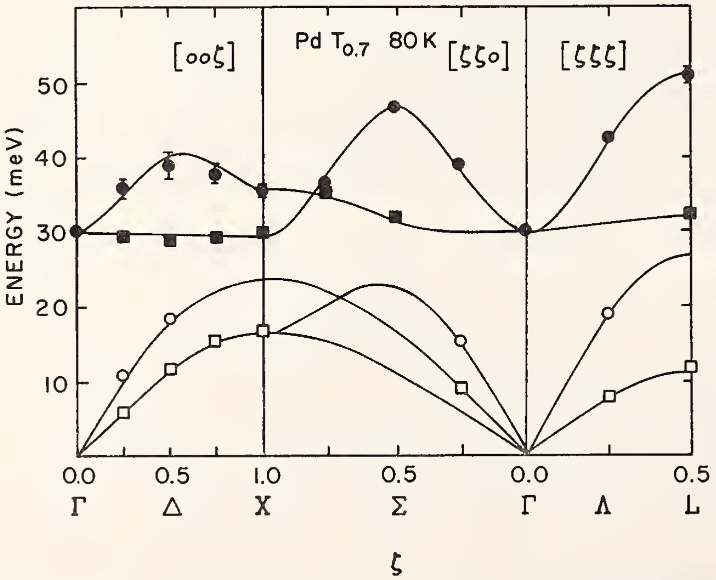

Figure 1: Measured dispersion relation for $PDT_{0.71}$ at 80 K. Solid lines a result of a fit to a Born-von Karman model.

results, shown in figure 1, demonstrate conclusively that anharmonicity alone cannot explain the reverse isotope effect, although it does go in the correct direction. A re-analysis of earlier incoherent neutron scattering results for $PdH_{0.6}$ and $PdD_{0.6}$ (summarized in 1985 annual report) shows that even for PdH and PdD, anharmonicity cannot explain the measured T_c's. The present results show that the theory of superconductivity must be re-examined as it applies to materials with the large mean-square displacements characteristic of PdH, PdD, and PdT.

HYDROGEN PAIRING AND ANISOTROPIC POTENTIAL FOR HYDROGEN ISOTOPES IN YTTRIUM

I. S. Anderson, J. J. Rush, T. Udovic and J. M. Rowe

The properties of the YH_x system in the α or solid solution phase have been the subject of a great deal of study and controversy in recent years, especially since, for $x < 0.2$, the α-phase persists down to very low temperatures. In the present work we have investigated the potential for H and D in α-phase $[Y(H,D)_{0.18}]$ by neutron spectroscopy, using the BT-4 crystal spectrometer with either Be or a new Be/graphite composite filter for final energy analysis. The spectroscopic results for a $YH_{0.18}$ single crystal, with energy scans arranged so that the momentum transfer $\bar{Q}$ was almost parallel or almost perpendicular to the c-axis of the hexagonal crystal, are shown in figure 1. For $\bar{Q} \parallel$ c-axis a single prominent peak is observed at 100 meV, while for $\bar{Q} \perp c$ a dominant single peak is observed at 134 meV. These results not only show clearly that virtually all the hydrogen resides in tetrahedral type sites (as opposed to the suggestion of partial octahedral-site occupancy from previous results on polycrystalline samples). More importantly these spectra demonstrate that the potential of the tetrahedrally bound H (and D) is highly anisotropic and (in the c-direction) anharmonic, in spite of the fact that the t-sites are only slightly distorted from regular tetrahedral symmetry. Measurements of higher harmonics of these vibration modes for both H and D samples also demostrate clearly that the c-axis vibrations show a much higher degree of anharmonicity than those in the ab plane.

Further measurements, using a high resolution composite Be/graphite filter-analyzer, are shown in figure 2. These results show that there is a splitting of the c-axis vibration modes at low temperature, which further demonstrates the analomous hydrogen bonding potential in this crystal direction and, in fact, confirms the presence of pairing of hydrogens on either side of the Y atoms at low temperature,

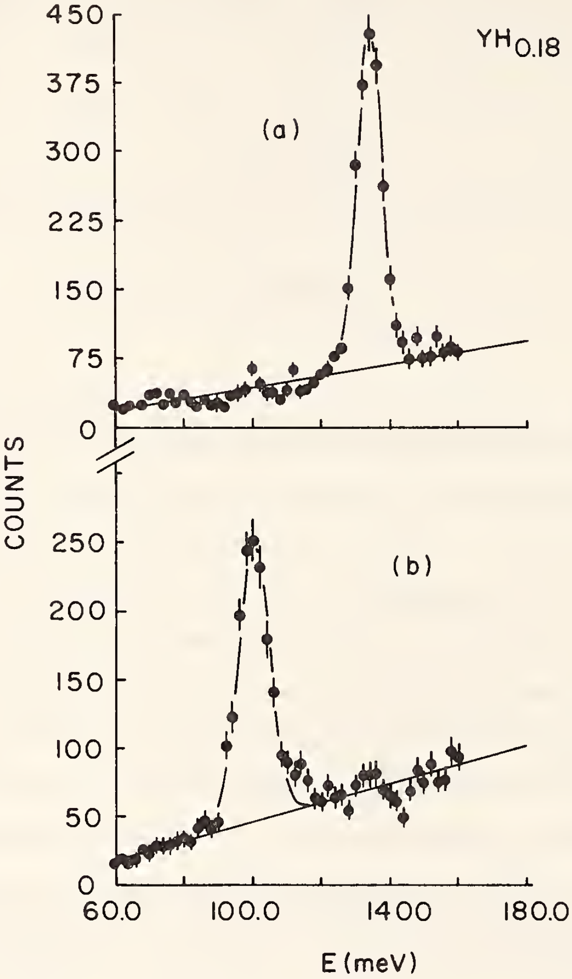

Figure 1. Measured neutron spectra of $YH_{0.18}$ single crystal, for $\bar{Q} \perp$ c-axis (a) and $\bar{Q} \perp$ c-axis (b).

previously suggested by neutron diffuse scattering patterns. The spectral changes as a function of temperature in figure 2 also show the existence of an increasing fraction of unpaired protons at higher temperature (peak at 74.7 meV at 240 K), and is consistent with the interpretation of diffuse scattering results. This is the first example of such pairing in metal-hydrogen systems, which must reflect an associated perturbation of the local electronic structure.

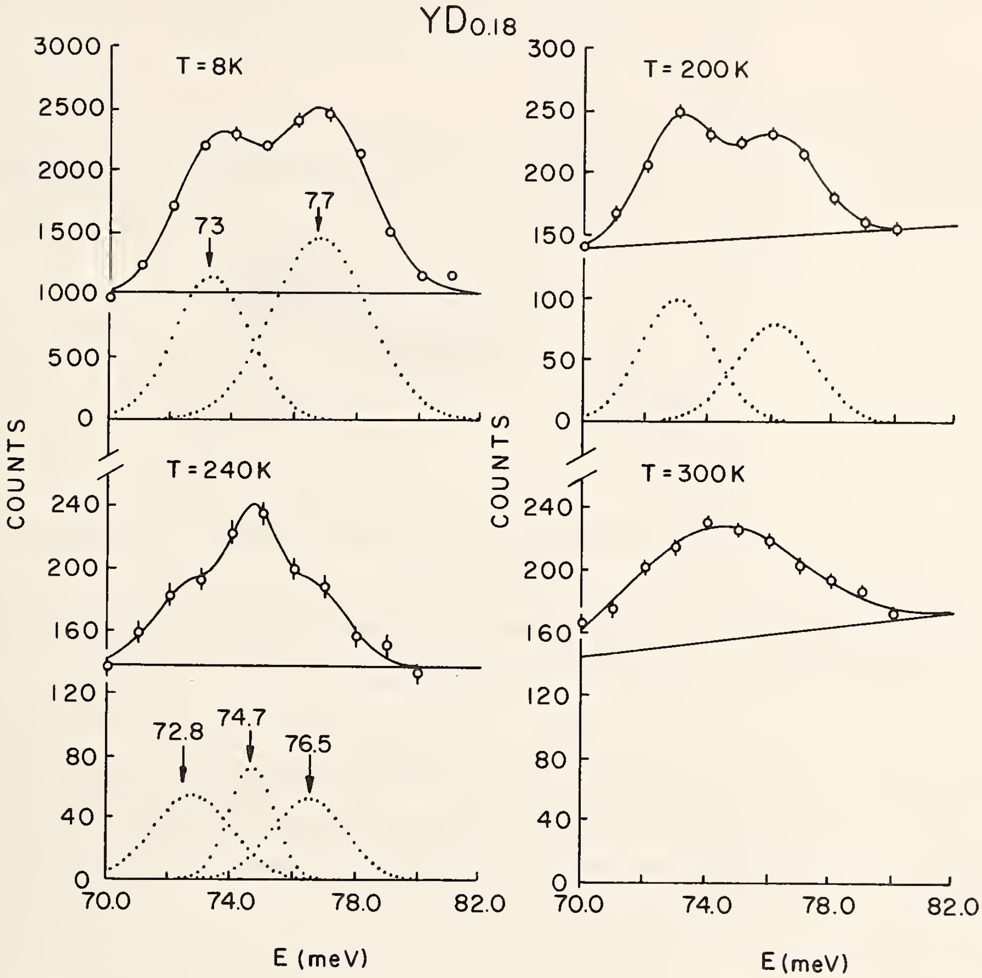

Figure 2. Measured spectra for polycrystalline $YD_{0.18}$ as a function of temperature. Solid lines are the results of fits assuming Gaussian peak shapes.

NEUTRON SPECTROSCOPIC STUDY OF HYDROGEN ADSORPTION ON RUTHENIUM SULFIDE CATALYSTS

T. J. Udovic and J. J. Rush

and

W. H. Heise, K. Lu, Y.-J. Kuo, and B. J. Tatarchuk
(Auburn University, Auburn, AL)

Hydrodesulfurization (HDS) selectivity over ruthenium sulfide (RuS_2) catalysts can be altered by varying the surface pretreatment conditions. For example, reaction experiments have indicated that thiophene HDS proceeds primarily via direct hydrogenolysis over catalysts pretreated in 10% H_2S/H_2 at 673 K, whereas the pathway for thiophene hydrogenation to tetrahydrothiophene followed by hydrogenolysis becomes

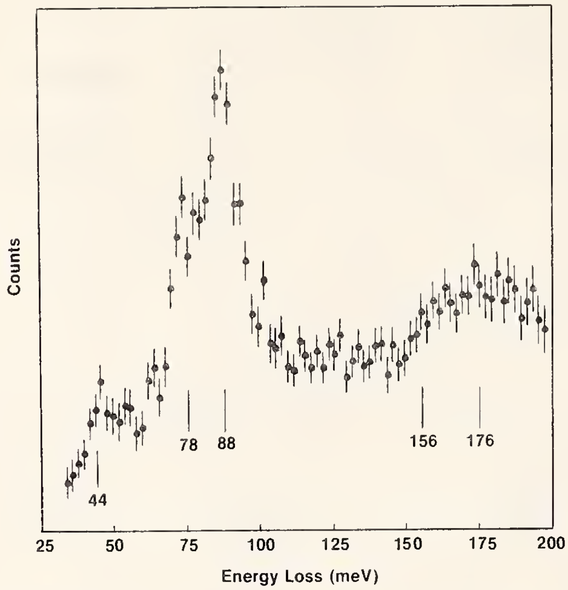

Figure 1. IINS spectrum at 80 K for hydrogen adsorbed on RuS_2 after surface pretreatment with 10% H_2S/H_2 at 673 K.

comparable to the direct HDS pathway over catalysts pretreated in 100% H_2S. To help understand the role of hydrogen in this reaction system, incoherent inelastic neutron scattering (IINS) is currently being utilized to probe the adsorbed nature of hydrogen on unsupported RuS_2 catalysts.

Hydrogen adsorption results in table 1 indicate that the irreversible H_2 uptakes on RuS_2 increase with both adsorption temperature and degree of surface sulfidization. Ruthenium sulfide surfaces pretreated in 100% H_2S at 673 K possess the maximum H_2 adsorption capacity at 373 K, 63% of the adsorption capacity for Ru metal surfaces. Yet, Ru metal surfaces pretreated in 10% H_2S/H_2 at 673 K are fully poisoned toward H_2 adsorption due to the formation of a "skin sulfide" barrier containing one-half monolayer of surface sulfur atoms in a different chemical state (as evidenced by x-ray photoelectron spectroscopy and reaction experiments) than in the bulk sulfide RuS_2.

Recent neutron scattering results have indicated that the H/RuS_2 vibrational spectra, and therefore the surface species, are qualitatively independent of adsorption temperature and pretreatment conditions; only scattering intensities vary, reflecting the differences in H_2 uptake. The IINS spectrum for hydrogen adsorbed at 373 K on RuS_2 pretreated in 10% H_2S/H_2 at 673 K is depicted in figure 1. The main scattering features appear as a doublet at 78 and 88 meV with the corresponding second harmonics near 156 and 176 meV. These are assigned to the bending modes of a sulfhydryl (SH) group in agreement with the vibrational spectra for (SH) on other

Table 1 - Sulfidization and temperature effects on H_2 chemisorption

Catalyst Surface	Pretreatment (673 K)	Irreversible H_2 Uptake (μmoles/m^2) 300K	373K
Ru	100% H_2	-	10.2
Ru	10% H_2S/H_2	0	0
RuS_2	10% H_2S/H_2	1.0	2.2
RuS_2	100% H_2S	1.4	6.5

sulfide surfaces (1-3). The weak scattering feature at 44 meV is tentatively assigned to H motion associated with a sulfur phonon mode in agreement with the expected energy for such a mode. Substitution of deuterium for hydrogen resulted in the harmonic isotopic energy shifts to 55 and 64 meV. Isotope dilution neutron spectroscopy experiments utilizing 15% H/85% D indicated no significant change in the H vibrational peak structure for the Ru-S-H bending modes, suggesting that the doublet at 78 and 88 meV represents two different vibrational modes rather than the phonon dispersion of a single bending mode due to adsorbate-adsorbate dynamic coupling interactions.

---

1. C. J. Wright, D. Fraser, R. B. Moyes, and P. B. Wells, Appl. Catal. 1, 49 (1981).
2. C. Sampson, J. M. Thomas, S. Vasudevan, and C. J. Wright, Bull. Soc. Chim. Belg. 90, 1215 (1981).
3. R. J. Koestner, M. Salmeron, E. B. Kollin, and J. L. Gland, Chem. Phys. Lett. 125, 134 (1986).

AN INCOHERENT INELASTIC NEUTRON SCATTERING STUDY OF THE ADSORPTION AND ABSORPTION OF HYDROGEN BY PALLADIUM BLACK

J. M. Nicol
(University of Maryland, College Park, MD)

and

R. D. Kelley and T. E. Madey
(Surface Science Division)

and

J. J. Rush

The interaction of hydrogen with palladium surfaces is of considerable interest because of its catalytic properties in reactions such as the selective hydrogenation of alkynes to alkenes and its ability to form metallic hydrides for hydrogen storage. Studies of the interaction of hydrogen with both single crystal and polycrystalline Pd samples have been carried out using such techniques as high-resolution electron energy loss spectroscopy, low energy electron diffraction, thermal desorption, and inelastic incoherent neutron scattering (IINS).

In the present work we have used IINS to study the interaction of hydrogen with Pd black, and exceptionally high surface area metal powder with an initial surface area of 40 m^2/gm. Unlike similar studies of surface hydrogen species on Raney Nickel and platinum black, the Pd-hydrogen system is more complex due to the ability of Pd to absorb hydrogen. The α- and β-Pd hydrides have been well characterized by IINS, particulary at NBS. In addition to the surface and bulk species there is strong evidence for a "sub-surface"hydrogen species, formed below the topmost layer of Pd atoms, which may act as an intermediate between the surface and bulk hydrogen. It was the aim of the present work to investigate the adsorption of hydrogen on Pd black, the existence of subsurface hydrogen by IINS, and the interaction of chemisorbed oxygen with these species. The initial results of these studies (along with preliminary interpretations) are described here.

The IINS spectra were measured on the BT4 spectrometer at the NBS reactor, operating with a liquid nitrogen cooled Be filter analyzer. The spectrum of Pd black after hydrogen titration at 80 K, followed by evacuation and heating at 373 K is shown in figure 1a. Scattering intensity observed at 58, 94, 100 and 119 meV shows the presence of a significant amount of residual hydrogen (ca. 0.6 - .75 monolayers). This suggests that all of the residual hydrogen is much more strongly bound than bulk hydrogen, which would have been removed during evacuation at 373 K. We thus assume that all of the features seen in figure 1a are associated in some way with surface

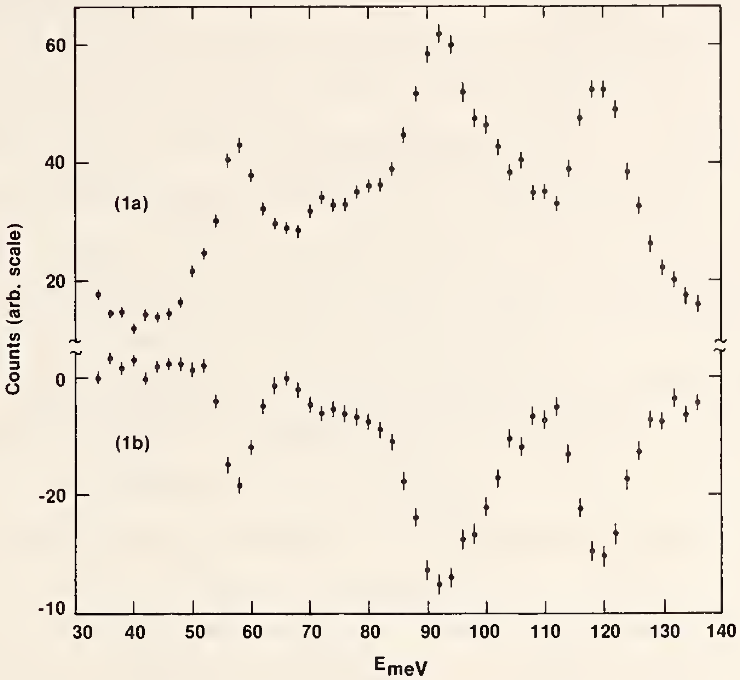

Figure 1. (a) IINS Spectrum at 80 K of cleaned Palladium black
(b) difference spectrum after the addition of 1 monolayer of oxygen to 1(a), 1 warming to 293 K and cooling to 80 K. (Negative scattering intensity represents species removed by oxygen attack.)

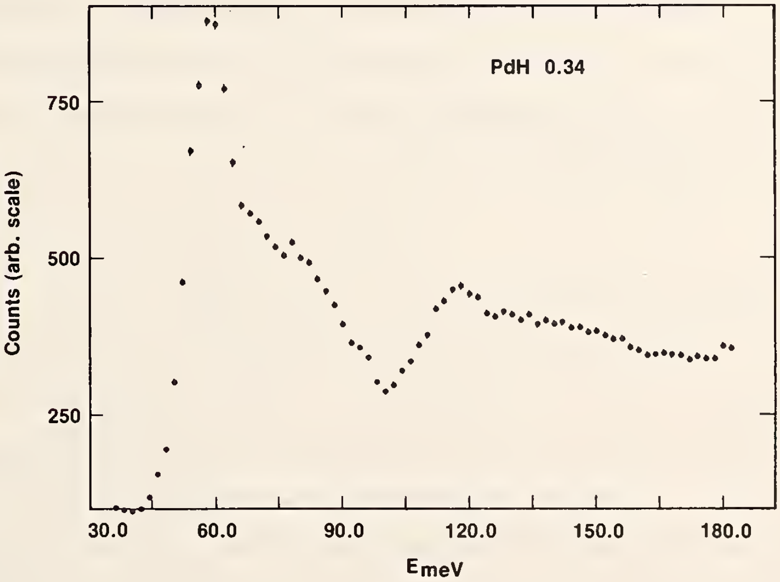

Figure 2. IINS Spectrum of the β-hydride of Palladium black at 80 K.

sites. This was confirmed by an interesting chemical titration experiment. When oxygen was adsorbed (1 monolayer of O atoms) on the surface at 80 K, very little change in the spectrum was observed. On warming the sample to 293 K and cooling again to 80 K all features in the spectrum associated with hydrogen disappeared (figure 1b). As no features due to surface OH groups were observed, the residual scattering intensity is felt to be due to weakly bound water. The removal of the hydrogen scattering intensity due to the reaction of surface oxygen is also a good argument that the features in a Figure 1a are due to chemisorbed H species, and not due to impurity modes such as H bound to surface carbon or oxygen.

The feature at ca. 58 meV, which is removed by oxygen, is suggestively close in frequency to that of the bulk β-hydride. For comparison the spectrum of the β-hydride of Pd black is shown in figure 2. The mode due to interstitial hydrogen is observed at 60 meV. However, a comparison of the width of the peak for β-hydride in Figure 2 and the peak observed in the Pd black spectrum (figure 1a) suggest that they are due to quite different species. In addition, since it is known that the α and β hydrides of Pd are easily removed by evacuation at ambient temperatures, the cleaning of the Pd black surface should have removed all hydride species. We also observe this feature to react with surface oxygen, its intensity to be independent of temperature, and its concentration to increase only at hydrogen concentrations of greater than 1 monolayer. These factors lead us to speculate that the feature we are observing is due to subsurface hydrogen, whose site symmetry is similar to that of the β-hydride.

Force constant calculations and further experimental work are currently being undertaken to try to establish site geometries. We also hope to improve the procedure for removing residual hydrogen from the palladium surface without a significant reduction in the surface area.

ADSORBATE DYNAMICS AND THE DEAMMONIATION PROCESS IN AMMONIATED ZEOLITE RHO

T. J. Udovic, R. R. Cavanagh, and J. J. Rush
and
J. M. Nicol
(University of Maryland, College Park, MD)
and
(National Bureau of Standards, Gaithersburg, MD)
and
G. D. Stucky
(University of California, Santa Barbara, CA)
and
M. J. Wax
(W. R. Grace and Co., Columbia, MD)
and
G. A. Jones and D. R. Corbin
(E. I. duPont de Nemours and Co., Wilmington, DE)

Quasielastic and inelastic neutron scattering experiments involving ammoniated zeolite rho have been performed in order to investigate the rotational dynamics of bound NH_4^+ as well as characterize the deammoniation process over the temperature range 473 - 723 K. Figures 1 and 2 illustrate the IINS spectra reflecting the deammoniation process. Vibrational features of the bound NH_4^+ near 180 meV (bending modes) and below 60 meV (large amplitude rotational and translational modes) are found to diminish as the deammoniation temperature is increased. The low-energy spectra show initial intensity loss in the 28 - 35 meV region at the earliest stage of deammoniation followed by intensity loss in the 38 - 45 meV region during the latter stages of deammoniation. This is suggestive of NH_4^+ ions bound at two different kinds of sites in zeolite rho, the more weakly bound and the more strongly bound species desorbing below and above ca. 623 K, respectively. The desorption process for both species involves NH_3 formation leaving behind a bound proton. This process is evident in the IINS spectra during the latter stages of deammoniation by the gradual appearance of the scattering features for H-rho: the large-amplitude doublet feature at 44 and 50 meV, the feature at 93 meV associated with proton coupling to a symmetric T-O stretching mode, and the features at 142 and 131 meV associated with in- and out-of-plane T-O-H bending modes.[1]

The reorientation of NH_4^+ ions has been characterized by low-energy quasielastic neutron scattering. The dependence of the elastic incoherent structure factor on momentum transfer suggests that the more strongly bound NH_4^+ undergoes 120°

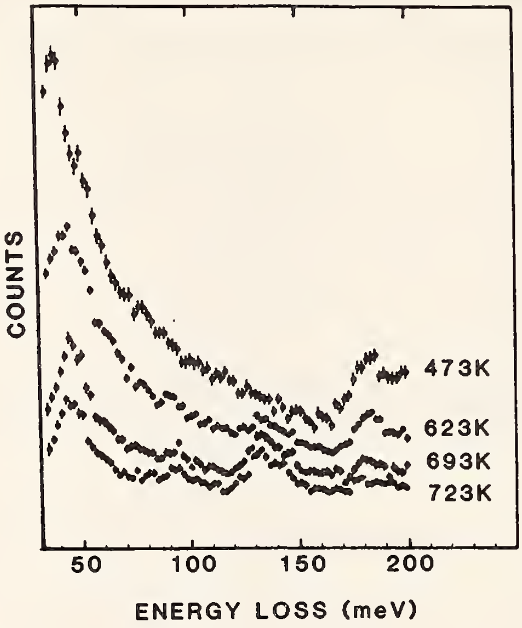

Figure 1. High energy IINS spectra at 80 K of ammoniated zeolite rho following deammoniation at 473-723K, collected using the BT-4 beryllium filter detector.

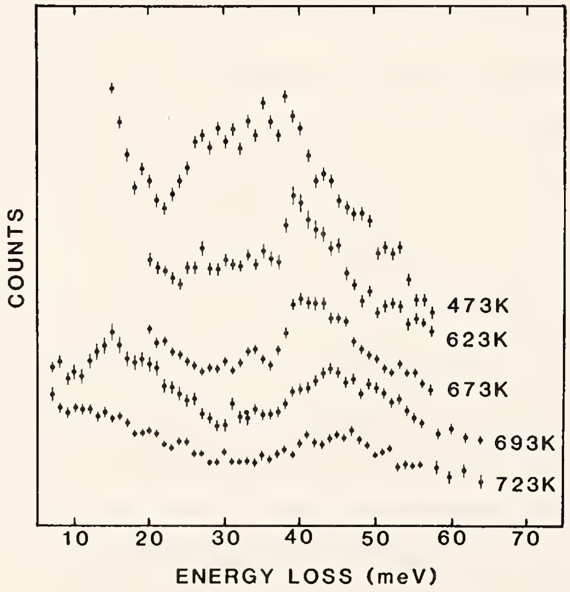

Figure 2. Low-energy IINS spectra at 80K of ammoniated zeolite rho following deammoniation at 473-723K, collected in the BT-4 triple-axis configeration at 13.8 mev constant final energy.

reorientations around a random axis and is coordinated through a single hydrogen to the zeolite framework. The temperature dependence of the quasielastic component indicates a very low (ca. 20 meV) barrier to reorientation of the more tightly bound NH_4^+ ions, which have been located by x-ray diffraction to be approximately in the center of the "windows" (eight-membered rings) which separate the cages in the zeolite-rho structure.[2]

Current studies are investigating the reversibility of the deammoniation process by characterization of H-rho after the reintroduction of NH_3.

---

1. M. J. Wax, R. R. Cavanagh, J. J. Rush, G. D. Stucky, L. Abrams, and D. R. Corbin, J. Phys. Chem. 90, 532 (1986).
2. L. B. McCusker, Zeolites 4, 51 (1984).

NEUTRON SCATTERING STUDIES OF ULTRASTABLE ZEOLITE Y

J. M. Nicol
(University of Maryland, College Park, MD)

and

(Surface Science Division)

and

T. J. Udovic and J. J. Rush

A study of the acid sites (protons) in ultrastable zeolite Y has been initiated by inelastic incoherent neutron scattering. Spectra at temperatures between 80 and 373 K have been collected using the BT4 spectrometer, with a nitrogen cooled Be filter analyzer. The initial results indicate a rearrangement of the protons with increasing temperature. A similar behavior has been previously reported for zeolite H-rho.[1]

Further studies are planned over a wider energy range by quasielastic and inelastic neutron scattering. A Force constant analysis will also be undertaken.

---

1. M. J. Wax, R. R. Cavanagh, J. J. Rush, G. D. Stucky, L. Abrams and D. R. Corbin, J. Phys. Chem., 90, 532 (1986).

COHERENT SCATTERING OF LOW ENERGY NEUTRINOS FROM CRYSTALS

R. C. Casella

I have considered the problem of neutral current neutrino scattering from macroscopic crystals. It has been known since the work of Freedman[1] that neutral-current scattering of neutrinos from the nucleons in a nucleus can be coherent, leading, for sufficiently long wavelengths, to cross sections which are proportional to the square of the nuclear baryon number. When extended to macroscopic objects containing N nuclei, it has recently been reported that coherent cross sections proportional to N^2 have been observed.[2] Normally, one expects such N^2 enhancements to occur only when the wavelength of the incident particles is larger than the sample size. The question of the existence of coherence is relevant to but not identical with that of possible N^2 effects. I find that coherent scattering can indeed occur on the scale of an entire crystal for incident neutrino wavelengths comparable to the internuclear separation or less, but that the cross section remains linear in N.[3] Hence coherence cannot explain the reported observation of a macroscopic force exerted on a crystal by reactor antineutrinos.[2]

For sufficiently small momentum transfers, $|q^2| \ll M_{Z^o}^2$, neutral current neutrino processes follow from the standard-model Hamiltonian

$$H = (G/\sqrt{2})[\bar{\nu}\, \gamma_\mu(1 - \gamma^5)\nu][\bar{q}(C_V\gamma^\mu + C_A\gamma^\mu\gamma^5)q], \qquad (1)$$

where $C_V = I_3 - 2Q \sin^2\Theta_W$ and $C_A = - I_3$, G is the Fermi coupling and q is an elementary weak isodoublet: $q = (\nu,\ell)$, (u,d'), (p,n), or (A_+,A_-). The first entries are the leptons and quarks of each family. For smaller momentum transfers the nucleon isodoublet is treated as elementary, while for sufficiently low energies we may treat the entire nucleus as elementary with $A_\pm$ the $I_3 = \pm 1/2$ components of q. When, in the latter case, vector coupling dominates, the scattering amplitude $a(E,\Theta)$ in the neutrino-nucleus c.m. frame satisfies

$$a(E,\Theta) = (1/\sqrt{2})(GE/2\pi)[Z(1 - 4 \sin^2\Theta_W) - N_n] \cos(\Theta/2). \qquad (2)$$

Here E and Θ are the incident energy and scattering angle in the c.m. frame and Θ_W is the weak angle. This leads to cross sections which are quadratic in baryon number $A = Z + N_n$. I have calculated directly the net force exerted on a crystal by the coherent scattering of every neutrino from the N nuclei, assuming phase coherence is maintained even for neutrino wavelengths much smaller than the lattice constant, but larger than nuclear dimensions. Letting b denote the constant multiplying the quantity E cos(θ/2) in Eq.(2) for a(E,θ) and F_z, the net force exerted by a current-density source distribution $J_z(E)$ of (anti)neutrinos, I find[3]

$$F_z = (4\pi/3)\ N\ e^{-2W}\ b^2 \int^{E_c} dE\ E^3\ J_z(E). \qquad (3)$$

Here E_c is a cut-off energy above which the scattering becomes incoherent and exp(-2W) is the temperature dependent Debye-Waller factor due to thermal vibrations of the nuclei. F_z is linear in N. While coherence can occur in the scattering of neutrinos of wavelengths much smaller than the sample size, an N^2 enhancement is possible only for ultra-low-energy neutrinos with wavelengths of order the linear dimensions of the crystal. Therefore, the reported observation[2] of a macroscopic force exerted on a crystal by antineutrinos from a fission reactor cannot be explained by an N^2 enhancement at the crystalline level of the nuclear cross-section due to coherence.

---

1. D. Z. Freedman, Phys. Rev. D, 9, 1389 (1974).
2. J. Weber, Phys. Rev. C, 31, 1468 (1985).
3. R. C. Casella, "Coherent Scattering of Low Energy Neutrinos from Macroscopic Objects", Proc. of the 2nd Conf. on the Intersections Between Particle and Nuclear Physics, Lake Louise, Canada, 1986, Am. Inst. of Physics (in press).

X-RAY DIFFRACTION STUDIES OF THE AMORPHOUS $(FE_{1-x}Ni_x)_{77}Si_{10}B_{13}$ ALLOYS

S. C. Yu and J. W. Lynn
(University of Maryland, College Park, MD)
and
(National Bureau of Standards, Gaithersburg, MD)

The atomic structures of single roll-quenched amorphous $(Fe_{1-x}Ni_x)_{77}Si_{10}B_{13}$ (atomic %, 0 ≦ x ≦ 1) alloys have been studies by x-ray diffraction. Interference functions, atomic distribution functions and radial distribution functions were calculated from the data. We find that the nearest neighbor distance decreases from 2.54 ± 0.01 Å for x = 0 ($Fe_{77}Si_{10}B_{13}$) to 2.49 ± 0.01 Å for x = 1 ($Ni_{77}Si_{10}B_{13}$), while the average coordination number (CN) of 12.50 ± 0.18 is independent of x. The values corresponding to the nearest neighbor distance were 2.493 Å (for $Fe_{77}Si_{10}B_{13}$), 2.448Å (for $Ni_{77}Si_{10}B_{13}$), 2.498 Å (for $Fe_{78}Si_{10}B_{12}$) and 2.453 Å (for $Ni_{78}Si_{10}B_{12}$), calculated from the radii of each element for CN = 12 using the homogeneous crystalline model. We can see that the nearest neighbor distance of $Fe_{77}Si_{10}B_{13}$ is larger than $Ni_{77}Si_{10}B_{13}$. From an earlier report[1] we can see that this tendency still holds in the amorphous state. For example, the nearest neighbor distance of amorphous $Fe_{78}Si_{10}B_{12}$ alloy is 2.58 Å and that of amorphous $Ni_{78}Si_{10}B_{12}$ alloy is 2.55 Å. In addition, the nearest neighbor distance in $TM_{77}Si_{10}B_{12}$ (TM = Fe, Ni) is shorter than $TM_{78}Si_{10}B_{12}$ alloy. These trends are in good agreement with our results but there are some numerical differences which are likely due to differences between the amorphous alloys, and to the crystalline model. These results are consistent with the measured densities of the samples, which are found to increase with increasing Ni content.

---

1. Y. Waseda, "The Structure of Non-crystalline Materials", (McGraw-Hill, New York, 1980) p. 128.

THE MAGNETIC STRUCTURE IN DY-Y SUPERLATTICES

R. W. Erwin and J. J. Rhyne
and
J. Borchers, M. B. Salamon, R. Du and C. P. Flynn
(University of Illinois, Urbana, IL)

It has been shown by neutron diffraction techniques that a superlattice of 15 atomic planes of Dy alternated with 14 atomic planes of Y orders magnetically in a helix which remains phase coherent across the magnetically 'dead' Y layers and is incommensurate with the bilayer periodicity.[1] This is shown in figure 1, where diffraction scans along the [000ℓ] direction of the hcp structure are plotted for several temperatures below the Neèl point $T_N \approx 170$ K. A primary nuclear Bragg peak of the superlattice is evident at $Q = 2.22$ Å^{-1} representing approximately the average spacing of the superlattice growth planes. Only the first order nuclear satellite at higher Q is visible which arises from the lattice mismatch between the Dy and Y layers.[2] The remaining peaks grow in intensity as the temperature is decreased and are thus magnetic. The spacing of these peaks is $2\pi/L$ as for the nuclear peaks (L = bilayer thickness), but they are otherwise incommensurate with the nuclear peaks. Note that the intensities of the magnetic satellites do not follow an obvious pattern, but that the relative intensities are strongly temperature dependent. We have been able to describe this effect by a simple model for the superlattice structure factor, which shows that the turn angle of the helical order is different

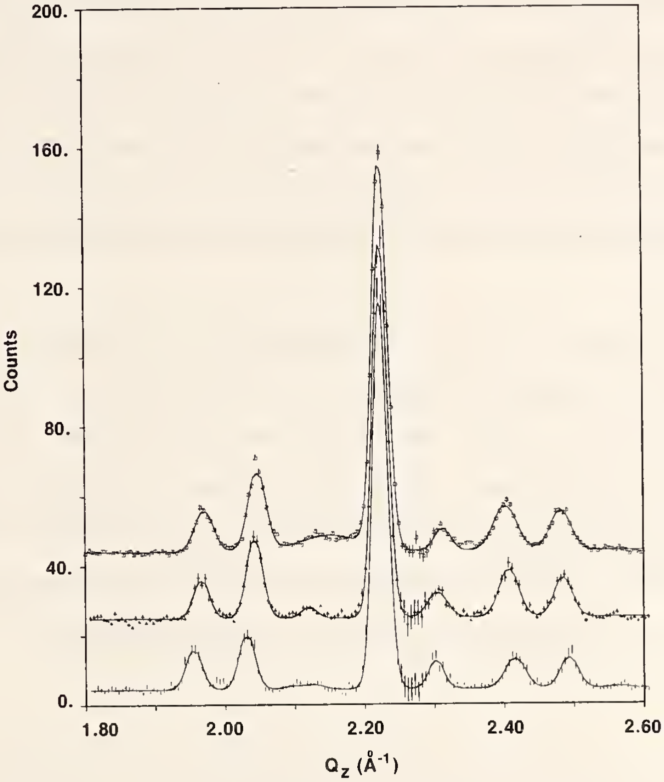

Figure 1. The temperature dependence of the diffraction scans along the [000ℓ] direction shows that the Dy-Y superlattice orders in a helix which is incommensurate with the bilayer thickness. Since several magnetic satellites are clearly distinguishable, this coherence extends across several layers of magnetically 'dead' yttrium.

in the Dy and Y layers.[2] The superlattice thus retains in the separate layers approximately the Fermi surface features which determine the magnetic periodicity in bulk Dy and Y. However, the ferromagnetic transition found in bulk Dy at 85 K is absent in the superlattice down to 5 K. This is the result of the strain clamping of the Y inter-layers, which inhibits the γ-magnetostriction associated with the ferromagnetic transition.[3]

Several features in the magnetization process in an applied field have been found to be unique to the superlattice. In Figure 2 are shown the diffraction scans as in figure 1, but after a 25 kOe field has been applied in the basal plane. At 110 K the magnetic field weakens the coherence of the helical order as evident in the broadening of the magnetic satellites (this occurs even in fields of only 1 kOe). The breakdown of the long-range order possibly results because the external field couples as a random field to the net Dy layer moment (the helix does not have an integer number of wavelengths in the Dy layer).[2] At 10 K, on the other hand, the phase coherence is not destroyed by low fields. Instead an irreversible transition is obtained to a remanent ferromagnetic state. Thus there is an extra magnetic intensity on the main Bragg peak even after the magnetic field is switched off, and the magnetic satellites of the helical order are not restored. We have also shown that the original helical order can be restored by raising the temperature to about 40-60 K. The ramanent state is beleived to be the result of the energy barriers to spin rotation caused by the strong increase of basal plane single-ion anisotropy at low temperatures.[1]

The coherence range of the helimagnetic order has been estimate from the observed peak widths and known instrumental resolution to be about 350 Å or four bilayers. This coherence implies that the handedness of the helix is preserved across the Y layers, so that the coupling can not be described as a simple scalar RKKY interaction (unless some intrinsic effect chooses the same handedness in each Dy layer). We beleive that this is strong evidence for an incipient conduction band spin density wave in Y stabilized by the Dy local moments.[1]

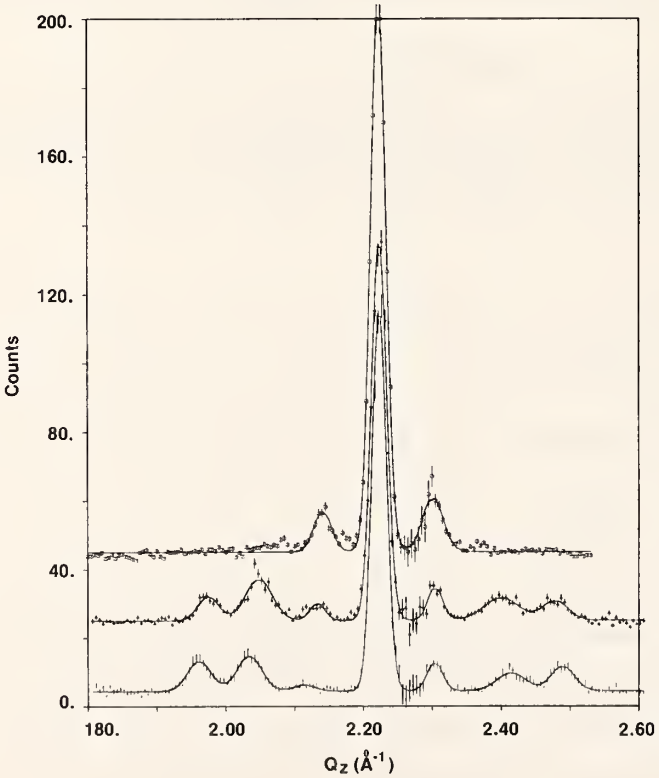

Figure 2. The diffraction scans are shown for the remanent state at several temperatures. At high temperatures (110 K) the coherence of the helimagnetic state is reduced by the applied magnetic field, while at low temperatures (10 K) a metastable ferromagnetic remanent state is frozen in by the strong basal plane anisotropy.

is obtained to a remanent ferromagnetic state. Thus there is an extra magnetic intensity on the main Bragg peak even after the magnetic field is switched off, and the magnetic satellites of the helical order are not restored. We have also shown that the original helical order can be restored by raising the temperature to about 40-60 K. The ramanent state is beleived to be the result of the energy barriers to spin rotation caused by the strong increase of basal plane single-ion anisotropy at low temperatures.[1]

The coherence range of the helimagnetic order has been estimate from the observed peak widths and known instrumental resolution to be about 350 Å or four bilayers. This coherence implies that the handedness of the helix is preserved across the Y layers, so that the coupling can not be described as a simple scalar RKKY interaction (unless some intrinsic effect chooses the same handedness in each Dy layer). We beleive that this is strong evidence for an incipient conduction band spin density wave in Y stabilized by the Dy local moments.[1]

---

1. J. J. Rhyne, R. W. Erwin, M. B. Salamon, Shantanu Sinha, J. Borchers, J. E. Cunningham and C. P. Flynn, to be published in Journal of the Less-Common Metals 1986; M. B. Salamon, Shantanu Sinha, J. J. Rhyne, J. E. Cunningham and C. P. Flynn, Phys. Rev. Lett. 56, 259 (1986).

2. R. W. Erwin, J. J. Rhyne, J. Borchers, M. B. Salamon, R. Du and C. P. Flynn, to be published.

3. B. R. Cooper, Phys. Rev. 169, 281 (1968); B. R. Cooper, Phys. Rev. Lett. 19, 900 (1967).

ANTIFERROMAGNETIC STRUCTURE OF THE CUBIC SUPERCONDUCTOR $ErPd_2Sn$

J. W. Lynn and H. B. Stanley
(University of Maryland, College Park, MD)

and

(National Bureau of Standards, Gaithersburg, MD)

and

R. N. Shelton and P. Klavins
(Iowa State University, Ames, IA)

$ErPd_2Sn$ is a Heusler alloy which crystallizes into the cubic Cu_2MnAl-type structure[1] (a=6.68 Å). In common with some other Er containing ternary compounds, $ErMo_6Se_8$[2] and $ErMo_6S_8$[3], this alloy exhibits the coexistence of long-range antiferromagnetic order and superconductivity. It differs from these however, by having a significantly higher percentage of magnetic Rare Earth ions, and in having a higher site symmetry (cubic). We have investigated the magnetic properties of this interesting alloy by means of neutron scattering.

The powder sample was loaded into an aluminum flat-plate sample holder with a thickness of approximately 1 mm to minimize the effects of absorption. The fixed incident neutron wavelength of 2.35 A together with horizontal Soller collimators of 10'-10'-10' (no analyzer) gave a wave vector resolution of between about 0.012 A^{-1} at a scattering angle of 17° and 0.023 A^{-1} at 60°. $ErPd_2Sn$ has been shown[1] to have a superconducting transition at T_s = 1.17 K, and has a heat capacity anomaly at 1 K. Measurements were therefore taken between 0.35 K and 4 K; the 4 K data representing the non-magnetic (flat) background.

Four magnetic Bragg peaks were observed between 10 and 60 degrees which we have identified as the (111), (113), (313) and (333) reflections of a fcc type-II antiferromagnet (space group Fd3m). This structure is characterized by the doubling of the fcc Er unit cell along all three crystallographic directions. Satellites of these allowed reflections were also observed, however, which indicates that this basic structure must be modulated.

All linewidths were found to be broader than instrumental resolution and clearly non-Gaussian in shape (see Figure 1). This may arise from an inelastic spin

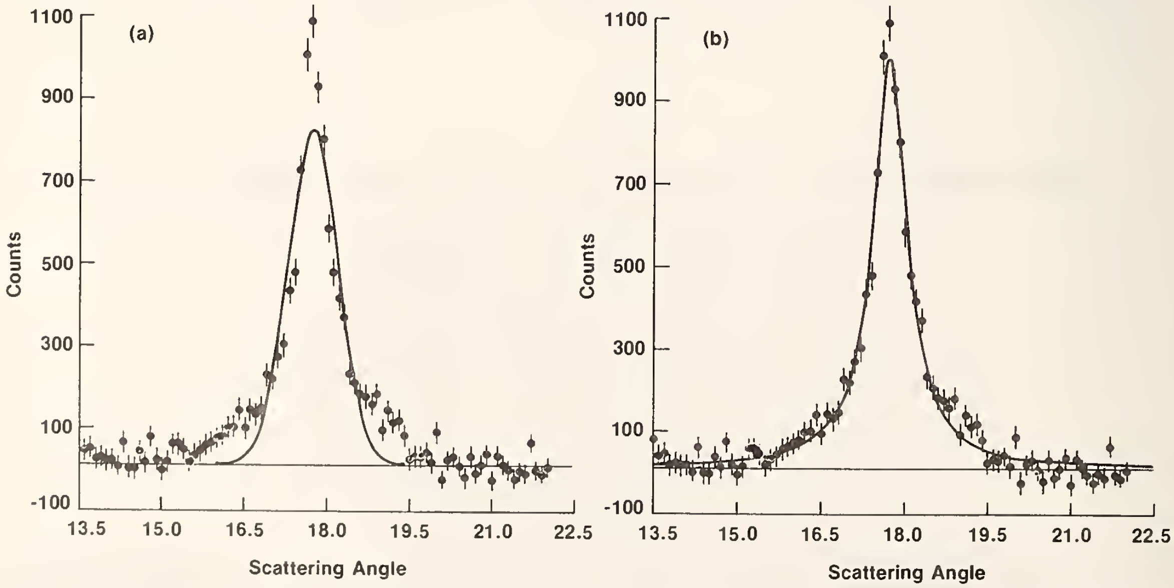

Figure 1. (111) magnetic Bragg reflection at 0.35 K. Background scattering, represented by data taken at 4 K, has been subtracted.
(a) solid line is a Gaussian fit to the data
(b) Lorentzian fit to the data

wave contribution to the scattering which maximizes at reciprocal lattice points, although increasing the temperature decreased the overall intensity without altering the lineshape. Inelastic measurements revealed that there are indeed magnetic excitations in the ordered state with energies below ~ 1 meV. In addition, we observed two crystal field excitations with energies of 7.4 and 11.1 meV.

---

1. R. N. Shelton, L. S. Hausermann-Berg, M. J. Johnson, P. Klavins and H. D. Yang (to be published)

2. R. N. Shelton, R. W. McCallum, H. Adrian, Phys. Lett. A56 213 (1976)

3. O. Fischer, A. Treyvaud, R. Chevrel and M. Sergent, Sol. St. Commun. 17 721 (1975)

SPIN DYNAMICS OF AMORPHOUS $Fe_{90-x}Ni_x Zr_{10}$

J.A. Fernandez-Baca and J. W. Lynn
(University of Maryland, College Park, MD)

and

(National Bureau of Standards, Gaithersburg, MD)

and

J.J. Rhyne

and

G.E. Fish
(Allied Corporation, Morristown, NJ)

The iron rich $Fe_{90-x}Ni_xZr_{10}$ amorphous system exhibits Invar characteristics[1], where the thermal expansion and a large positive spontaneous volume magnetostriction nearly cancel below the Curie temperature. This system also has the peculiarity that for x = 0 there is no long range ferromagnetic order. Small angle scattering experiments by Rhyne and Fish[2] have shown that the spin correlation length at low temperatures remains small (≈ 20 Å) and nearly temperature independent, reflecting the effect of competing ferromagnetic and antiferromagnetic exchange. The addition of Ni in the system induces long range ferromagnetic order as it has been shown in $Fe_{20}Ni_{10}Zr_{10}$, where spin waves have been observed in the whole range of temperatures studied (0.55-0.89 T_c).[3]

In order to obtain a better understanding of how this transition to long range ferromagnetic order occurs we have performed inelastic neutron scattering experiments to study the spin dynamics of $Fe_{90-x}Ni_xZr_{10}$ for x = 5, 10. The experiments were performed at the BT-9 triple axis spectrometer at the NBSR. The amorphous nature of the system required that measurements be taken near the forward (000) beam position. A fixed incident energy of 13.5 meV was used and a PG filter was placed after the monochromator to suppress higher order wavelength contaminations. Soller slit horizontal collimators of 15'-12'-11'-25' were used to produce a FWHM of 0.35 meV at the elastic position. Well defined spin waves were observed in all the range of temperatures studied (0.33-0.90 T_c for $Fe_{85}Ni_5Zr_{10}$, and 0.28-0.83 T_c for $Fe_{80}Ni_{10}Zr_{10}$). In analyzing the data, spin-wave energies and linewidth information were obtained by convoluting a double Lorentzian-type cross section with the instrumental resolution and least-squares fitting to the observed spectra, after subtraction of the background scattering.

The spin-wave energies at all temperatures under study were found to obey the quadratic dispersion relation expected for an isotropic ferromagnet:

$$E= \Delta + D(T)q^2 + \ldots \qquad (1)$$

where $\Delta \approx 0.05$ meV is an effective anisotropy gap which originates mainly from the dipole interaction, and shows no significant temperature dependence. The spin-wave stiffness parameter 'D' exhibited a temperature dependence of the form :

$$D(T) = D(0)[1-a(T/T_c)^{5/2}] \qquad (2)$$

with D(0) = 42.05 ± 0.37 and 78.03 ± 0.49 meV-$Å^2$ for the samples with x = 5 and 10, and a = 0.83. The value of the coefficient 'a' is of the same order of magnitude of the ones found in the Fe-B amorphous Invar system,[4] and is significantly larger than expected for a Heisenberg ferromagnet with short range interactions.

The intrinsic spin-wave linewidths Γ_q in the two systems under study did not show significant temperature dependence in the temperature range 0.55-0.90 T_c. These linewidth data could be fitted to a q^4 dependence (predicted by hydrodynamic spin-wave theory) or to a q^5 dependence (predicted from the topological disorder in amorphous systems). Also the ratio Γ_q/E_q ,that measures the relative damping of the spin-wave excitations, was found to be significantly larger than in the Fe-B system. These findings suggest that there might be spin-wave broadening mechanisms, presumably due to the magnetic disorder, in addition to the magnon-magnon interaction in the system.

---

1. K.Shirakawa, S.Ohnuma, M.Nose and T. Masumoto. IEEE Trans. Mag. 16,910 (1980).
2. J.J. Rhyne and G.E. Fish. J. Appl. Phys. 57,3407 (1985).
3. J.A. Fernandez-Baca, J.J. Rhyne and G.E. Fish. J. Magn. Magn. Mat. 54-57, 289 (1986); and NBS Technical Note 1217, ed. F. J. Shorten (1985) page 55.
4. J.A. Fernandez-Baca, J.W. Lynn, J.J. Rhyne, and G.E. Fish, J. Appl. Phys. 57,(1985).

NEUTRON SCATTERING STUDY OF THE SPIN FREEZING IN AMORPHOUS $Tb_{45}Fe_{55}$ AND $Tb_{25}Fe_{75}$

M. L. Spano*
(Naval Surface Weapons Center, Silver Spring, MD 20903)
and
(National Bureau of Standards, Gaithersburg, MD 20899)
and
J. J. Rhyne

We have made small angle neutron scattering measurements (SANS) on $Tb_{45}Fe_{55}$ and $Tb_{25}Fe_{75}$ as a function of temperature. These alloys, like others of the Tb-Fe system, do not become ferromagnets at low temperature, but rather undergo a transition to a spin frozen state. This is characterized by the formation of clusters of spin ordering which can be observed in SANS. There is a strong temperature evolution of the scattering intensity reflecting the change in the order parameter with temperature. The spin correlation length does not diverge at T_f reflecting the destruction of the conventional second order phase transition by the random anisotropy field. In the present study, both samples exhibit conventional Lorentzian lineshapes in Q for $T > T_f$, but depart from this form below T_f. We have fitted the latter lineshapes with the Lorentzian plus Lorentzian squared form appropriate for random field systems. In the $Tb_{45}Fe_{55}$ alloy the correlation length, ξ, rises, with decreasing temperature, to a rounded maximum of about 90 Å occurring about 20 K below $T_f = 298$ K, as determined from magnetization results, before decreasing to about 60 Å at 4 K. This is in marked contrast to the $Tb_{25}Fe_{75}$ alloy, in which ξ reaches an experimental infinity near its transition temperature of about 400 K. For both alloys the coefficient of the Lorentzian term rises sharply as $T \to 0$, whereas the Lorentzian squared coefficient follows approximately the square of the order parameter times ξ^{-1}.

MAGNETIC EXCITATIONS IN THE XY-HEISENBERG SYSTEM Tb_xSc_{1-x}

R. W. Erwin and J. J. Rhyne
and
B. Beaudry
(Iowa State University, Ames, Iowa)

Although well defined spin waves have been observed in rare-earth alloys with the non-magnetic diluent yttrium[1], there is very little known about the magnetic excitations in the analogous alloys diluted with scandium. Such a study is of

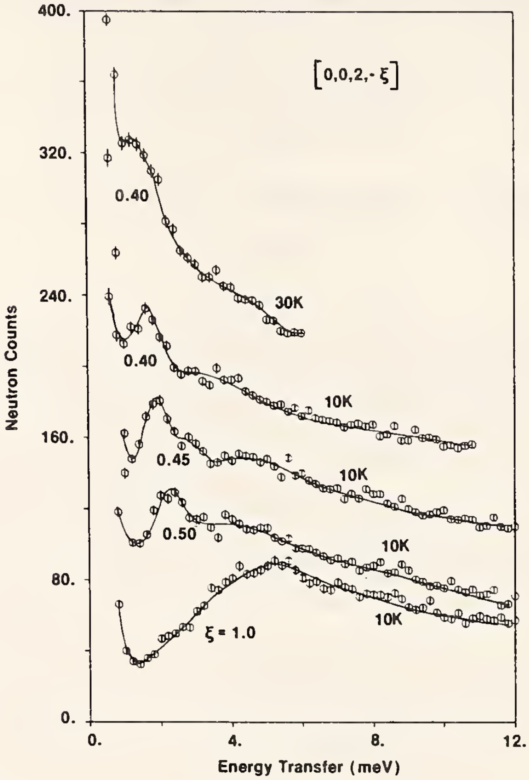

Figure 1. Scans of the energy transfer for wave vectors along the c^* direction show that the magnetic excitations in $Tb_{0.6}Sc_{0.4}$ are extremely broad. The observed peak positions do move to smaller energy transfer as the reduced wave vector decreases and the peak widths concomitantly become sharper as in conventional spin-wave behavior. The curves through the data points serve as a guide to the eye.

interest since there is considerable experimental data which indicates that Sc alloys have quite different magnetic properties from their Y counterparts[2]. It is then important to understand how these differences are related to the dynamic magnetic excitations in these materials.

We have begun an investigation of the Tb_xSc_{1-x} dilution system by probing the magnetic excitations in a single crystal of $Tb_{0.6}Sc_{0.4}$ with inelastic neutron scattering techniques.

These alloys have hcp crystalline structures and order in a magnetic structure consisting of a helix with the directions of the basal plane (XY) ferromagnetic sheets modulated along the c-axis (perpendicular to the basal plane). The spins are restricted to align in the basal plane by strong crystal field anisotropy. For large concentrations of Tb ($x \geq 0.85$) the low temperature ordered state is ferromagnetic[3] as in pure Tb for which $T_N = 225$ K and $T_c = 217$ K. As the Tb concentration is decreased below about 0.4 the helix coherence length becomes finite and the magnetic behavior becomes increasingly spin-glass like[2,4]. We have observed that the presently studied alloy ($x = 0.6$) has a resolution limited correlation length with $T_N = 115$ K.

In figure 1 are shown the low temperature ($T = 10$ K) energy scans for a range of wave-vector transfers along the c^* direction. The magnetic excitations should be most straightforward to observe in the c^* direction for these basal plane helimagnets as has been shown experimentally in a number of systems[5]. However, our data in figure 1 show that the magnetic excitations are extremely broad even for the excitations at the smallest reduced wave vectors measured $\xi = 0.4$ (40% of the way from the Brillioun zone center to the zone boundary) and at low temperatures (10 K = 0.12 T_N). The peak positions do move towards smaller energy transfer as ξ decreases and in addition the peak width does become sharper, as expected for conventional spin-wave behavior. Note that the effect of raising the temperature is to increase the intensity at small energy transfers until at 80 K ($\approx 0.7\ T_N$) a peak is no longer discernable at finite energy transfer as shown in figure 2 for $\xi = 0.6$. Also shown in figure 2 is the scan for $\xi = -0.6$, demonstrating that the observed inelastic scattering is predominantly due to magnetic excitations instead of phonons (the phonon intensity would increase as Q^2 where $Q = 2 + \xi$).

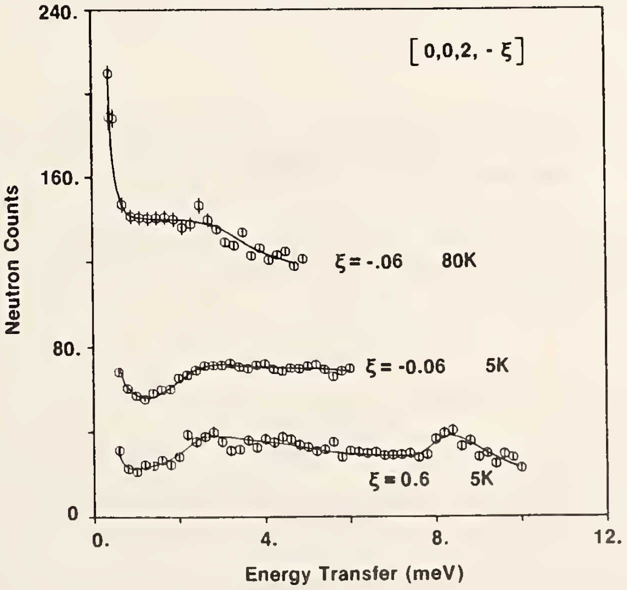

Figure 2. The energy scans along c^* at high temperatures show that the distribution of scattering has become broadened to the point that a peak in the intensity can no longer be observed at finite energy transfer. The scans at $\xi = \pm 0.6$ show that the observed scattering is predominantly magnetic in origin.

One possible method of explaining the observed broadening of the excitations is to invoke a distribution of exchange interactions between the Tb spins. This distribution might then be much sharper in the yttrium dilution systems than in the corresponding Sc systems, due to the verydifferent conduction band susceptibilities of Y and Sc[6]. The fact that the excitations become visible at low temperatures may be the result of the opening of a gap at zero energy transfer due to the strong increase of basal plane anisotropy, as has recently been predicted[7].

---

1. N. Wakabayashi and R. M. Nicklow, Phys. Rev. B10, 2049 (1974).

2. R. Abbundi, J. J. Rhyne, D. M. Sweger and R. Segnan, Phys. Rev. B18, 3313 (1978); J. H. Ferrick, J. J. Rhyne and R. Segnan, J. Appl. Phys. 53, 2232 (1982); K. Baberschke, P. Pureur, A. Fert, R. Wendler and S. Senoussi, to be published.

3. H. R. Child and W. C. Koehler, J. Appl. Phys. 37, 1353 (1966).

4. B. V. B. Sarkissian and B. R. Coles, Comm. Phys. 1, 17 (1976); R. W. Erwin and J. J. Rhyne, to be published.

5. A. R. Mackintosh and H. Bjerrum Moller, in Magnetic Properties of Rare Earth Metals, edited by R. J. Elliot, Plenum Press, New York, 1972.

6. S. H. Liu, R. P. Gupta and S. K. Sinha, Phys. Rev. B4, 1100 (1971).

7. A. A. Kumar, C. L. Henley and W. M. Saslow, to be published.

STATIC AND DYNAMIC SPIN CORRELATIONS IN DILUTE MAGNETIC SEMICONDUCTORS WITH HIGH Mn CONCENTRATIONS

T. M. Giebultowicz and J. K. Furdyna
(Purdue University, W. Lafayette, Indiana)

and

J. J. Rhyne

and

W. Y. Ching
(University of Missouri, Kansas City, MO)

and

D. L. Huber
(University of Wisconsin, Madison, WI)

Inelastic scattering spectra have been measured in $Cd_{0.35}Mn_{0.65}Te$ for several points in Q-space along [120] and $[1\bar{1}0]$ directions in the (001) plane. These directions have been chosen to avoid distortions of inelastic spectra due to twinning

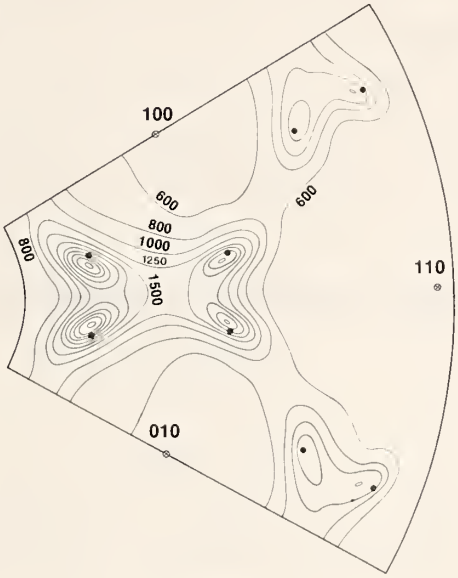

Figure 1. Contour map of elastic scattering intensity in $Zn_{0.45}Mn_{0.55}Se$ at 4.2 K for a 60° section of the basal plane. Crossed circles indicate the positions of nuclear Bragg reflections. Black dots show the ideal positions of magnetic superstructure reflections.

effects, which almost invariably occur in $Cd_{1-x}Mn_xTe$ crystals with high x. Comparison of the measured data (corrected for instrumental effects, such as resolution, or $\lambda/2$ contamination in the incident beam) with the dynamic structure factors $S(\vec{Q},E)$, calculated using the method by Ching and Huber[1], shows that this model gives an excellent description of the spin dynamics in $Cd_{1-x}Mn_xTe$, except for Q-points close to the zone center (the origin of a "gap" in E that occurs in this point is yet not clear). Fitting the theoretical lineshapes to measured spectra yields $2J_{NN}$= (13.8 0.2)K. This results provides the most accurate existing measurement of J_{NN} for $Cd_{1-x}Mn_xTe$ in the region of high Mn concentrations.

Studies of the wurtzite-structured DMS system $Zn_{1-x}Mn_xSe$ have been continued. Results of systematic measurements of elastic diffuse scattering intensity within the basal plan (shown as a contour map in figure 1) confirm that the short-range magnetic order in this compound is closely related to the type of antiferromagnetic structure which occurs in hexagonal β-MnS. The data reveal additionally two intriguing effcts: a strong anisotropy of the diffuse peak lineshapes, and a small shift of the centers of these peaks from ideal suprestructure positions. The first of these effects likely arises due to a "configurational" anisotropy of the Mn-Mn exchange interactions, which also occurs in cubic DMS systems. It is less clear, however, whether the shift is an intrinsic feature in this type of short-range ordering, or caused, e.g., by defects such as stacking faults.

---

1. W. Y. Ching, D. L. Huber, Phys. Rev. B25, 5761, and B26, 6164 (1982).

MAGNETIC PHASE TRANSITION UNDER PRESSURE IN THE REENTRANT SUPERCONDUCTOR $Tm_2Fe_3Si_5$

J.A. Gotaas

and

J.W. Lynn
(University of Maryland, College Park, MD)
and
(National Bureau of Standards, Gaithersburg, MD)

and

R.N. Shelton
(Iowa State University, Ames, IA)

The system $Tm_2Fe_3Si_5$ is an ordinary antiferromagnet with a transition temperature of 1.1 K at ambient pressure [1]; under applied pressures of 2 to 21 kbar there is a superconducting phase transition at a temperature $T_{c1} > T_N$, followed by a return to the normal state at a temperature T_{c2} in the vicinity of T_N as measured by ac susceptibility. The existence of thermal hysteresis under pressure suggests some first-order character to the reentrant transition [2]. Previous neutron diffraction measurements have shown no change in the nature of the magnetic state between ambient pressure and 2.3 kbar (just above the critical pressure for the appearance of superconductivity) [3].

We have now examined the nature of the magnetic ordering at higher pressures of 4.5 and 5.8 kbar, where the superconducting state is fully established before the magnetic transition occurs. The magnetic structure remains unchanged under the application of pressure. In particular, we find no evidence for the existence of any ferromagnetic component to the structure which could be responsible for quenching the superconducting state. Figure 1 displays the peak intensity of the first magnetic peak (100) as a function of temperature for both 2.3 and 5.8 kbar. It can be seen that intensity develops in the ordered state in the same way and that the sharp rise which normally defines the transition occurs at approximately the same temperature. The only apparent difference between the measurements at different pressures is the presence of additional intensity above the transition temperature at 5.8 kbar. There is a measurable increase in the peak width of the scattering above the transition, which indicates that this extra intensity results from short range correlations. There is no measurable thermal hysteresis in the magnetic peak intensity under pressure, in contrast to the observed hysteresis in the reentrant phase transition at higher pressures.

The destruction of the superconducting phase by an antiferromagnetic transition is unique experimentally, although a number of theories predict suppression of the superconductivity under some conditions [4, 5]. The absence of any increase in the observed T_N, in contrast to the observed rise in the reentrant temperature T_{c2}[2], may suggest that the superconducting state is not destroyed by the long range order of the magnetic moments, but by the dynamical fluctuations of the moments in the vicinity of the transition, as some theories have suggested [4]. In this case, there may be a second superconducting transition at still lower temperatures as the spin wave fluctuations become frozen out in the ordered state. The theory of Machida et al. [5] also predicts the destruction of superconductivity at the magnetic phase transition on different grounds, which is again followed by a second transition to the superconducting state at lower temperatures. Our neutron diffraction measurements would be insensitive to such a transition; such a possibility needs to be explored by polarized beam techniques, or by susceptibility or resistivity measurements.

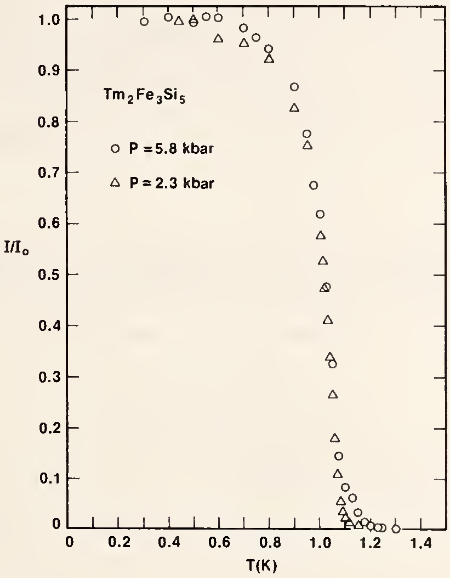

Figure 1: Peak intensity of the (100) magnetic reflection as a function of temperature, for pressures of 2.3 and 5.8 kbar.

---

1. A.R. Moodenbough, D.E. Cox and C.B. Vining, Phys. Rev. B32, 3103 (1985).
2. C.B. Vining and R.N. Shelton, Solid State Commun. 54, 53 (1985).
3. J.W. Lynn, J.A. Gotaas and R.N. Shelton, NBS Technical Note 1217, 58 (1985).
4. T.V. Ramakrishnan and C.M. Varma, Phys. Rev. B24, 137(1981); K. Levin, M.J. Nass and Charles Ro, in Superconductivity in Magnetic and Exotic Materials, ed. T. Matsubara and A. Kotani (Springer-Verlag) 1984, p. 104.
5. K. Machida, K. Nokura and T. Matsubara, Phys. Rev. B22, 2307 (1980).

SPIN DYNAMICS IN THE HEUSLER ALLOY NiMnSb

J.A. Gotaas and J.J. Rhyne
and
R.A. Robinson
(Los Alamos National Laboratory, Los Alamos, NM 87545)

We have begun neutron scattering measurements on the ferromagnetic Heusler alloy NiMnSb (T_c = 750 K [1]), which band structure calculations have shown to possess the unusual electronic property [2] that the majority spin electrons are metallic while the minority spin electrons exhibit a band gap, leading to a semiconducting nature.

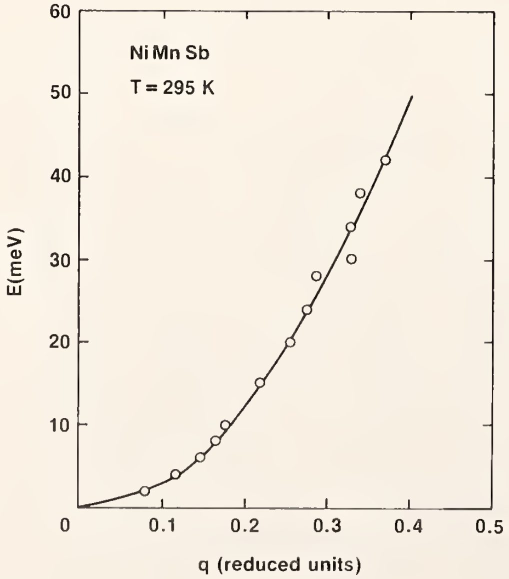

Figure 1. Magnon dispersion curve for NiMnSb at room temperature (q is in reduced units.

In the related conventional Heusler alloy Ni_2MnSb, which has a normal band structure, the moments are localized on the Mn atoms and the spin dynamics can be well described by the standard Heisenberg model. It is known that the moment remains localized on the Mn atoms in NiMnSb, so that one might also expect a Heisenberg description to be valid here, although the Curie temperature is considerably greater than that of Ni_2MnSb (where $T_c = 334$ K [1]). It is possible, however, that the peculiar band structure may lead to significant differences in the spin dynamics, and it is the goal of this work to explore that possibility.

To date, we have utilized BT6 and BT4 in the constant E mode to make measurements at room temperature on a single crystal sample weighing 9.5 gm. We have performed scans around the (111) and (220) reciprocal lattice points along the major symmetry directions (00ξ), $(\xi\xi0)$ and $(\xi\xi\xi)$. We have found the magnon dispersion to be isotropic along the major symmetry directions, and can be fit well by a simple quadratic law up to energies of 42 meV, with a dispersion constant of 218 $meV\text{-}A^2$. Figure 1 displays the data for all measurements (with q in reduced units), along with the fit $E = D q^2$, where D in reduced units is 311 meV.

Future experiments will extend these measurements to higher energies, as well as probing the behavior at elevated temperatures.

---

1. Y. Ishikawa and Y. Noda, AIP Conf. Proc. 24, 145 (1975).
2. R.A. de Groot, F.M. Mueller, P.G. van Engen and K.H.J. Buschow, Phys. Rev. Lettr. 50, 2024 (1983).

MAGNETIC FIELD-INDUCED TRANSITION IN $Y_{1-x}Gd_x$

J.A. Gotaas and J.J. Rhyne

and

L.E. Wenger
(Wayne State University, Detroit, MI)

and

J.A. Mydosh
(Kamerlingh Onnes Laboratorium, Rijksuniversiteit Leiden,The Netherlands)

Neutron scattering measurements have continued on the dilute alloys $Y_{1-x}Gd_x$ (x = 0.01,0.022,0.03 and 0.044). As reported earlier[1], for x=0.022, this system orders in a helical spin state at T=6.64K, with the spins lying in the basal plane and a modulation wave vector of 0.28c*. We have demonstrated that all compositions studied order in the same way with transition temperatures which depend on concentration (T_N=

2.4, 12.0 and 18.5K for x= 0.01,0.03 and 0.044, respectively)[3]. In order to clarify the origin of the long range order in this system, we have carried out additional neutron diffraction measurements in an applied magnetic field for the concentrations x=0.022 and 0.044.

We have studied the c axis satellites of the origin and (002) reflections in magnetic fields of up to 7 Tesla applied in the basal plane of the sample and find no change in the modulation wave vector of 0.28c* and no evidence for the development of higher harmonics which would indicate intermediate field-induced metastable periodic spin states. Below a critical field which depends on concentration and temperature (H_c = 0.25 T at 5.5K for x = 0.022 and 1.15 T at 4K for x = 0.044) the only observed change in the scattering is a gradual decrease in the magnetic intensity at 0.28c*, corresponding to the development of a net moment which should contribute a ferromagnetic component at the nuclear Bragg peak positions, although this additional contribution is too small to be observed in these dilute alloys. At H_c, there is an abrupt reduction by a factor of two in the intensity at 0.28c* (see figure 1), followed by a further gradual decrease as the applied field is increased. This result is consistent with a change in magnetic structure from the helical state to a linear modulated state in which the moments remain collinear in the basal plane but undergo a sinusoidal modulation in magnitude along the c axis. Such a magnetic transition is predicted by a spin density wave model[3] for the system, in which the Y conduction electrons are able to support a spin density wave through the interaction

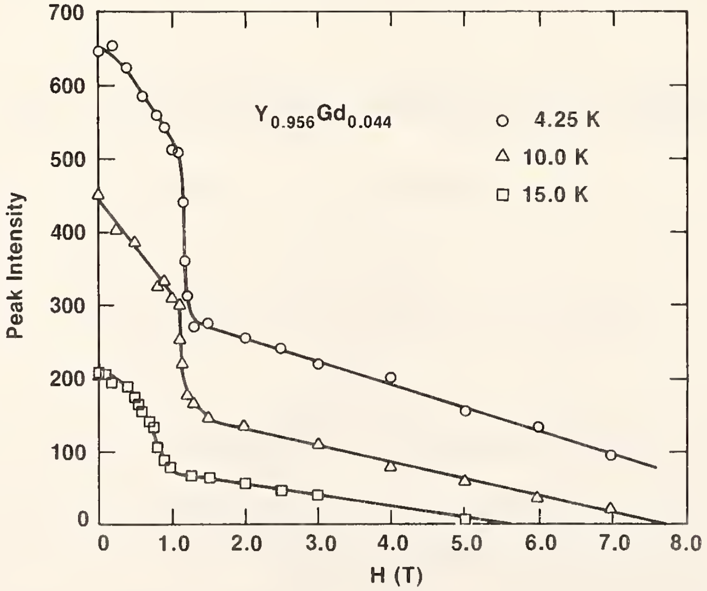

Figure 1. Magnetic peak intensity at 0.28c* as a function of the applied magnetic field for x = 0.044 at T = 4.25, 10.0 and 15.0K, displaying the sharp transition to the field induced state.

with the localized Gd moments in the matrix. Such a model is able to furnish semiquantitative agreement with measurements of susceptibility and specific heat[2].

Further experiments in applied fields will be carried out to verify the precise nature of the field-induced state.

---

1. J.A. Gotaas, J.J. Rhyne, L.E. Wenger and J.A. Mydosh, NBS Technical Note 1217, 49,(1985).
2. L.E. Wenger, Gary W. Hunter, J.A. Mydosh, J.A. Gotaas and J.J. Rhyne, Phys. Rev. Lett. 56, 1090(1986).
3. A.W. Overhauser, Phys. Rev. Lett. 3, 414(1959).

INELASTIC SCATTERING STUDIES OF VERY DILUTE MAGNETIC (SEMIMAGNETIC) SEMICONDUCTORS

T. M. Giebultowicz and J. K. Furdyna
(Purdue University, W. Lafayette, Indiana)

and

J. J. Rhyne

and

W. Y. Ching
(University of Missouri, Kansas City, MO)

and

D. L. Huber
(University of Wisconsin, Madison, WI)

Recently, it has been demonstrated that inelasic[1-3] neutron scattering can be used as a method for studying the excitation levels of isolated pairs of magnetic ions, and for direct determination of the nearest-neighbor exchange constant J_{NN}. We have applied this technique for investigating the Mn-Mn exchange interactions in a series of DMS compounds $Zn_{1-x}Mn_xS$, $Zn_{1-x}Mn_xSe$, and $Zn_{1-x}Mn_xTe$. Several single crystal and polycrystalline samples with concentrations x=0.01-0.05 have been studied using a triple-axis spectrometer in constant-Q mode. Energy transfer between the excited states does not depend on temperature and momentum transfer, in contrast to the scattered intensity[1]. Taking advantage of this property, we have carried out measurements at various temperatures and various points in Q-space in order to distinguish pair scattering from other possible inelastic effects (e.g., phonon scattering). Peak corresponding to the first and second excitation levels have been identified for most of the studied specimens (see figure 1), and in some measurements three levels have been observed. The values of $2J_{NN}$ have been determined to be 2.8, 2.1, and 1.6meV, respectively, for the three studied materials. Our result for $Zn_{1-x}Mn_xTe$ is slightly higher (≈5%) than the earlier reported value which was based on observation of only one excited level[3]. Practically, no reliable J_{NN} data existed before for the other two materials.

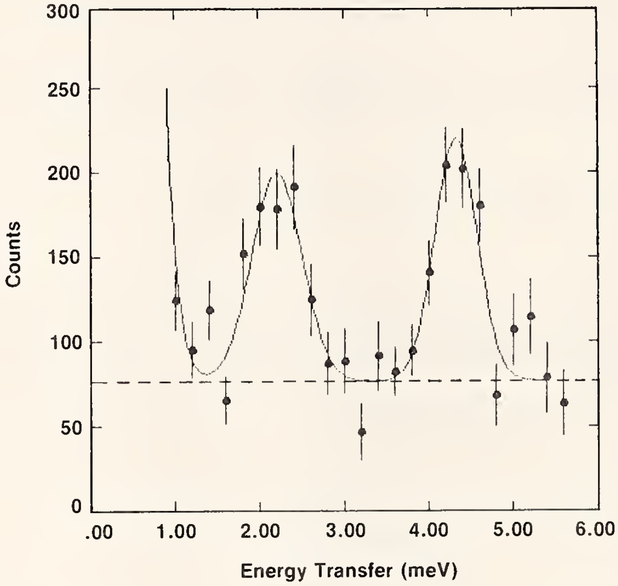

Figure 1. Pair scattering spectrum for $Zn_{1-x}Mn_xSe$ (with x = 0.062% per weight) showing peaks corresponding to the first and second excited level. The dashed line is the background level.

---

1. A. Furrer and H. U. Gudel, J. Mag. Mag. Mat. 14, 256 (1979).

2. W. L. J. Buyers et al., Phys. Rev. B30, 6521 (1984).

3. L. M. Corliss et al., Phys. Rev. B33, 608 (1986).

NEUTRON POWDER DIFFRACTION STUDIES OF LITHIUM AND SILVER EXCHANGED ZEOLITE RHO

G. D. Stucky and M. M. Eddy
(University of California, Santa Barbara, CA)

and

D. R. Corbin, L. Abrams and G. Jones
(E. I. du Pont de Nemours & Co., Wilmington, DE)

and

E. Prince

In molecular sieve chemistry fine tuning and design of connectivity, ordering and surface chemistry are required at the nanometer level in order to control electronic, chemical and transport properties. The ability to manipulate channel openings and thereby control access to the active centers has long been recognized as a major step in achieving more selective and efficient catalysts. To establish the mechanism by which site preference alters pore dimensions and void characteristics, the positions of the metal atoms in the structures of dehydrated lithium and silver exchanged zeolite rho were determined and refined using neutron powder diffraction methods. The framework of zeolite rho, which is composed of large α cages linked by double eight-rings, is particularly flexible[1], with distortions from an ideal structure (space group Im3m) varying greatly with different cations used for charge

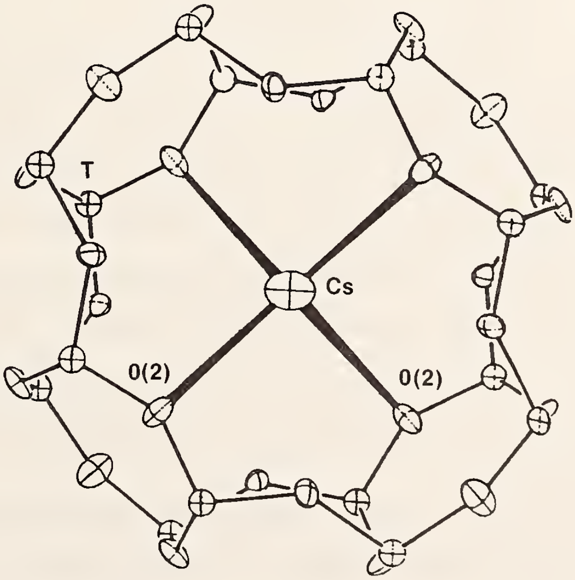

Figure 1. The tetrahedral site at the center of the double-8-ring which is occupied by cesium.

balance. Most compositions have structures with space group $I\bar{4}3m$.

We have studied by neutron powder diffraction two samples of zeolite rho, one with the composition $Si_{37.5}Al_{10.5}Na_{1.3}Li_{4.8}Cs_{4.3}O_{48}$ (lithium rho), and the other with composition $Si_{35.7}Al_{12.3}Na_{0.03}Ag_{10.8}Cs_{0.06}O_{48}$ (silver rho). The refined parameters for both structures are shown in table 1. The cesium in lithium rho occupies a nearly ideal tetrahedral site in the middle of the distorted double eight ring (figure 1). In this site it blocks the channels and also prevents any further distortion, leaving a cell parameter at room temperature (300 K) of 14.4925(5) Å. The cesium is very difficult to remove, but there was reason to believe that lithium rho did not represent the limit of distortion of the framework. Silver rho was therefore prepared with very little cesium. Its lattice parameter, 14.2251(6) Å, is the smallest yet observed in any sample of zeolite rho, and the framework is therefore the most distorted ever observed.

---

1. J. B. Parise, L. Abrams, J. D. Jorgensen & E. Prince, J. Phys. Chem. 88, 2303 (1984).

A STRUCTURAL STUDY OF $(Sr,Nd)Cl_{2.15}$

Harry A. Eick
(Michigan State University, East Lansing, MI)

and

E. Prince

Anion-excess fluorite structures have been an area of research activity for many years. In 1964 Willis, in an attempt to explain the structure of fluorite-type UO_{2+x} postulated "Willis Clusters"[1]. These clusters presumably developed because the excess anions relaxed from the (1/2, 1/2, 1/2) and related sites sites along <110> and <111>. To avoid extremely short anion-anion distances, it was necessary to postulate clusters. The cations remained fixed at (000). Subsequently, Cheetham et al.[2] examined by neutron diffraction $(Ca/Y)F_{2.10}$ and determined that the cluster model was consistent with their observations. Two types of clusters designated 2:2:2 and 3:4:2[2] were postulated.

Mason and Eick[3] examined by single crystal x-ray diffraction the structure of fluorite-type $(Sr/Y)Cl_{2.05}$. They observed the presence of weak non-face-centered reflections which were not accounted for by the cluster models. The superstructure reflections were so weak, however, that structural data could not be deduced from them.

Bendall and co-workers[4] effected a single crystal neutron diffraction study of (Sr/Pr)$Cl_{2.10}$. In contrast to Mason and Eick, they do not report the presence of superstructure reflections. Furthermore, their report does not indicate that they even looked for such reflections! From difference Fourier sections, three features were identified: (1) nuclear density was observed at (1/2, ν, ν); (2) intensity at (w,w,w) with w ≈ 0.4 was less than that at (1/2, ν, ν), indicative that the 2:2:2 cluster model was inappropriate and (3) nuclear density was observed at (x,x,x), x ≈ 0.28.

As might be expected, these workers encountered refinement difficulties with high correlations between some parameters. Furthermore, they found that the cation appeared to be slightly displaced from (000), but their attempts to refine a displaced cation were unsuccessful.

Bendall <u>et al</u>.[4] also examined by neutron powder diffraction $SrCl_2$, $Sr_{0.9}La_{0.1}Cl_{2.10}$, and $Sr_{0.82}La_{0.18}Cl_{2.18}$. These specimens were prepared by quenching in water molten samples of the appropriate molar ratios sealed in dried silica ampoules. For the analysis of the $Sr_{0.82}La_{0.18}Cl_{2.18}$ data five structural models were considered:

a. No anion interstitials; anion occupancy refined.

b. (1/2, ν, ν) interstitials, T-factors independent.

c. (w,w,w) interstitials, T-factors independent.

d. (1/2, ν, ν) and (w, w, w) interstitials, T-factors independent

e. (1/2, ν, ν) and (x, x, x) x = 0.286 interstitials, T-factors independent.

Models b and e gave R_{prof} values of 8.2 and 8.3 percent, respectively. Because Fourier sections indicated the same features as those observed for the single (Sr/Pr)$Cl_{2.10}$ crystal, model e was considered the best model, even though it had more parameters. Again, Fourier maps suggested that some cations were displaced from the ideal site, but attempts to account for the displacement failed because of high correlations between the magnitude of the displacement and the temperature factor. In addition, these authors found a modulated background which they attributed to interactions betweeen defects.

Laval and Frit[5] reviewed the $Ca_{(1-x)}Y_xF_{2+x}$ data and proposed a new structural model based upon an archimedian antiprism, a 4:4:3 cluster. This cluster which contains square antiprismatic, rather than cubic cation coordination, fits all the previously reported data for this fluorite system and elimates some of the very short anion distances that result from the 2:2:2 or 3:4:2 cluster. These authors suggest that nearly identical 4:4:4 or 4:4:5 clusters could equally well be present.

Bevan and Lawton[6] from geometrical considerations propose for heavily doped anion excess fluorite structures (i.e., MF_x, $X > 2.26$), regular polyhedral models based also upon cation centered square antiprisms. They indicate that these polyhedral models are good approximations for anion-excess fluorite structures, and can be the starting point of successful x-ray structural refinements.

In view of these recent developments in structural models for the anion-excess fluoride fluorite structure, it seemed appropriate that they be considered for the strontium chloride doped systems. Furthermore, since the structural studies reported for $Sr_{0.82}La_{0.18}Cl_{2.18}$ indicated possible cation displacements, and since the samples on which the analyses was performed were quenched, it was thought that carefully annealed homogeneous samples should be examined.

The sample was prepared by a homogeneous preparatory route. The appropriate molar quantities of Nd_2O_3 (99.9%, Michigan Chemical Company, principal impurity, 500 ppm Ca) and $Sr(OH)_2 \cdot 8H_2O$ (Baker Chemical Company) together with a 6x molar excess of NH_4Cl/mole of cation, were dissolved in an HCl/H_2O solution, evaporated to dryness, and thermally decomposed in accordance with the procedure described by Meyer and Ax.[7]

The reaction product was placed in two outgassed alundum boats which were subsequently sealed under vacuum into outgassed quartz tubes. The specimens were heated to 870° C, above the melting point of the mixture, in a MINI BRUTE furnace whose temperature was controlled to ± 0.1° C. They were held molten for 1 hour, then cooled to 680° C. The temperature was then decreased slowly over the course of 13 days to 400° C, then to room temperature over a 12 hour period. A sample of the product mixed with NBS certified Si [a = 5.43062 (4) Å] was examined by the Guinier x-ray diffraction procedure. The product was cubic, with a = 6.976 (2) Å.

Data analysis is still in progress.

---

1. B. T. M. Willis, Proc. Br. Ceram. Soc. 1, 9 (1964).

2. A. K. Cheetham, B. E. F. Fender and M. J. Cooper, J. Phys. C. 4, 3107 (1971).

3. E. Mason and H. A. Eick, J. Solid State Chem. 47, 314 (1983).

4. P. J. Bendall, C. R. A. Catlow and B. E. F. Fender, J. Phys. C. 17, 797 (1984).

5. J. P. Laval and B. Frit, J. Solid State Chem. 49, 237 (1983).

6. D. J. M. Bevan and S. E. Lawton, Acta Cryst. B42, 55 (1986).

7. G. Meyer and P. Ax, Mat. Res. Bull. 17, 1447 (1982).

THE STRUCTURES OF THE TRANSITION ALUMINAS AND THEIR PRECURSORS

R.S. Zhou and L. Snyder
(Alfred University, Alfred, NY)

and

E. Prince

The transition aluminas are a series of hydroxyl and microstructure stabilized materials which result from heating gibbsite, bayerite or boehmite. They are not true polymorphs of Al_2O_3 but rather contain varying amounts of residual hydroxyl ions. The hydroxyl concentration, equivalent to a loss on ignition, ranges from more than 10% for "amorphous alumina" to less than 1% for the best crystallized high temperature phases like theta and kappa. The final high temperature product is the irreversible transformation to alpha alumina.

The low temperature products are often called activated aluminas, in that they have high surface activity and very large specific surface areas. These materials are of high technological importance being widely used as catylitic substrates.

On heating the trihydroxides of aluminum, proton migration occurs, allowing the formation of water which vaporizes. The resulting structure and the role of the remaining hydrogens in stabilizing it are unknown. It is reasonable to speculate that the layers $Al(OH)_6$ octahedra lose their interconnecting hydrogen bonds first, which induces the observed fine cracking in the material. In the first stage of heating, the structurally ordered regions are on the order of 100 Angstroms, rendering the material x-ray amorphous. Diffusion and ion rearrangement follows, increasing the size of the structurally ordered regions. The reordering takes place within the framework of the original hydroxide crystal and thus the starting material helps determine the structure at any subsequent temperature.

Structural information is desired on these materials because of their technological importance. However, the minimal effect of hydrogen scattering on x-ray diffraction patterns has resulted in no information on the role of hydrogen in stabilizing these structures. This investigation is looking at a number of aluminum hydroxides and the various deuterated transition products using neutron diffraction. The pattern fitting Rietveld method is being used to structurally characterize these phases. A considerable effort has been expended on attempts to prepare the phases of interest in a pure state. We have had success with eta and theta to date and have taken neutron data on these phases. We are currently preparing the delta and kappa phases and hope to get neutron data on these in the near future.

A neutron powder diffraction pattern of deuterated transition theta-alumina was run on the five detector high resolution NBS Neutron diffractometer. This pattern contains 180 independent reflections but is poorly resolved due to specimen broadening resulting from poor crystallinity. The pattern has been refined using the NBS version of the Rietveld refinement program in conjunction with Fourier analyses and normal probability analyses.

Analysis of the Fourier and difference Fourier, after refinement of the x-ray parameters, clearly shows a deficient Al site and the presence of the deuterium. The x-ray structure has space group C2/m. The current reliability factor Rw in space group C2/m without protons is 6.42%. Removing the mirror results in space group C2 and adding 0.135 protons per asymmetry unit produces a current residual error of 6.37%. The true space group will be established in later refinements. The hydrogen is 1.129 Angstroms away from one of the three oxygens and about 0.6 Angstroms away from the density deficient aluminum position. The defect configuration is consistent with an sp2 hybridized bond to the oxygen. Other disordered positions for the deuterium are being investigated.

The neutron diffraction pattern of a deuterated eta alumina has been recorded. A newly proposed model is being refined using the Rietveld method with initial success.

NEUTRON POWDER DIFFRACTION AND RIETVELD REFINEMENT OF CERIUM ALUMINATE PHOSPHORS

G. P. Hamill
(GTE Laboratories, Inc., Waltham, MA)
and
E. Prince

The Rietveld refinement of the cerium aluminate phosphor, $CeAl_{13.5}O_{21.75}$, room temperature and 20ZK. neutron diffraction patterns indicates some structural properties which have been anticipated but never observed or confirmed in this material. As in the similar structures of cationic conductors (eg. lithium impregnated Beta"-alumina battery electrodes) there is a highly asymmetric thermal motion of the principal cation, Ce, in the plane sandwiched between the spinel blocks. One can picture the preferred vibrations of the cerium atoms as disk-shaped in the x-y plane with very small motion along the crystallographic "c" axis. This is an indication of a strong bonding between the cerium atoms and the nearest neighbor oxygens in the spinel blocks. Any vacancies in nearby oxygen sites therefore occur in the conducting plane with a corresponding anisotropic motion of the cerium position with only ten or eleven nearest neighbor oxygens instead of the normal twelve.

The analysis of the nearby aluminum atom in the conducting plane also shows a highly anisotropic thermal motion. In this case, however, it is needle-shaped along the "c" axis. The site in the conduction plane has three nearest neighbor oxygens in an equilateral triangle geometry. Directly above and below this site are more stable tetrahedral sites into which the aluminum atoms can "fall" in response to some oxygen vacancy in a nearby site. The 20°K. data are encouraging in this respect. Since one would expect a "freezing" of thermal motion at low temperatures, the atoms are expected to reduce their motion if they are in stable sites. The aluminum atom exhibits higher relative motion at low temperatures (assuming fixed location). The potential for several aluminum sites - tetragonal and triangular coordination - is high.

Further refinement will aim at checking for additional sites for the cerium and aluminum atoms in response to local vacancy/occupancy of oxygen atom sites. A correlation between specific site vacancies and the symmetrical or asymmetrical configuration surrounding the cerium atoms will be tested. Note that although the data obtained at room temperature and the subsequent structure refinements may be less clear than those at cryogenic temperatures, the samples of greater interest are those at a room temperature which provide the proper emission spectra.

In an associated research project, a more complete set of EXAFS data at both room and cryogenic temperatures will be obtained through a Principal Research Team at Beam Line 18B at Brookhaven's National Synchrotron Light Source. In this way, data on the average crystal structure and localized site geometry will be combined to obtain a full understanding of these structures and the effects on the emission spectra of the two materials.

NEUTRON POWER DIFFRACTION STUDY OF THE ZEOLITES BA1SI$_2$O$_6$ WITH B=Cs, Rb, K, and Na

Francis W. Beech
(University College of London, London, England)

and

A. Santoro and R. S. Roth

This study was undertaken to compliment the recent investigations of Block and Piermanini (1986) into the pressure induced phase transitions displayed by these

Table I Results of the refinement of CsAlSi$_2$O$_6$ in space group I41/a cd-Ions Si and Al disordered.

Atom	Position	x	y	z	B	n
Cs	16	0.3824(6)	0.6324	1/8	3.76	1/2
Al(1)	16	0.1576(7)	0.4076	1/8	1.31	1/6
Si(1)		"	"	"	"	1/3
Al(2)	32g	0.1184(8)	0.6610(7)	0.5813(7)	1.30	1/3
Si(2)	"	"	"	"	"	2/3
O(1)	32g	0.1047(8)	0.1382(6)	0.7199(6)	2.52	1.0
O(2)	"	0.7239(7)	0.1149(7)	0.1340(8)	2.52	1.0
O(3)	"	0.1297(7)	0.7132(6)	0.0980(8)	2.52	1.0

R_N=11.19 R_p=7.91 R_W=10.08 R_E=4.66 X=2.163

a=13.6748Å

c=13.7087Å

Table II Results of the refinement of CSAlSi$_2$O$_6$ in space group I4./a . Si and Al Al disordered.

Atom	Position	x	y	z	B	n
Cs	16 f	0.126(1)	0.127(1)	0.124(1)	3.5(2)	1.0
Al(1)	"	0.121(1)	0.662(1)	0.583(1)	1.3(4)	1/3
Si(1)	"	"	"	"	"	2/3
Al(2)	"	0.591(1)	0.134(1)	0.667(1)	0.8(3)	1/3
Si(2)	"	"	"	"	"	2/3
Al(3)	"	0.659(1)	0.592(1)	0.123(2)	1.3(3)	1/3
Si(3)	"	"	"	"	"	2/3
O(1)	"	0.120(1)	0.1462(9)	0.724(1)	2.3(3)	1.0
O(2)	"	0.7264(9)	0.116(1)	0.134(1)	3.0(3)	1.0
O(3)	"	0.135(1)	0.725(1)	0.099(1)	2.3(3)	1.0
O(4)	"	0.8716(9)	0.3379(8)	0.5316(9)	2.6(3)	1.0
O(5)	"	0.849(1)	0.9641(9)	0.120(1)	1.7(3)	1.0
O(6)	"	0.4618(7)	0.386(1)	0.139(1)	1.3(2)	1.0

R_N8.13 R_p6.47 R_N=8.28 R_E=4.65 X=1.781

x-rays a=13.6632 c/a = 1.004
c=13.7227

Neutrons a=13.675 c/a = 1.002
c=13.709

materials. Their results have reopened the controversy concerning the basic structural arrangements in these materials. This problem is exemplified in the Cesium case by the inability to reconcile the observed optical birefrigence with the cubic space group suggested for the material by Newman. Due to the multile twinning displayed in single crystals of these materials powder neutron diffraction data was were collected on the instrument BT1 which was subsequently analysed using the Richield technique.

The Powder samples were synthesised by means of a soft-gel technique. The reactants Al $(i(C3H_2O)_3$, Si $(C_2H_5O)4$ and the alkali metal acetates were obtained from commercial sources and used without further purification. Due to the hydroscopic nature of some of the materials considered in this study all operations were conducted either in an argon atmosphere drybox or under argon purge. It was discovered that the tetraethyl onthesillicate has a significantly lower hydrolyis rate than the other reaction components and this factor resulted initially in diphasic materials. The key to obtaining single phase materials in this case lie in prehydrolysing the tetraethyl on the silicate. The single phase amphorous gels produced by this route were crystallised by subsequent heat treatments and the crystalline powders were characterised by x-ray techniques.

The neutron data for the cesium material were analysed in the cubic space group $Ia\bar{3}d$ suggested by Newman and the deniative tetragonal space groups I41/acd and I41/a. Significantly not all peaks in the data set could be accounted for in the cubic setting which rules the possibility out. The final values for the refinements in the tetragonal settings are reported in Tables 1 and 2.

In the case of the rubidium and potassium analogues refinements to differentiate between the tweo tetragonal possibilities clearly showed that the space group for these materials is I41/a. All the above results are being prepared for publication.

The above refinements were postponed using the assumption that the framework Al/Si were statistically distributed over the possible crystallographic positions. Attempts to induce ordering of these ions into the refinement have so far met with little success due to the apparent insensitivity of the space group to ion ordering in the framework. Work is continuing on this intriguing problem. Work is also in progress to relate these synthetic materials with their hydrated geological equivalents in an attempt to understand the role of absorbed water molecules in etermining the observed molecular structure.

BISMUTH VALENCE ORDER-DISORDER STUDY IN $BaBiO_3$ BY POWDER NEUTRON DIFFRACTION

C. Chaillout and M. Marezio
(Laboratoire de Cristallographic, Grenoble, France)

and

A. Santoro

and

J. Remeika
(AT & T Bell Laboratories, Murray Hill, NJ)

Two structural arrangements have been shown to exist for the perovskite-like compound $BaBiO_3$ by powder neutron diffraction data. The first is characterized by a partial (75%) order of the Bi^{3+} and Bi^{5+} cations on the two crystallographically independent sites, while in the second arrangement the two cations are almost 100% disordered. The structure of eleven differently-prepared $BaBiO_3$ samples showed that the deciding factor for obtaining one or the other arrangement is the temperature at which the sample is prepared or subsequently heat-treated. On the contrary, the cooling rate and the atmosphere (air or oxygen) do not seem to be important parameters. DTA measurements indicated that $BaBiO_3$ undergoes an additional phase transition at 860°C on heating and 810°C on cooling. This transition probably corresponds to the disproportionation of the Bi into Bi^{3+} and Bi^{5+} cations. This conjecture explains why the heat-treatment at 800°C yields compounds containing partial cation ordering. Since the symmetry is cubic above and below the 810°C transition, the 75% ordered $BaBiO_3$ stable between 810°C and 480°C would contain a trigonal dynamical distortion which would be the precursor of the static trigonal distortion which takes place at 480°C. In every compound the partial ordering is always 75%. This has been interpreted as an indication that an additional ordering of Au_3Cu type could exist on the two Bi sublattices.

STUDIES OF TITANIUM ALUMINUM ALLOYS

R. M. Waterstrat
(American Dental Association Health Foundation Research Unit)

and

E. Prince

The phase diagram of the titanium-aluminum system is complex near the Ti rich end, and it has proved difficult to determine it unambiguously because precipitates of low temperature phases form rapidly even when the sample is quenched from high temperature.[1] Because of the negative scattering amplitude of Ti for neutrons, neutron powder diffraction is well suited to the study of these alloys. A vacuum furnace has been constructed to enable powder diffraction measurements in situ at temperatures up to 1200°C, and samples of Ti-Al with compositions ranging from 14 to 45 atomic percent Al have been studied at 900°C and 1000°C. 14% and 16% samples have the disordered α-Ti structure at both temperatures. At 20% Al the superlattice lines of ordered Ti_3Al are present. The sample with composition 82% Ti - 18% Al was particularly interesting. At 900°C, well crystallized Ti_3Al is present. At 1000°C the diffraction pattern is very weak, although the composition is a long way away from the "null matrix" composition. This may be due to short range order, which can produce a large "effective temperature factor".

---

1. R. D. Shull, A. J. McAlister and R. C. Reno, Proceedings of the Fifth International Conference on Titanium (1984).

TEXTURE MEASUREMENTS IN DEFORMED METALS USING NEUTRON DIFFRACTION

R. C. Reno
(University of Maryland - Baltimore County, Baltimore, MD)

and

(National Bureau of Standards, Gaithersburg, MD)

and

R. J. Fields
(Fracture and Deformation Division)

Since crystallographic texture in deformed metals has a profound influence on mechanical properties, methods which quantify texture are extremely useful. Using a four-circle neutron diffractometer at the NBS Reactor, we have begun a study of texture in several materials, including copper rods, high-strength low alloy (HSLA) steel, and rolled 5052 aluminum sheet. The diffractometer is used to generate pole figure data (see figure 1 & 2) which can be analyzed to determine preferred crystallographic orientation in each specimen. The advantages of using neutron diffraction to create pole figures stem from the deep penetration of neutrons into metallurgical samples. This is especially important when one must examine samples which cannot be made thin enough for x-ray pole figure studies or which contain large grains or large-scale inhomogeneities. The use of neutrons for texture studies does, however, have its drawbacks. Neutron measurements are slow and expensive and must be

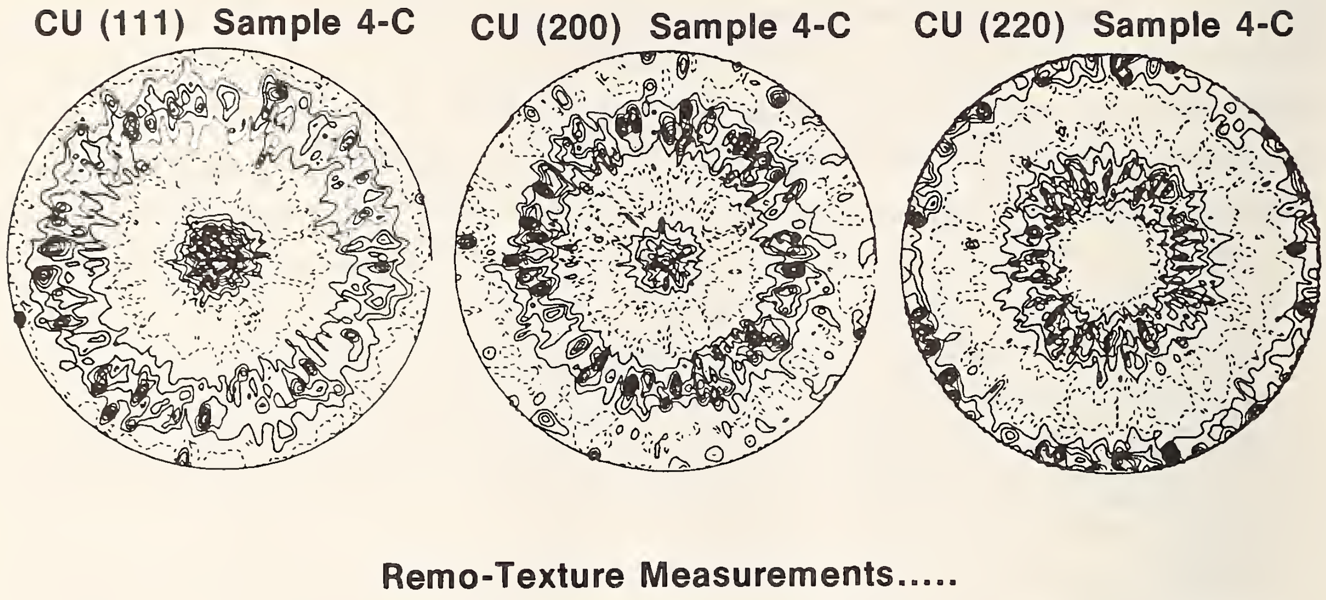

CU (111) Sample 4-C

CU (200) Sample 4-C

CU (220) Sample 4-C

Figure 1. Neutron pole figures for creep-cavitated copper. These show that [100] and [111] directions are aligned preferentially along the rod axis. Also, [111] texture is stronger than the [100] texture.

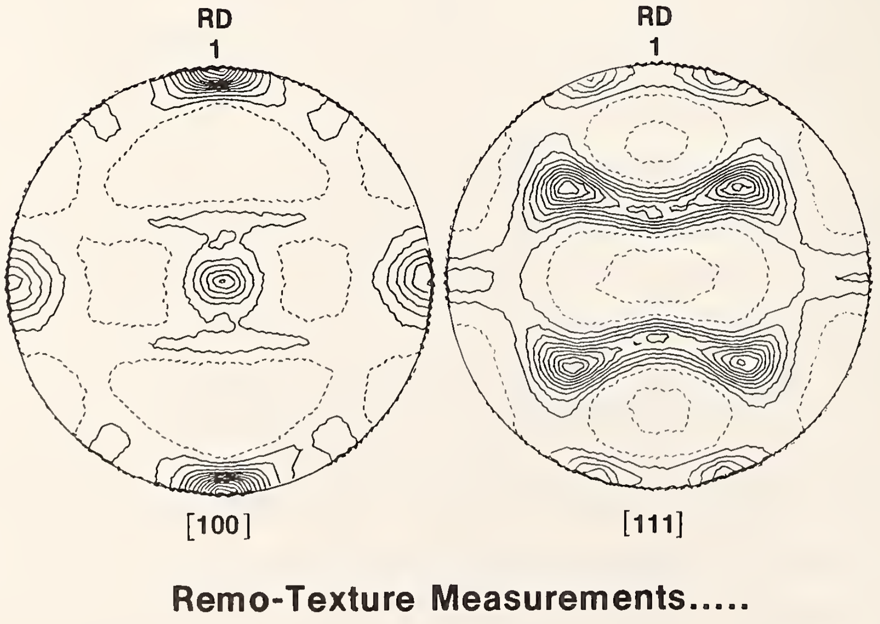

Figure 2. Neutron pole figures for 5052 rolled aluminum sheet. [100] directions are predominantly parallel to the rolling and transverse directions.

carried out at a reactor. When rapid determinations of texture must be made, perhaps on materials still on a production line, an alternative is desirable. In these cases we rely on ultrasound velocity measurements to provide texture information. Since, however, ultrasonic propagation is sensitive to sample inhomogeneities as well as texture, it is essential that results from both techniques be compared before the structure of a sample is fully understood. Figure 1 shows pole figure data for copper rods that have been subjected to low tensile stress at high temperatures. An analysis of this data indicates that the fiber texture of these rods consists of a mixture of [111] and [100] orientations along the axis, approximately a 72% contribution from the [111] orientation. This data is useful in understanding the ultrasound velocity measurements which, in this material, are sensitive to voids.[1]

Figure 2 shows pole figures for rolled 5052 aluminum sheet. It can be deduced from the figures that most crystals are oriented so that [100] directions are parallel to the rolling and transverse directions of the sheet. A fit of the pole figures to an expansion in spherical functions up to order $\ell = 4$ gives w-coefficients[2] as follows:

$$W_{400} = 0.122 \pm 0.006$$
$$W_{420} = -0.022 \pm 0.006$$
$$W_{440} = 0.043 \pm 0.007$$

---

1. H. M. Ledbetter and R. J. Fields, submitted to Acta Metallurgica

2. Ryong-Joon Roe, J. Appl. Phys. 37, 2069 (1966)

MICROSTRUCTURE STUDY OF AGE-HARDENED U - 0.75WT% Ti ALLOY

C. S. Choi and H. J. Prask
(U. S. Army Armament R & D Center, Dover, NJ)
and
(National Bureau of Standards, Gaithersburg, MD)

It is well known that heat treatment (i.e. quenching and subsequent aging) of depleted uranium alloys increases the mechanical strength of the alloys through precipitation hardening. This study is aimed at understanding the mechanism of the precipitation hardening (or aging) by characterizing the crystallographic and microstructural properties of the alloys as function of aging amount. The cast ingot of depleted uranium alloy containing 0.75% titanium was hot rolled to a plate form with a thickness of approximately 0.2 inches, about 10% reduction at each step, in a

Table 1. Sample preparation data.

Samples were prepared in the following sequence.
Cast ingot, hot rolled to 0.2" in 10% steps, γ-phase treatment at 800C for 3 hours, water-quenched, cold rolled (1 - 2%) and then aged.

Samples	aging dosages	hardness(HRC)
No. 1	no aging	31.9(4)
No. 2	500C / 10^2 sec	38.0(10)
No. 3	500C / 10^3 sec	52.3(8)
No. 4	550C / 10^3 sec	52.3(6)
NO. 5	550C / 10^4 sec	43.6(18)
No. 6	600C / 10^4 sec	38.4(6)
No. 7	pure uranium	

vacuum oven. The plates were homogenized at 800C for 3 hours and quenched in water, and then cold-rolled and cut to platelets of approximately 2 x 10 x 30 mm size. The platelets were divided into six groups, and aged differently as shown in table 1. The hardness of the aged alloys was measured for one of each group using a Rockwell Hardness Tester. The results are included in table 1.

1. Neutron Powder Diffraction (wide angle) Measurement

The diffraction patterns of the aged samples, measured by the multi-detector high resolution diffractometer, showed a two phase structure consisting of α-U and U_2Ti. Therefore the refinements were performed in two steps: the first step was the normal Rietveld refinement for the uranium phase, excluding the regions of the delta-phase peaks; the second step was a delta-phase refinement for the whole pattern using a multi-phase Rietveld refinement program. The structural parameters of α-U as obtained in the earlier study was used for all samples throughout the refinements. The width function parameters, unit cell dimensions, and preferred orientation parameters of the uranium phase and other profile parameters including backgrounds were refined in the first step. In the second step of the refinement (i.e., two-phase refinement), the scale factors of the two phases were determined, with all other parameters as obtained in the first step kept unchanged, using the entire profile. The scale factors obtained by this multi-pattern refinement were used for the determination of the delta-phase concentration. To examine the trend of lattice distortion as a function of the heat treatment, the b-axis lengths and the unit cell volumes were normalized to the corresponding value of α-phase as-cast DU (DUAC) alloy, i.e. b = 5.8537(2), V = 83.17(1), and plotted as a function of aging. The two curves showed essentially an identical aging-dependence: both parameters are reduced after the γ-quench; further shrinkage occurs in the initial stage of aging; maximum shrinkage occurs at the aging dosage of sample No. 3 (10^3 sec. at 500C); expansion occurs with subsequent aging.

2. Neutron Small Angle Scattering Study

The SANS facility at the NBS reactor was used for the study of the particle size distribution of the precipitates (or aggregate) and the internal structure of the aggregate. Since the wavelength spread and the angular spread of collimators are the two main factors of the instrumental resolution, the uncertainty of distance determination (or size uncertainty) becomes;

$$\Delta r \approx 2\pi\{(\Delta\lambda/\lambda)^2 + (4\pi\Delta\Theta/\lambda Q)^2\}^{1/2}/Q \qquad (1).$$

Since the size uncertainty is inversely proportional to Q, the SANS intensity function I(Q) of an aggregate should show the characteristics of a homogenious density particle at the lower Q region. The characteristic scattering of the internal structure occurs only at higher Q region where Δr is smaller than the individual element of the aggregate. To study the overall size of the aggregate and the internal structure of the aggregate, the measurements were made in two ways; the lower Q-ranges ($.007 < Q < .08$) using 9Å wavelength neutrons for the former and the higher Q-ranges ($.01 < Q < .15$) using 5Å neutrons for the later.

a. Particle Size Distributions

We assume that the scatterers are globular particles in the Q-ranges below the crossover point, and hence the scattering intensity distribution of 9Å neutron measurement obey Guinier's law. A multi-group guinier particle model;

$$(d\sigma/d\Omega) = K\sum_i (n_i\rho^2 v_i^2 \exp(-R_i^2 Q^2/3)) \qquad (2)$$

was used for the analysis of the particle size distribution. The least-squares parameters determined were the amplitude A_i ($= Kn_i\rho^2 v_i^2$) and the radius of gyration R_i. Four different size-groups were required to describe the entire scattering profile for each sample. The distribution of the particle sizes obtained were quite similar between the five aged samples, ranging between 20Å - 31Å, 58Å - 76Å, 116Å - 140Å, and 239Å - 286Å, respectively, for the four size-groups. Therefore, the size distributions were reanalized using an identical set of size-groups (20Å, 60Å, 130Å, and 260Å) for all samples. Then the amplitudes of the four particle sizes were refined simultaneously by the non-linear least squares method. The particle-size

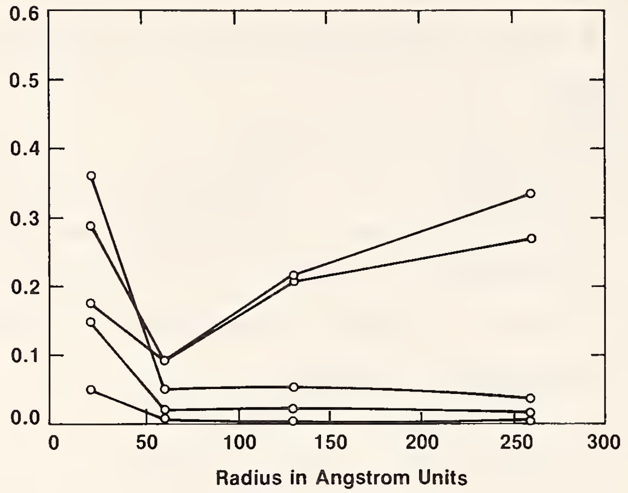

Figure 1. The particle size distributions (volume fraction vs Guinier radius) of the delta-phase precipitates in the aged samples, as obtained by SANS study with 9Å neutrons.

distributions thus obtained are shown in figure 1. The amount of the smallest particles of the precipitates increases with aging until it reaches a maximum at sample #4 (550C/1000sec), then it decreases with increased aging. On the other hand, the concentrations of the larger size-groups increase monotonically with increased aging. The number of precipitate particles increases rapidly up to sample No. 4 and then gradually decreases with increasing aging. This analysis also supports the two-stage aging model derived from the crystallographic parameters.

b. Fractal behavior

The intensity distributions of 5Å neutron measurement were plotted as log(I) vs log(Q) to search for straight lines at the higher Q-ranges up to experimental Q limit ($0.15Å^{-1}$). The exponent of the power-law was determined from the slope of the straight line obtained by the least-squares fit to the log-log data within selected Q-ranges (by visual estimation). The results are shown in table 2. The Porod regions ($D = 4$) have not been observed up to $0.15\ Å^{-1}$ (the experimental Q limit) for any of the five samples. If the distributions represent the power-law property of a fractal, the observed fractal dimensions of the five aged samples are about 1.5 for sample #2 and then becoming gradually larger with increasing aging to about 2.4 for sample #6, as shown in table 2.

3. The effect of the temperature gradient by rapid quench.

In the quenching of a large cylindrical uranium alloy sample, the outer surface cools first while the interior remains hot because of the finite thermal conductivity. This temperature gradient creates a radially varying residual stress

Table 2. The fractal dimensions D, the Q ranges and the chi-squares of the refinement for the aged DU samples, as determined by the power-law properties of fractals.

Sample	D	Q_{min} (A^{-1})	chi
2	1.51(1)	.08 - .15	4.23
3	1.84(1)	.085 - .15	3.54
4	2.03(1)	.07 - .15	3.65
5	2.24(1)	.06 - .15	2.85
6	2.39(1)	.06 - .15	2.81

distribution with highly compressive tangential and axial stresses in the outer surface and tensile stress in the interior, and causes a void formation in the interior of cylindrical alloys. An additional concern for specimens of radius greater than ≈1 cm is the uniformity of the γ to α' conversion throughout the sample, because of the quench-rate difference by positions.

A thin, disk-shaped sample, 24mm diameter and 2mm thichness, was obtained from a 33 mm diameter gamma-quenched U - 0.75wt% Ti alloy rod. To search for any evidence of delta-phase formation in the sample, an x-ray powder diffraction pattern was measured from 5 to 70° in scattering angle, using Mo-K_α radiation. The diffraction pattern revealed clearly the UO_2 peaks but no trace of TiU_2 compound.

Subsequently, SANS measurements were conducted on this sample at four different radial positions of the disk, at R = 0, 3, 6, and 9mm. The sample was mounted perpendicularly to the incident beam (5.5A wavelength) with a beam cross-section of 6mm diameter. The scattering intensities at the four positions were measured under identical conditions including the monitor counts. The result indicated that the scatterer size distribution could be represented by three particle-sizes, approximately 6, 22, and 44A, for the two outer positions, and by four sizes which included 100A particles in addition to the above three sizes. Probably the three smaller particles are combination of UO_2 particles and the lattice dislocations, and the 100A particles are voids.

STRUCTURE FACTOR OF HE-4 IN THE VICINITY OF THE GAS-LIQUID PHASE TRANSITION

B. Mozer

and

B. LeNeindre
(Laboratoire des Interactions Moleculaires et des Hautes Pressions,
CNRS, Universitaire Paris Nord, France)

and

B. Farnoux
(Laboratoire Leon Brillouin, Centre des Etudes Nucleaires - Saclay, France)

The structure factor of He-4 in the region of the gas-liquid antical point has been measured by neutron scattering for small wave vector differences, $q = 4\pi \sin\Theta/2$, and at large wave vector differences. These measurements provide the data which can permit an evaluation of the cross-over behavior between large and small wave length fluctuations as described in the modern theories of critical phenomena.

The sample all was designed and built at NBS to fit onto an I.L.L. type cryostat in use at Saclay. The cell was in an adiabatic configuration and from our measurements of the thermodynamic behavior of the system, we could ascertain a temperature regulation of 1 - 2 μK around the critical point $T_c = 5.2$ K. This regulation was measured by a calibrated NBS germanium thermometer kindly furnished to us by E. Pfieffer of the Temperature Division. Other resistance thermometers were used to measure the temperatures at various parts in the cell. The density of the behavior was measured via the capacitance of the liquid and evaluated from published thermodynamic data. Our preliminary diffraction data was obtained mostly for reduced temperatures below the critical point and one point above the critical point. Neutron diffraction data was taken at 5, 8, and 15 Å at the small angle spectrometer, PAXY, and at 5 Å on the banana detector spectrometer in the guide hall. These measurements cover a q range from 0.001×10^{-3} Å^{-1} to 0.25 Å^{-1} for the small angle measurements and from 0.2 to 2.5 Å^{-1} for the banana detector. Figure 1 shows the log of the intensity versus log q for all our measurements except at the smallest angles. The regions of overlap are evident from the figure. The structure factor is normalized so as to be unity for very large q and corresponds to a reduced temperature of $t = (T - T_c)/T_c = -0.5 \times 10^{-4}$. Figure 2 shows the data including that at the smallest q values and part of the data obtained with the banana detector.

We have found from our data a value for the compressibility exponent, $\gamma = 1.158$ if we take the accepted value of the exponent for the correlation lengths, $\nu = 0.63$. We also find that the ratio of the prefactors for the correlation length at temperatures above the transition to that below the transition to be

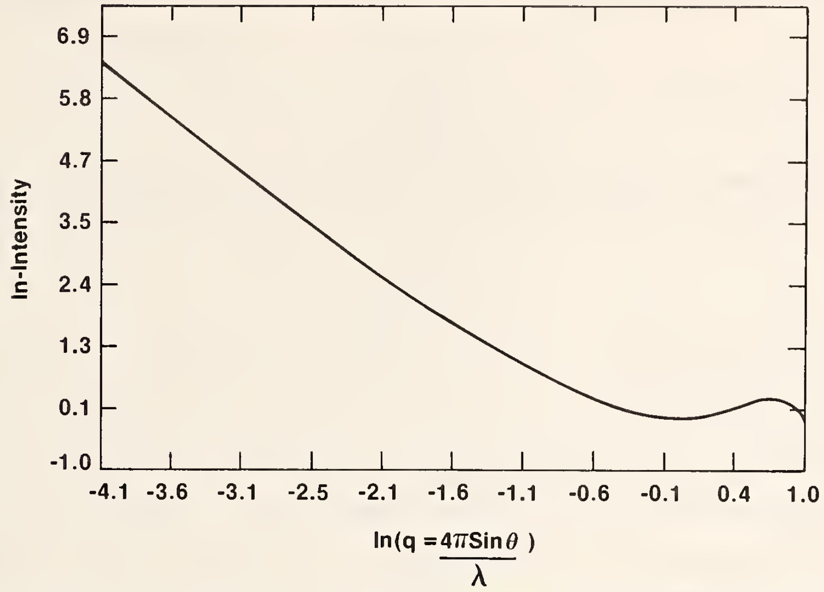

Figure 1. Ln intensity versus ℓn q for the structure factor of helium at $T = (T - T_c)/T_c = -2.5 \times 10^{-4}$. All the data taken is represented here except that for the smallest q values.

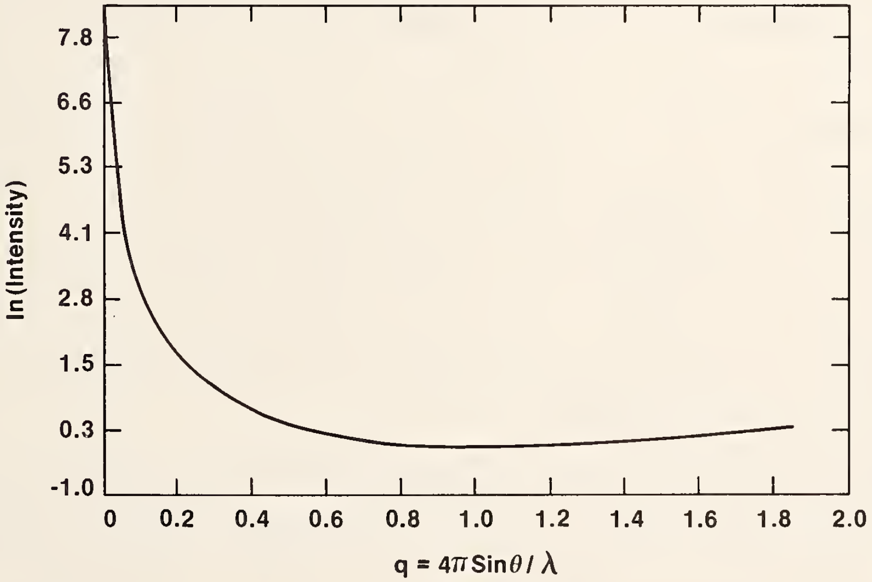

Figure 2. Singular contributions to scattering, $I_s(q)$, as regulated by dispersion in wavevector pool, with $\Delta k = k/20$. a) $c = 0.04$, $c_1 = 0.45, 0.37, 0.29, 0.21$. b) $c_2 = 0$, $c_1 = 1 - c_s$ and $c_s = 0.5, 0.6, 0.7, 0.8$.

$$R = \xi_o/\xi_o^- = \frac{2.40}{1.14} = 2.11.$$

We are in the process of analyzing this data to determine the cross-over region and other critical exponents.

THE STRUCTURE FACTOR OF LIQUID HE-4 AT SMALL ANGLES FOR SEVERAL TEMPERATURES

B. Mozer

and

B. LeNeindre
(Laboratoire des Interactions Moleculaires et des Hautes Pressions,
CNRS, Universitaire de Paris Nord, France)

and

B. Farnoux
(Laboratoire Leon Brillouin Centre d'Etudes Atomiques - Saclay, France)

Preliminary small angle neutron scattering experiments were performed at Saclay on a sample of liquid He-4 at the liquid-gas phase transition, the λ-transition, and temperatures between these transitions. The sample cell in adiabatic configuration was designed and made at NBS. The sample cell was attached to an insert for an I.L.L. type cryostat in use at Saclay. Temperature regulation was in the range of 1 - 3 μK using an NBS calibrated germanium resistor and carbon resistors for secondary thermometers. The thermodynamic states of the He-4 was determined by measuring the capacitance of the helium and converting this to the density via the Clausius-Mosotti equation, knowing the temperature, and using published thermodynamic data of other workers.

The neutron diffraction data at small angles was obtained on the PAXY spectrometer at Saclay using 3, 5, 8 and 15 Angstrom neutrons in order to cover a range of wave vector differences from $q = 0.0008$ Å to 0.25 Å^{-1}.

The most striking results away from the phase transitions and nearer to the λ transition is shown in Figure 1 where we observe the structure factor to decrease from its value at $q = 0$, which can be determined from thermodynamics, to almost zero at $q = 0.06$ Å^{-1} and then rise again.

This behavior of the structure factor explains our difficulty in attempting to measure the quasi-elastic scattering around the λ-transition using the spin-echo spectrometer at I.L.L. in collaboration with F. Mezei. The spin-echo experiments were performed at the smallest of q values for that machine and unfortunately they lie in the region of the hole in the structure factor.

There has been no other measurements of the structure factor in this region of q-space and all other measurements have suggested a smooth liner extrapolation of other data from the smallest q's measured, 0.16 Å^{-1} to the value at $q = 0$ given by thermodynamics. Our preliminary measurements indicate the occurence of possible oscillatory behavior of the structure factors at small q values. We are proposing additional measurement to see just how the small angle scattering joins the have been documented so that the database can readily be implemented on several international on-line systems.

To permit scientists to use the database, we are developing software tools that can be distributed with the database or used to search the database on-line at a central site. NBS software (NBS*LATTICE), which is an integral part of the CRYSTAL DATA Distribution Package, is designed to carry out a variety of functions. With the lattice-matching program function, an unknown compound can be identified by comparison of its lattice with those in the database. The required lattice parameters are determined using x-ray or neutron diffraction techniques. The lattice-matching method offers and excellent way to characterize solid-state materials and is now being used at NBS, in industrial analytical laboratories, and crystallographic data centers. Currently a concerted effort is being made to extend the method to analyze data obtained from electron diffraction experiments.

Using the on-line NRCC-NBS CRYSTAL DATA Search System, the database can be accessed by scientists worldwide. This system integrates scientific with database management software. The scientific software has been expanded to facilitate its application to materials analysis and design. All key data elements can be searched and answers to queries can be obtained using highly efficient Boolean type search strategies. Statistical analyses for all of the data items, and combinations of items, can readily be carried out. During the year, this system has been used by scientists to solve a variety of problems in chemistry and solid-state physics. On-line demonstrations of the System at scientific meetings have been well attended.

Future efforts of the Crystal Data Center will focus on several areas of activity. First, in 1987 the next version of the NBS CRYSTAL DATA Distribution Package will be released. Both the database and the software components of this package will be upgraded. The database will be expanded and will include ~115,000 entries with 1.7 million data records. Each entry will include all data types that are input or created by the NBS*AIDS83 program. All of the data will be used to upgrade the on-line NRCC-NBS CRYSTAL DATA Search System. Second, minerals data will be processed and evaluated in order to produce a comprehensive minerals subfile with at least one entry for each known mineral. Third, research will be carried out, scientific software will be developed, and scientific papers on CRYSTAL DATA products will be written.

previously measured part of the structure factor for $q \geq 0.16$ -- as well as to try to pin down the behavior of the smallest q values.

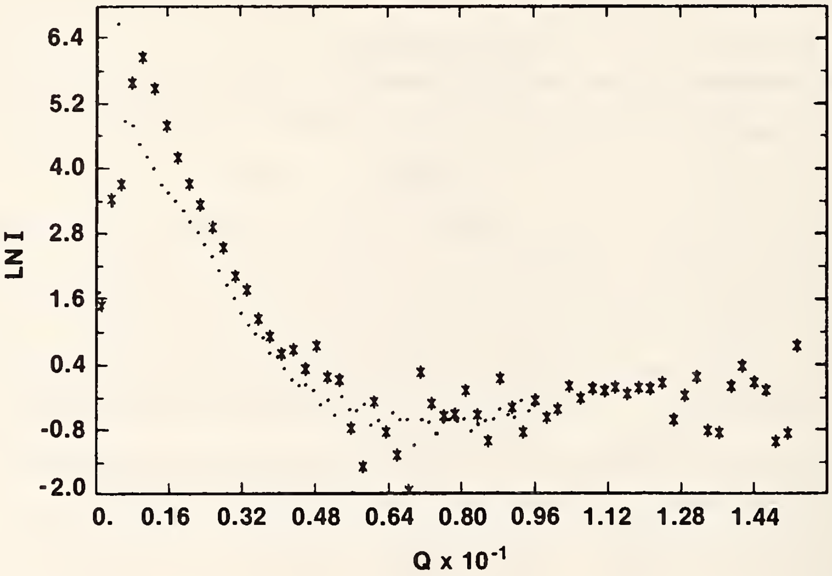

Figure 1. The long of the intensity of the small angle sctterimg from liquid He-4 at 3K for 5 Å - * and 8 Å - • incoming neutron beams versus the wave vector difference $q = 4\pi \sin\theta/\lambda$. The decrease in the scattering to almost zero in the region 0.06 $Å^{-1}$ has been shown by us in a number of measurements at different temperatures not near the liquid-gas phase transition.

CRYSTAL DATA CENTER

A. D. Mighell, J. K. Stalick, and V. H. Himes

The Crystal Data Center is concerned with the collection, evaluation, and dissemination of data on solid-state materials. The Center maintains a database which includes chemical and crystallographic information on all types of substances with known unit cells. The materials fall into the following categories: inorganics, organics, organometallics, metals, intermetallics, and minerals. For each substance, there are a variety of input and derived data parameters including: the conventional and reduced cell parameters, the space group, the compound name and formula, calculated and observed densities, literature reference, and critical comments.

During the year, the database has been significantly upgraded and expanded with respect to the number of entries and the number of records per entry. The database now contains more than 100,000 entries with an average of fourteen 80 character records per entry. Detailed specifications and definitions for all of the data items

NEUTRON ACTIVATION AUTORADIOGRAPHY STUDY OF PAINTINGS

Y. T. Cheng and J. S. Olin
(Smithsonian Institution, Washington, DC)

and

M. Ganoczy

The Smithsonian Institution initiated a project to study by neutron induced autoradiography and gamma spectroscopy the works of painter Thomas Wilmer Dewing (1851 - 1938) in the National Museum of American Art as well as selected key paintings from other locations. Of special importance to the Smithsonian Institution, due to his representation by 24 works at the National Museum of American Art and 42 works at the Freer Gallery of Art, Dewing was a significant turn of the century painter, and a noted member of "The Ten" American Impressionists.

Neutron induced autoradiography stands alone as the only available technique that allows the observation of multiple pigment applications beneath the surface of an oil painting. It offers the art historian, therefore, an unparalleled opportunity to observe the working method of an artist, quite literally, from the ground up. Previously dependent upon the x-ray radiograph and documentation external to the canvas, such as related sketches, surviving letters, and diaries, the art historian now is able to witness firsthand the artist's creative process as it moves from the preliminary drawing to the subsequent paint layers comprising the final image. The pigments used by the artist are also of special interest, and can, in part, be determined from the gamma ray energy spectra measurements conducted simultaneously with the autoradiography process.

This study will provide unique information on each individual painting examined, and establish a standard against which other works by the artist can be compared in the future. The range of works autoradiographed, as well as their distribution throughout Dewing's career, will provide the necessary scope or base for an accurate overview of his working methods. The results can lead to further studies of the artist's technique to include investigations of the pigments and painting media used. While extensive pigment studies have been done on European paintings, less investigation has been conducted on American works of art. The research will contribute to our knowledge of pigments used in this country. The results can be applied to future autoradiographic studies of works by Dewing's contemporaries and perhaps, ultimately, a body of information will be established illustrating the working methods and pigments used by American painters.

Thomas Wilmer Dewing was member of "The Ten American Painters", a group of artists who banded together in 1898 and subsequently have been associated with the impressionist movement in America. Dewing's colleagues in "The Ten" included William Merritt Chase, Willard Metcalf, John H. Twachtman, J. Alden Weir, Childe Hassam, Robert Reid, Frank Benson, Edmund Tarbell and others who are now considered major figures in late nineteenth century American Art. Today the works of these artists, Dewing included, are widely exhibited, bring large prices and are subjects of catalogues raisonne. Dewing's oeuvre, which include oils, pastels and silverpoints, is relatively small. Such comparative rarity has driven sales of his work to very high princes while his exquisite paintings and sensitive drawings are sought by collectors and museums alike. In addition to the significant holdings at the Smithsonian Institution, Dewing is also represented at the Metropolitan Museum of Art, New York City; The Museum of Fine Arts, Boston; The Philadelphia Museum; The Detroit Institute of Fine Arts; The Terra Museum and the Art Institute, both in Chicago; and smaller institutions across the country.

Interest in applying the neutron induced antoradiography method to the works of Thomas Wilmer Dewing (1851 - 1938) first arose when the artist's canvas Tobit and the Angel (1887, Metropolitan Museum of Art) was lent to Brookhaven National Laboratories for autoradiography in 1975. While x-rays revealed little more than the structure of the ground, autoradiographs recorded the dramatic changes that occurred while the painting was being executed. The Metropolitan Museum's subsequent autoradiography of works by Rembrandt, Van Dyck and Vermeer demonstrated that a full understanding of an artist's methods could only be achieved by studying a series of works systematically.

Collaboration between the art historian and the scientist in interpreting the data generated was proved to be a crucial aspect of the Metropolitan Museum of Art's project. Likewise, this study will require similar effort.

Thus far eight works by Thomas Dewing have been autoradiographed using the NBSR facility, four during the past year, as part of an on-going research project, most of which show that the artist employed significant changes in his compositions. Moreover, several reveal extensive overpainting. As the latter have darkened under the brown and black pigments, it is only through autoradiography that the original design can be seen. The study and visual presentation of Dewing's distinctive and complex type of paint application can be facilitated by means of autoradiography.

Autoradiographs of Tobit and the Angel (1887, Metropolitan Museum of Art), Lady with a Rose (catalogued 1924, National Museum of American Art), The Duet (1922, Kennedy Galleries and Edward Shein), A Nude (catalogued 1922, Akron Art Museum), Portrait of Mrs. Houston (1880, National Museum of American Art), have revealed these various aspects of Dewing's work. They indicate that Dewing altered his compositions in most of the paintings studied thus far. Details of the alterations are not apparent in the x-ray radiographs. Often the information is obscured by the canvas weave and the supporting structure. Figure 1 is a picture of the painting, A Nude as we see it today and figure 2 shows the corresponding x-ray radiograph. For comparison, figure 3 is the fifth autoradiograph of A Nude representing distribution of pigments containing manganese; figure 4 is the sixth autoradiograph showing the area of sodium containing pigments and figure 5, the ninth autoradiograph, shows the distribution of cobalt containing pigments. These figures demonstrate that neutron induced autoradiography is more than a complementary technique to conventional x-ray radiography for painting examination and study.

Thomas Dewing's working methods are complex. Each of the five paintings that have been autoradiographed appear to have been constructed in a different manner. For example, A Nude, as in figure 5, was begun with line drawing; Lady with a Rose, (figures 6 and 7) was begun by blocking the background around the figure and the Portrait of Mrs. Houston (figures 9 and 10), was painted premier coup with no preparatory drawing at all. The original pose of Lady with a Rose, revealed by the autoradiography process, shows a placid figure with folded hands, a youthful face with upturned nose, high cheekbones and a demure cap of hair (figure 7). Subsequently overpainting the work, Dewing made the sitter more animated by raising her arm. He further added an element of sophistication by giving her an aquiline profile. The autoradiographs also delve below the deceptively smooth surface of the painting to reveal its structure. He laid in the initial background hue with rough palette knife marks that were blocked in around the figure (figure 3). Subsequent strokes of another pigment were placed in another direction in order to soften and smooth the underpainting. The final effect of the first version was a precisely rendered figure surrounded by a shimmering, mottled atmosphere. The remarkable similarity of the underpainting to The Garland (figure 8), a well documented painting by Dewing at the Freer Gallery of Art, assisted the art historian in suggesting a date of 1916 for the original painting underneath Lady with a Rose.

Figure 1. A NUDE, oil on panel, 10.5" x 13.5".

Figure 2. X-ray radiograph of A NUDE.

Figure 3. Fifth autoradiograph of A NUDE, taken 3 hours after painting activation.

Figure 4. Sixth autoradiograph of A NUDE, taken 1 day after painting activation.

Figure 5. Ninth autoradiograph of A NUDE, taken 20 days after painting activation.

Figure 6. LADY WITH A ROSE, oil on canvas, 24" x 20".

Figure 7. Seventh autoradiograph of LADY WITH A ROSE, taken 10 days after painting activation.

Figure 8. THE GARLAND, oil on canvas, 25" x 19".

Figure 9. PORTRAIT OF MRS. HOUSTON, oil on canvas, 19.5" x 14.5".

Figure 10. Fifth autoradiograph of PORTRAIT OF MRS. HOUSTON, taken 3 hours after painting activation.

ADVANCED NEUTRON METHODS

1. Small Angle Neutron Scattering (SANS)

The SANS instrument operated virtually without interruption during the past year. A record number of scientists (60) from government, university and industrial laboratories and eight NBS Divisions used the facility for experiments in polymers (41%), metallurgy (17%), chemistry and physics (12%), magnetism (11%), ceramics (9%) and biology (7%), where the percentages give the distribution of beam time in each area. Included in these totals are the first proprietary measurements carried out on the facility, by Eastman Kodak Company and IBM Almaden Research Laboratories, in which the full costs of operating the facility are borne by the users' laboratory in accord with recently established NBS guidelines. In the following paragraphs, some of the past year's SANS highlights are briefly noted. In many cases more complete summaries of the work alluded to can be found in articles elsewhere in this report.

The first application of SANS to characterize the adsorbate structure in chemically modified microporous particles used in chemical separation and processing has been carried out by the Reactor Radiation (C. Glinka), Ceramics (W. Haller) and Organic Analytical Research (L. Sander) Divisions. Using contrast variation techniques, dramatic scattering signals from the adsorbate phases have been observed which are directly related to their conformation on the pore surfaces of the particles. In a closely related effort, researchers from Exxon (S. Sinha and J. Huang), the University of Delaware (S. Satija), and the University of Maryland (H. Stanley) have conducted measurements on binary fluids entrained in porous media to investigate the onset of preferential wetting and the effects of the pore structure on the miscibility of the fluids.

The tendency of low concentrations (~0.5%) of hydrogen in α-Pd to cluster under the influence of large internal stresses was convincingly demonstrated in a collaborative effort (J. Rush and C. Glinka) with the Max Planck Institute (R. Kircheim). Characteristic cluster sizes of about 100 Å were observed in mechanically deformed Pd foils while no evidence for clustering was seen in strain-relieved foils; a result with significant implications for studies of hydrogen embrittlement.

Scientists from General Electric's Advanced Materials Laboratory (C. Austin and R. Darolia) used SANS to monitor the effects of extended exposure to high temperatures on the microstructure of single-crystal, superalloys being developed as turbine blade materials for advanced aircraft. These measurements were successful in correlating a drop in stress-rupture strength of certain alloys, containing a few percent rhenium, with the formation of an unwanted phase of small, incoherent precipitates. The relationship between precipitate size and distribution and the mechanical strength of real engineering alloys was also the subject of SANS measurements by C. S. Choi and H. Prask, of the Army's Materials Commmand, who examined uranium-titanium alloys, and of R. Fields (Fracture and Deformation Division) who analyzed copper-rich precipitates in high strength, low alloy steels. In a fundamental study of the kinetics of precipitate formation, M. Chisholm (Carnegie-Mellon University) followed the earliest stages in the growth of cobalt precipitates in CuCo binary alloys for comparison with computer molecular dynamics simulations of the precipitation process.

Through the use of deuterium labeling to highlight the network structure in epoxies, W. Wu and B. Bauer of the Polymer Division have recently obtained significant results regarding the molecular modes of deformation in strained epoxies. They have observed in epoxies with short crosslink spacings typical of commercial materials that there is essentially no change in the average crosslink distance in samples strained up to 30%. This remarkable result suggests that the macroscopic deformation is controlled by some type of defect motion, analogous to the way dislocations determine strain in metals.

The interest in developing low-temperature processing routes to achieve high density ceramics has prompted K. Rhyne and T. Coyle of the Ceramics Division to use SANS to study the first stages of the polymerization of silica in solution. By chemically controlling the rate of aggregation, they have been able to observe and characterize the cluster growth in real time.

The magnetic correlations which characterize the spin glass state continue to be central to recent SANS measurements in magnetism. P. Mangin (Institut Laue-Langevin) and J. Rhyne have recently measured the concentration, temperature and magnetic field dependence of the magnetic scattering in the reentrant spin-glass, amorphous FeCr. They find that below the spin-glass transition temperature the scattering can be separated into two components, the Lorentzian-shaped component and a Lorentzian-squared component. Furthermore, the Lorentzian-squared component, but not the Lorentzian component, depends on whether or not the sample has been cooled in an applied field, an observation that gives new insight into the physical origin of the correlations in the spin glass state.

The chain conformation in new varieties of polymer blends and microphase separated block copolymers has been systematically measured by C. Han (Polymers Division) and several collaborators. Han and coworkers have also studied the fluctuations in semidilute solutions of polystyrene that are precursors to gel formation in an effort to better understand how the gelation may be controlled.

SANS STUDY OF CHEMICAL ADSORBATES BOUND TO PORE SURFACES

C. J. Glinka and N. F. Berk

and

L. C. Sander
(Center for Analytical Chemistry)

and

W. Haller
(Ceramics Division)

Previous work[1] on the characterization of microporous silica particles by small angle neutron scattering (SANS) has been extended to the study of linear hydrocarbon chains chemically grafted to the internal pore surfaces of such particles. The aim of this work has been to relate the structure of the bonded adsorbate layers to the performance of chemically modified microporous particles used in chemical separation (e.g. in high performance, reverse-phase liquid chromatography) and processing.

The measurements were made on microparticles of silica controlled pore glass with pore diameters ranging from 7 to 30 nm. This material is prepared by controlled phase separation of the SiO_2-B_2O_3-Na_2O system and subsequent leaching of the boron-rich phase which results in an interconnected pore space and a narrow pore size distribution. Alkyl chain monomers of various length (ranging from 4 to 18 carbon atoms per monomer) were bonded to the pore surfaces and the pores then filled with a solution whose scattering density was chosen to match that of the skeletal material (silica). In this way the pore scattering is minimized while the signal from the thin (4 - 20 Å) bonded layers is accentuated.

A typical set of measurements is shown in figure 1 for a glass with 120 Å diameter pores. The crosses denote the scattering from the pores in the dry, unbonded glass. The position, Q_p, of the prominent peak in this pattern is closely related to the pore size, d, through $d = 2\pi\phi/Q_p$ where ϕ is the porosity. The three lower intensity curves in the figure are for bonded phase particles immersed in the pore masking solution. In these curves there is also a peak at Q_p, but also a weaker secondary feature at $Q_p' \sim 2Q_p$. This higher order peak shifts and becomes more prominent as the monomer chain length increases and thus is directly related to the effective thickness of the adsorbate layer.

The scattering from the unbonded particles can be accurately fitted using a model for phase separated glasses first proposed by Cahn.[2] Analytic and numerical calculations are now in progress to apply this model to the scattering from the adsorbate layers in order to extract quantitative information regarding the uniformity and thickness of the layers.

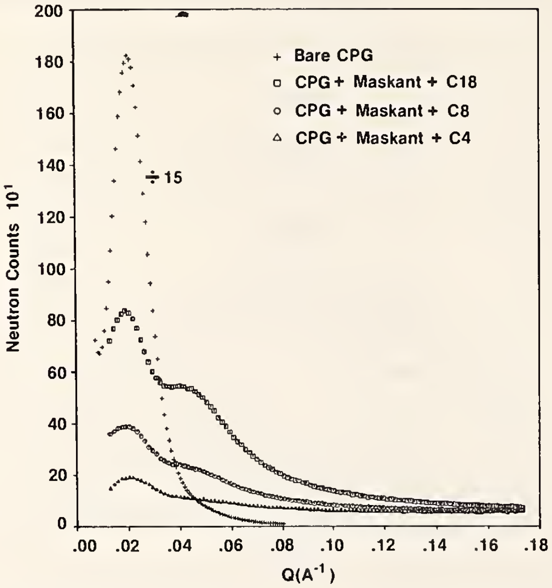

Figure 1. Small angle scattering from controlled pore glass (CPG) particles having 120 Å diameter pores.
(+) - pore scattering from unbonded particles
(Δ, o, □) - scattering from alkyl chains (C_4, C_8 and C_{18} monomers, respectively) bonded to the pore surfaces of the particles.

---

1. C. J. Glinka, L. C. Sander, S. A. Wise, M. L. Hunnicutt and C. H. Lochmuller, Analytical Chem., 57, 2079 (1985).

2. J. W. Cahn, J. Chem. Phys., 42, 93 (1965).

SMALL ANGLE NEUTRON SCATTERING STUDY OF PRECIPITATION IN HIGH STRENGTH LOW ALLOY STEELS

R. C. Reno
(University of Maryland - Baltimore County, Baltimore, MD)

and

(National Bureau of Standards, Gaithersburg, MD)

and

R. J. Fields
(National Bureau of Standards, Gaithersburg, MD)

In our continuing investigation of A710 steel, we have utilized small angle neutron scattering (SANS), transmission electron microscopy (TEM), and Mössbauer effect (ME) to study precipitation processes. SANS measurements on unaged steel, water quenched from 900°C, show Porod behavior ($I \alpha q^{-4}$) over the range $q > 0.005$ $Å^{-1}$.

Average particle size deduced from the SANS data is ~40 nm. Mössbauer measurements on this material show the presence of ~1% retained austenite. We are presently trying to determine if this austenite phase is responsible for the observed SANS results.

After aging the steel for one hour at 480°C, no austenite phase can be found by Mossbauer effect and the SANS results show a Porod region followed by a region where the intensity obeys a q^{-2} behavior (for $q > 0.05$ A^{-1}). Since the predominant impurity in this steel is copper, we have in the past attributed our SANS results to scattering from copper-rich precipitates. However, we are now investigating the possibility that significant scattering may result from manganese - or chromium - rich regions of this steel.

SANS STUDY OF STRENGTHENING MECHANISMS IN SINGLE-CRYSTAL SUPERALLOYS

C. Austin and R. Darolia
(General Electric Company, Cincinnati, OH)

and

C. J. Glinka

Single-crystal, nickel-based "superalloys" are complex, precipitation-strengthened alloys now widely used for turbine blades in high performance aircraft. The unusual high temperature strength and creep resistance of these alloys derives from a homogeneous dispersion of coherent γ' (Ni_3Al) precipitates and the absence of grain boundaries, respectively. The addition of various elements to the alloys' composition can further enhance their high temperature strength although the mechanisms for this enhancement are in many cases not well understood.

In this study, small angle neutron scattering (SANS) has been used to monitor changes, due to high temperature exposure, in the microstructure of superalloys containing a few weight percent rhenium. This work was prompted by mechanical tests which showed that the addition of rhenium produces an initial increase in strength which, however, is not maintained over long exposure times.

Figure 1 shows a typical SANS intensity contour plot for a superalloy specimen in its initial, "as prepared" state. The sample was oriented with a [100] cubic direction parallel to the incident beam. The γ' precipitates in the material, which are roughly one micron in size and account for over 70% of the volume, are cuboidal in shape with edges along [100] directions. The strong scattering seen in figure 1 along [100] directions is due to the narrow (~20 nm), planar γ-phase regions between

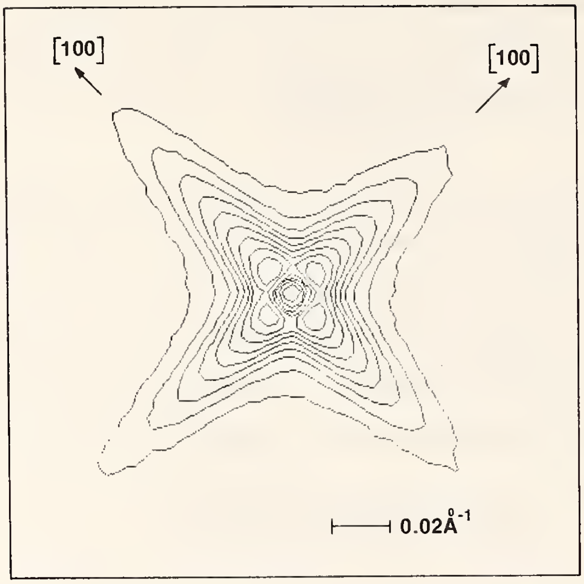

Figure 1. Isointensity contours observed on the two-dimensional SANS detector for a superalloy specimen oriented with its [100] direction parallel to the incident beam.

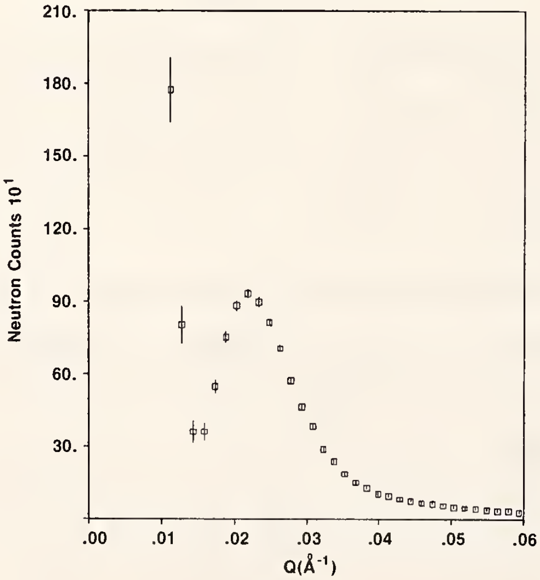

Figure 2. The net, circularly averaged, small angle scattering for a superalloy sample containing 3% rhenium after subtracting the scattering from a sample containing no rhenium. The peak in the scattering is due to a fine dispersion of small precipitates which develop in the rhenium containing alloy after 500 hours aging at 1050 C.

the precipitates and provides an indirect means of monitoring changes in the γ' morphology. Regions of the scattering pattern away from [100] directions are, on the other hand, relatively free from γ' scattering and thus are sensitive to microstructural changes unrelated to the γ' morphology.

SANS measurements were made on samples with and without rhenium which had been aged at 1050 C for up to 500 hours. After 500 hours the rhenium containing samples gave additional, isotropic scattering which is seen most clearly (see figure 2) by subtracting the scattering from an identically treated sample containing no rhenium. The residual scattering, shown in figure 2, is indicative of a fine dispersion of small precipitates with a mean spacing of 15 - 20 nm. The lack of any directional dependence in this scattering indicates that these precipitates are not coherent which may explain the decrease in mechanical strength of the rhenium containing samples at long aging times.

MOLECULAR RESPONSE TO LARGE STRAIN DEFORMATION IN EPOXIES - A SANS STUDY

Wen-li Wu & Barry J. Bauer
(Polymers Division)

The molecular mechanisms of deformation in crosslinked polymers has been a subject of extensive research. However, most of the effort has been concentrated on those materials with rather low crosslink density such as rubbers. Neutron scattering has been the main research technique for determining the molecular response to the deformation process. The junctions within the crosslinked materials were found to deform following a scheme closely predicted by a phantom network model. For materials of high crosslinking density such as epoxies, no experimental results about the changes in the molecular dimension using any direct measuring methods have been reported.

Based on our previous experience in the determination of the network structure of epoxies using neutron scattering techniques, it is apparent that the epoxies composed of partially deuterated DGEBA and Jeffamines are the ideal candidates for the deformation study. The average distance between crosslinks can easily be calculated from the positions of the scattering peaks. All of specimens were deformed in the pure shear mode. A pair of specially designed aluminum plates were used to keep the specimens in their deformed state during the scattering measurements.

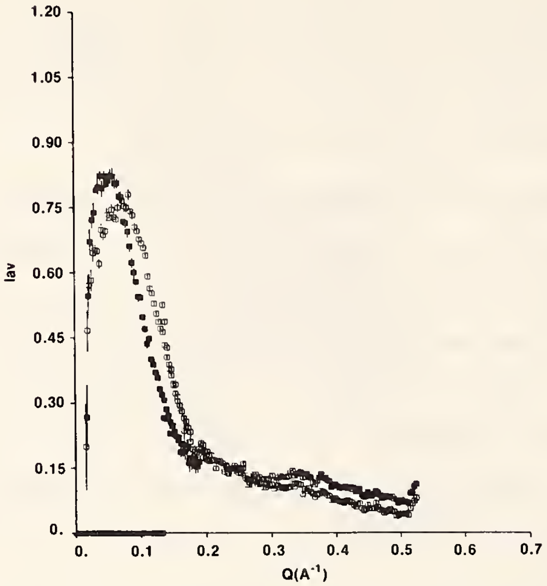

Figure 1. Neutron scattering curves of deformed epoxy containing a mixture of D-2000 to D-4000 amines. Stretch ratio was 25%.
- – along the stretch direction
- – along the undeformed direction

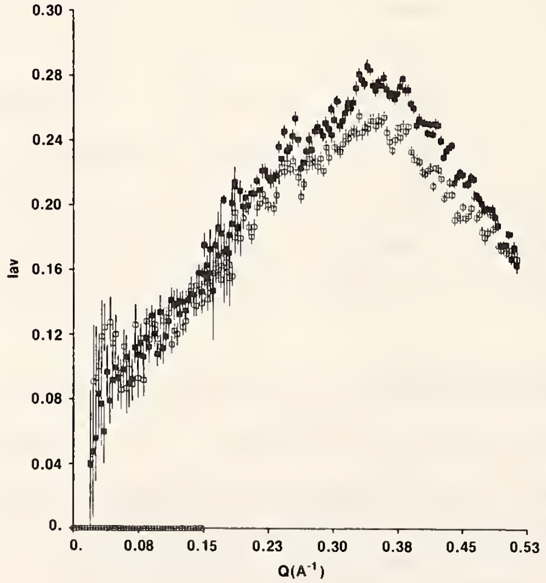

Figure 2. Neutron scattering curves of deformed epoxy containing D-400 amine. Stretch ratio was 24%.
- □ – along the stretch direction
- ■ – along the undeformed direction

For those epoxies containing a mixture of D-2000 and D-400 amines, the average distance between the crosslinks along the amine chains was found to be 60A and the distance along the epoxy links was 17A. The corresponding scattering maxima (Figure 1, open square) were located at 0.1 and 0.37 A^{-1}. The maximum amount of deformation before the samples rupture is about 50%. Within this strain limit, the amine chains were found to elongate with the macroscopic strain as reflected by the shift of the main scattering peak to a lower q (Figure 1, solid square). No elongation occured along the epoxy chains as evidenced by the fact that the position of the second peak remained unchanged upon deformation.

As the molecular weight of the amine decreased to 400 or D-400 amine was used by itself, the average distance between the cross links along the amine was about 17A while the distance along the epoxy chain stayed unchanged. The maximum strain before sample failure was 30%. No change in the distance between crosslinks along either the amines or the epoxy chains was noticed within this strain limit. The scattering curves of a D-400 epoxy along the stretch direction (solid square) and the undeformed direction (open square) are given in figure 2. The stretch ratio of this specimen was 24%.

The above observation is rather striking and may also have some important practical implications since most thermosetting resins used as composite matrices have molecular weights below 400. In light of the above observation, the question to be addressed is what is deformed in a specimen with a macroscopic strain up to 30%, given that the majority of the molecules do not deform. There are at least two possible explanations for the above observation. The first is a defect-control model; the deformation is concentrated in localized defect regions while the major portion of the molecules lie outside these defects. The analog of this defect model in metals or other crystalline materials is the dislocation. The generation and movement of dislocations accommodates the macroscopic strain while the lattice dimensions of the crystals remain unchanged. But the unanswered question for epoxies is what is the defect. The second possible explanation is the unfolding of the molecular networks; however, a prerequisite for such a mechanism is that the average network within a bulk sample is topologically two dimensional. Experiments are now underway to elucidate the deformation mechanisms in greater detail. Amines and epoxies with different functionality and composition are now included in this work to establish the generality of this finding.

STATIC AND KINETIC STUDIES OF POLYSTYRENE/ POLY(VINYLMETHYLETHER) BLENDS

C. C. Han, F. L. McCrackin and B. J. Bauer

and

M. Okada
(Tokyo Institute of Technology, Tokyo, Japan)

and

Y. Muroga
(Nagoya University, Nagoya, Japan)

and

Q. Tran-Cong
(Kyoto Institute of Technology, Kyoto, Japan)

The study of static and kinetic phase behavior provides not only a fundamental understanding of polymeric systems but also practical materials applications. This has long been recognized in the field of inorganic glasses and metallic alloys. In the polymer field, effort has been concentrated on the equilibrium studies of phase behavior. Although some kinetic studies have been carried out, so far relationships and subtleties between thermodynamics and kinetics have not been explored consistently. We have made a systematic study of the equilibrium phase behavior of deuterated polystyrene/poly(vinylmethylether) blends by the small angle neutron scattering (SANS) technique, and the phase separation kinetics by the temperature jump light scattering (TJLS) technique. Static properties, such as the spinodal temperatures and binary interaction parameters, χ, have been obtained from the static study and then used in the prediction of and comparison with kinetic results. The consistency and also the discrepancy between theories and experiments have been compared quantitatively in detail.

COMPATIBILITY OF HYDROGENATED AND DEUTERATED POLYSTYRENE

C. C. Han and B. J. Bauer

and

H. Yang and R. Stein
(University of Massachusetts, Amherst, MA)

and

E. Kramer
(Cornell University, Ithaca, NY)

A 50/50 blend of deuterated polystyrene (PSD.M_w = 255 x 10^3) and polystyrene (PSH.M_w 233 x 10^3) was studied by small-angle neutron scattering (SANS) for its interaction parameter, χ/ν_0, correlation length, ξ, and susceptibility, $S(q = 0)$ at various temperatures. The interaction parameter χ/ν_0 has a value of less than 10^{-6}, which is within the error limit of being zero in the measurement temperature range. The error bound cannot exclude the possibility of an upper critical solution temperature (UCST). However, this UCST, if it exists, will be well below the glass transition temperature for any PSD/PSH blends with reasonable molecular weight. Phase separation of PSD/PSH blends does not occur under common experimental conditions and phase separation of isotopically labeled polymers is not a general phenomenon but a specific property of individual polymers.

THEORY OF SPATIAL CORRELATION AND DIFFRACTION FOR THE LEVELED WAVE MODEL OF RANDOM BICONTINUOUS STRUCTURES AND INTERFACES

N. F. Berk

We are involved in a theoretical program for small angle scattering from extended open structures that is relevant to contemporary interests in problems of interfacial morphology, such as the study of hydrocarbon wetting of porous glass and phase separation in microemulsions. There is a need in such areas to generate well-defined mathematical models of substrate and interspace morphologies of extended bicontinuous structures in order to have firm bases for interpreting scattering data.

Our model generalizes an idea originally discussed by Cahn. The material density field, $\rho(\vec{r})$, of a two-phase system is defined by the following algorithm. One starts by constructing a field, $S_N(\vec{r})$, obtained by adding together N sinusoidal waves having common wavelength, $\lambda = k/2\pi$, but randomly chosen directions, $\hat{k}_n$, phase constants, ϕ_n, and amplitudes A_n:

$$S_N(\vec{r}) = \sum_{n=1}^{N} A_n \cos(k\hat{k}_n \cdot \vec{r}_n + \phi_n).$$

The set of all points $\vec{r}$ that satisfy the equality $S_N(\vec{r}) = a$ is called the a-set of the function $S_N(\vec{r})$ and determines a surface in three dimensions that everywhere separates regions where $S_N(\vec{r}) < a$ from regions where $S_N(\vec{r}) > a$. For given valves of level parameters a and b we define $\rho(\vec{r}) = 1$ wherever $a \leqq S_N(\vec{r}) \leqq b$ and $\rho(\vec{r}) = 0$, otherwise. Thus $\rho(\vec{r})$ is uniform over the interspace bounded by the non-intersecting a-set and b-set surfaces. We call this the leveled wave model. The prototype of such behavior is obtained with $b = 0$ and $a = -\infty$, which corresponds to an extended,

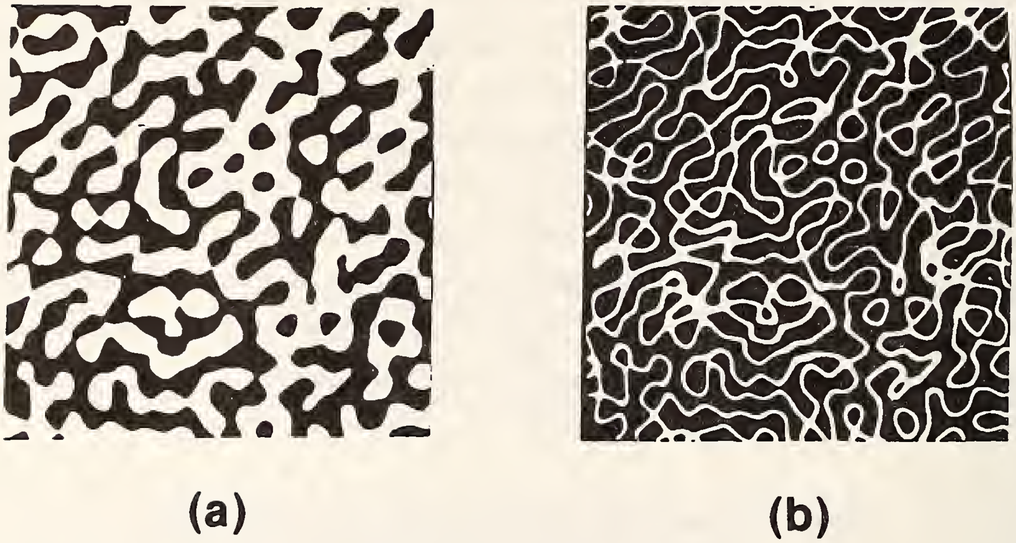

Figure 1. Computer simulations of leveled density fields ($\rho = 0$ is black) for $N = 50$. a) 0-set interface b) −1-set and +1-set interfaces. See text.

bicontinuous interface separating one phase with volume fraction $c = 1/2$ and $\rho(\vec{r}) = 1$ from the other with volume fraction $1 - c$ and $\rho(\vec{r}) = 0$. More generally, for finite a and b, the phase in which $\rho(\vec{r}) = 1$ has volume fraction c and the regions it separates, both with $\rho(\vec{r}) = 0$, have volume fractions c_1 and c_2, with $c_1 + c_2 = 1 - c$. Figure 1 gives examples of computer simulations in planar sections for $N = 50$. The regions in which $\rho(\vec{r}) = 1$ are shown in white, $\rho(\vec{r}) = 0$, in black. Figure 1a shows the prototype case while in Figure 1b, $-a = b << 1$ for the same $S_N(\vec{r})$. The morphology of Figure 1a suggests a highly porous, spongy structure while the white interspace of Figure 1b ($c<<1$, $c_1 = c_2 \approx 1/2$) may model the wetting of pore surfaces or a microemulsion surfactant interlayer. Simulations show that such morphologies stabilize rapidly with increasing N, so that the limiting averaged behavior as $N \to \infty$ is meaningfully identified with structures generated by large but finite N.

We have developed an exact method of study for the self-correlation function of the leveled wave model, $\langle \Delta\rho(\vec{r})\Delta\rho(0)\rangle = c(\Delta - c)\gamma(r)$ in the $N = \infty$ limit and have obtained analytic results in special cases. For example, for the prototype 0-set morphology, $\gamma(r) = \frac{2}{\pi} \arcsin(j_o(kr))$, where $j_o(x) = \sin x/x$. This exhibits both linear behavior a small r, a consequence of the sharp interface, and sinusoidal oscillations of wavelength λ at large r, reflecting the sinusoid population from which the field is constructed. In general we find the model has a Porod correlation length given by $\xi = \left|\frac{d\gamma}{dr}\right|_{r = 0}^{-1} = c(\Delta - c)\sqrt{3}\lambda/[e^{-\beta^2} + e^{-\alpha^2}]$, where α and β replace a and b in the infinite N limits and are scaled to the rms amplitude at the wave sum.

The exact scattering intensity, I(q), of the model consists of two singular parts and a non-singular, featureless, remnant we will not exhibit here. The singular contributions are represented by

$$I_s(q) = \frac{\pi V S^2}{k^2}\left[c_1 \delta(q - k) + \frac{c_2}{2q}\,\Theta(2k - q)\right] \qquad (1)$$

where $c_1 = (e^{-\beta^2} - e^{-\alpha^2})^2$ and $c_2 = (\beta e^{-\beta^2} - \alpha e^{-\alpha^2})^2$. Also in (1), δ = material contrast, V = sample volume, and $\Theta(\cdot)$ is the Heaviside function. The first term is a sharp line at q = k, which is caused by long ranged order, and is anticipated from various numerical and analogue simulations of the prototype model. The second term is a hyperbolic singularity at q = 0, also caused by long ranged order, which has no precedence in previous studies. Moreover these two singularities tend to exclude one another. In the case corresponding to Figure 1a, we have $c_1 = 1$ and $c_2 = 0$, so that only the sharp line persists; while in the complementary situation of Figure 1b, we have $c_1 = 0$ and $c_2 \neq 0$, so that only the hyperbolic divergence is manifest. We have also generalized the model to incorporate a polydispersive wavelength population into the unleveled wave sum. Figure 2 shows two families of analytic results corresponding to the singular contribution to the scattering $I_s(q)$, as regulated by a wavevector spread $\Delta k = 0.05k$. In Figure 2a c = 0.04 is constant but c_1, c_2 vary.

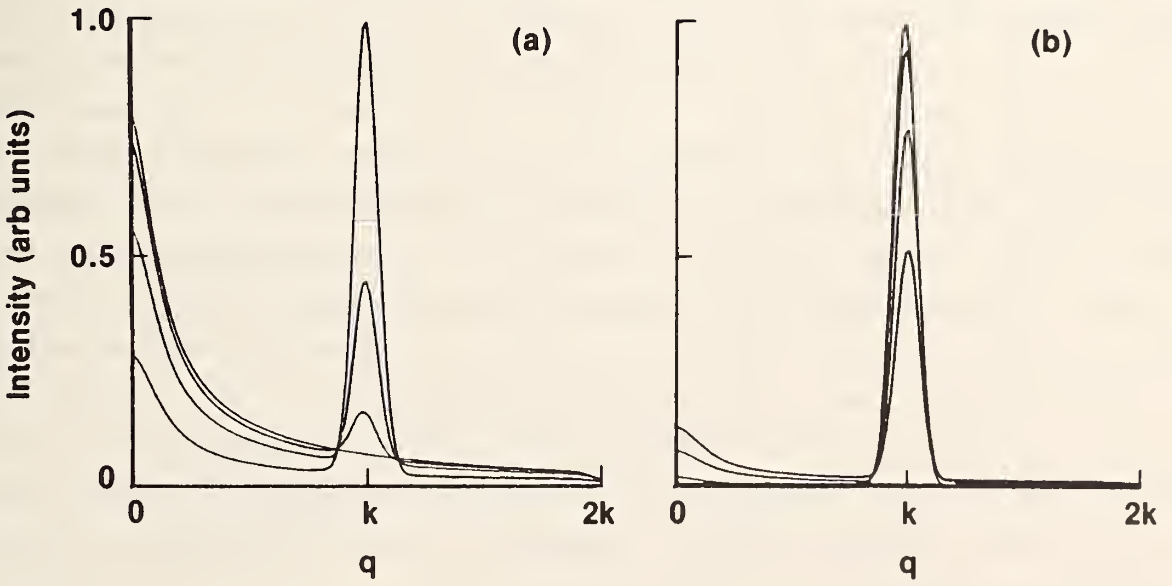

Figure 2. Singular contributions to scattering, $I_s(q)$, as regulated by dipersion in wavevector pool, with $\Delta k = k/20$. a) c = 0.04, c_1 = 0.45, 0.37, 0.29, 0.21. b) $c_2 = 0$, $c_1 = 1 - c_s$ and c_s = 0.5, 0.6, 0.7, 0.8.

The case $c_1 = c_2$ gives the curve without a peak at $q = k$ but with the largest amplitude at $q = 0$. As c_1, c_2 move away from the isometric configuration, the scattering at $q = 0$ diminishes while the peak at $q = k$ emerges and grows. Figure 2b corresponds to a single interface as in Figure 1a but with variable composition, $c_1 = 1 - c$, $c_2 = 0$. Here the line at $q = k$ diminishes and the intensity at $q = 0$ grows as c departs from 1/2.

In summary, the scattering from leveled wave structures reveals two distinctive but related singularities that reflect in different ways the underlying order in the model. The sensitivity of these features to compositional details may serve as important signatures for interpreting small angle scattering data from real systems that may be approximated by these mathematical methods.

RENEWAL THEORY APPROACH TO SPATIAL CORRELATIONS IN RANDOM TWO-PHASE MEDIA

N. F. Berk

The spatial self-correlation function P(r) of an isotropic two-phase medium can be expressed equivalently as the probability of finding both ends of a random $\vec{r}$-join lying within the same phase or as the relative volume of the intersection of a phase with its $\vec{r}$-translate. In the latter view, the system can be subdivided into thin straw-like tubes parallel to $\vec{r}$, and for a sufficiently random system the self-correlation of the bulk should be characteristic of that along an arbitrary (infinitely long) straw, as in a one-dimensional problem. This is true effectively by definition for models in which the only information is the spatial frequency distribution of intersections (nodes) of the interface with an arbitrary, infinite straight line. Then the calculation of the self-correlation can be posed as the question: for the given probability density f(x) of finding adjacent nodes separated by x, what is the probability that a randomly chosen r-join is cut by an even number of nodes, including none? The answer is equivalent to the required probability, P(r), that both ends of an r-join lie in the same phase (i.e., only in even numbered or in odd numbered intervals along the line). This can be couched as a problem in renewal statistics - the "renewals" being ordered occurrences of nodes - which we have solved using standard methods. (Analogous renewal problems have been discussed in different contexts.)

We have found P(r) to be given by

$$P(r) = \int_r^\infty P_e(x,r)dx,$$

where $P_e(x,r) = \lim_{x_o \to -\infty} P_e(x,r,x_o)$ and $P_e(x,r,x_o)$ satisfies the integral equation

$$P_e(x,r,x_o) = p(x - x_o,|x_o|) + \int_o^r p(x' - x_o,|x_o|)P_e(x - x',|r - x'|)dx'.$$

Here $p(x,r) = g(x,r)\Theta(x-r)$ is the conditional probability density that, given a node at $x = 0$, the first node to exceed r falls at x. $\Theta(\cdot)$ is the Heaviside unit step function and g(x,r) satisfies Samuelson's integral equation

$$g(x,r) = f(x) + \int_o^{\min(x,r)} f(x - y)g(y,r)dy,$$

where f(x) is the nodal frequency distribution for the interface. The relation of $P_e(x,r)$ to p(x,r) is essentially an extension of Samuelson's equation relating p(x,r) to f(x). This is our central result.

Two examples are useful.

1. $f(x) = \alpha e^{-\alpha x}$,

where α^{-1} is the mean nodal spacing. After some work, we find $P(r) = 1/2 + 1/2\ \gamma(r)$, where $\gamma(r) = e^{-2\alpha r}$, which is the Debye-Brumberger-Anderson formula. Thus, Debye's model of a random interface is equivalent to the Poisson nodal distribution, an observation that is well-known from several points of view.

2. $f(x) = 2\alpha x e^{-\alpha x}$,

where α^{-1} is again the mean nodal spacing. This first-order Poisson distribution has its mode at $x = \alpha^{-1}$, which can be interpreted as introducing some degree of short ranged order. Here one eventually obtains the deceptively simple result, $\gamma(r) = e^{-\alpha r} \cos\alpha r$. The scattering intensities for these models are proportional to

$$I(q) = \int_o^\infty r^2 \gamma(r) j_o(qr)dr,$$

and we have for the two cases

$$I(q) = 2\alpha/(q^2 + \alpha^2)^2, \qquad (1)$$

the well-known Debye scattering function, and

$$I(q) = 2\alpha q^4/(2\alpha^4 + q^4)^2, \qquad (2)$$

which fall sharply to zero at $q = 0$ and is peaked at $(12/5)^{1/4}\alpha$. Both scattering functions exhibit the Porod law, $I(q) \sim q^{-4}$ as $q \to \infty$, which is a consequence of the sharp interface of the two-phase model.

HIGH RESOLUTION, MULTIDETECTOR POWDER DIFFRACTOMETER

E. Prince and A. Santoro

A new, high-resolution neutron powder diffractometer is under construction that will enhance the capabilities for structure studies at the NBS reactor by extending the range in which high resolution data can be collected to shorter d-spacings and by increasing data rates for all patterns. A schematic layout of the instrument is shown in figure 1. The provision for several monochromator positions will enable a resolution curve to be chosen that is suitable for a particular sample, depending on the d-spacing range in which the important information is found. The thirty-two detectors will have Soller collimators with a horizontal divergence of 7' of arc and a vertical divergence of up to 9°, with provision for different vertical divergences for different detectors, according to the angle range they cover, so as to maximize sensitivity without sacrificing peak shape.

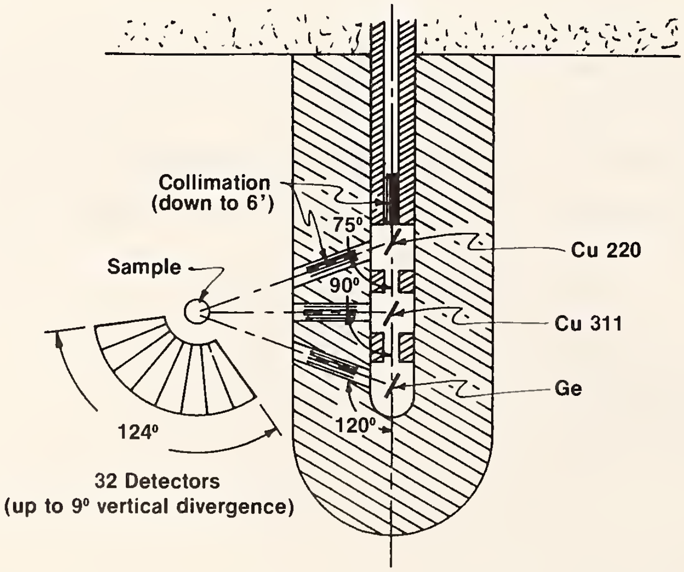

Figure 1. Schematic layout of the new NBS high resolution, powder diffractometer.

COLD NEUTRON RESEARCH FACILITY

J. M. Rowe, C. J. Glinka, T. Udovic, I. S. Anderson,
I. G. Schroder, J. LaRock, W. Knill, and R. Williams

No funds were appropriated for the construction of the new cold neutron research facility for Fiscal Year 1986, and therefore, no detailed design or construction could take place. Funds to begin construction were again included in the President's budget for FY1987, and the matter is now before the Congress. In the meantime, conceptual design efforts and construction and upgrading of the two instruments to be installed within the existing Reactor building continued. The cold source itself will be discussed in the following section.

1. Conceptual Design

A set of alternative possible arrangements of the neutron guide tubes to be installed in the cold source assembly has been explored, and the heating rates, guide illumination and total beam area have been varied to determine the optimum configuration. More detailed design of the actual guide tube insert is now underway, and the construction requirements are now being specified. Preliminary contact with the supplier of the neutron guides has been initiated in order to better estimate the cost of the assemblies. In addition, a set of options which will allow either a reduced or staged development of the facility are being prepared in order to determine costs, capacity and the possibility future expansion. A neutron filter to be used for intermediate wavelengths, based on the special properties of molecular hydrogen in the liquid state, has been designed, and will be tested in the coming year.

A concerted effort to refine the conceptual design of the new experimental hall is underway, with an emphasis on staged development and on more flexible use of available space. In particular, a different floor design which will provide better vibration isolation and a significantly reduced construction cost is being explored. Cost estimates are being refined, and a set of alternative proposals for project staging have been developed. As a result of this effort, detailed design of the new facility can begin immediately with the availability of construction funds.

2. Neutron Time-of Flight Spectrometer

Construction of the major components of this facility is now complete. Final testing of the monochromator assembly and the new data acquisition system, based on a 32-bit minicomputer using a Camac interface, is underway preparatory to installation of the monochromator during the scheduled August reactor shutdown for refuelling. This test period has been quite extensive in view of the fact that the assembly cannot be accessed during reactor operation, so that extreme reliability is required. This has allowed a thorough shakedown of the data acquisition software and refinement of the system design. As presently defined, it will be possible to control the instrument from any terminal on the NBS Reactor network, and to inspect the data and operating conditions at any time. In order to prevent inadavertent changes to the spectrometer operation, each experimenter will be allowed to choose a password that will be required before any operation parameter can be changed. The entire system is designed for maximum user friendliness, with single key strokes sufficient to access most information. The evacuated flight path, neutron detectors, and associated electronics have been assembled, and the final detector shielding has been fabricated and tested. On the basis of current tests, the irreducible background will meet or exceed the design requirement of less than one count per minute per detector. The full facility will be operational by October of this year, although some sample area refinements will not be completed until early 1987. Initial research applications planned include extensive work on catalysts, ionic conductors, and high technology alloys and magnetic materials.

3. Small Angle Neutron Scattering Instrument Upgrade

In order to make efficient use of the cold source flux, several aspects of the current SANS instrument are being improved. A spare 64 cm. detector has been ordered, with the new fill gas that has improved the γ-ray background. This detector will be delivered in 1987. In addition, a new data acquisition system based on the same hardware as that used for the neutron time of flight spectrometer is being assembled. This new system will include high speed histogramming memory that will allow rapid acquisition of data in separate memory areas that can be moved into the computer while a new area is being filled, thus allowing real time experiments. A new interface between the existing direct time to digital encoder and the histogramming memory has been fabricated, and is being tested. The new memory will also allow for larger data arrays, so that the data can be taken on a finer grid. The system is easily expandable for future needs. The data acquisition programs will be based on a concept similar to that described above for the time-of-flight spectrometer. The ability to control and interrogate the spectrometers from any terminal on the network will allow for routine operation from remote locations, using existing dial up lines on the network.

NBSR COLD NEUTRON SOURCE

R.S. Carter, P. A. Kopetka, M. Ganoczy, M. J. Kahn

The cold source cryostat (see figure 1) was received and underwent extensive testing. All components were helium leak tested and determined to be leak-tight. Procedures were developed for freezing ice in the ice chamber and several successful freezes were accomplished.

The cryostat was set up at the thermal column radiography port and neutron radiography used to determine the ice chamber volume and monitor the ice level as the freezing progessed. The ice was frozen in layers to prevent damage to the ice chamber. A neutron radiograph of the half full ice chamber is shown in Figure 2.

After the freezing tests were completed, the cryostat was moved to the refrigerator location and temporarily connected to allow low temperature cooling tests external to the reactor. Ice was again frozen in the cryostat and then cooled to low temperature. The tests were conducted successfully, but they indicated that some cryostat modifications were needed. These modifications are now underway.

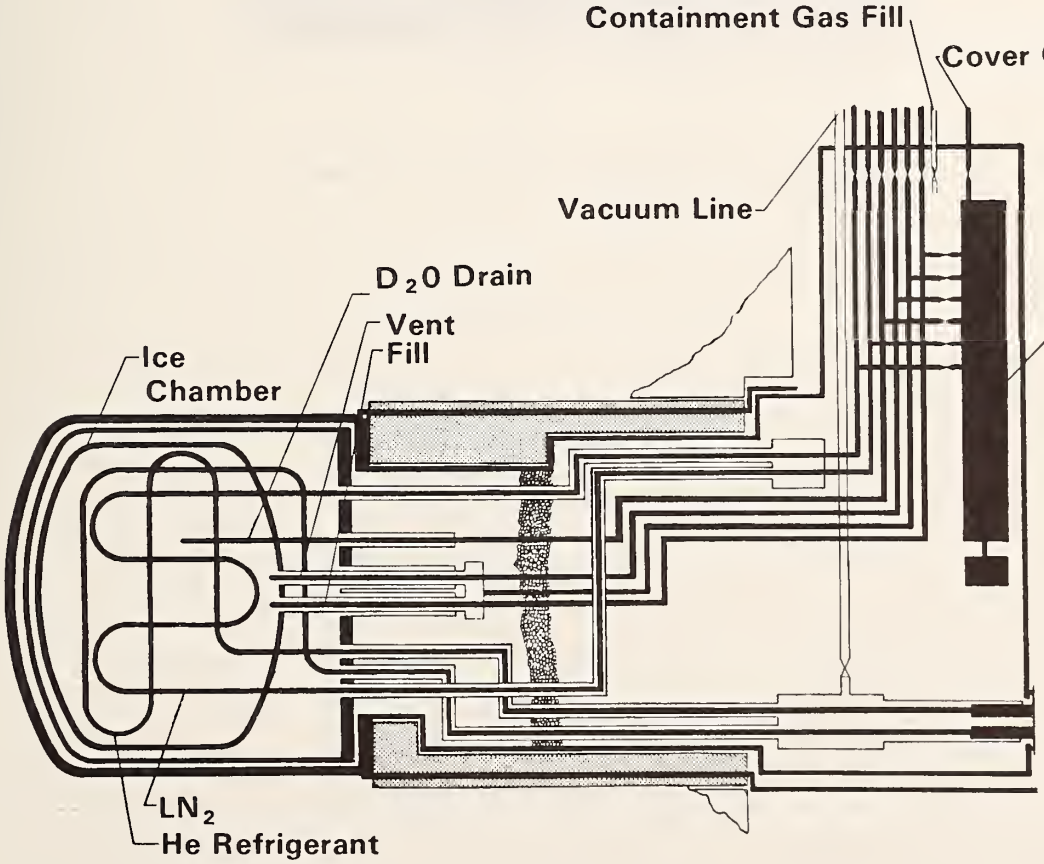

Figure 1. The Cold Source Cryostat.

Figure 2. The half filled ice chamber.

B. NON-RRD PROGRAMS

NUCLEAR METHODS GROUP: OVERVIEW

R. Fleming
(Center for Inorganic Chemistry)

The development and application of nuclear analytical techniques for greater accuracy, higher sensitivity and better selectivity are the goals of the Nuclear Methods Group. A high level of competence has been developed in reactor-based activation analysis, which includes instrumental and radio-chemical neutron activation analysis (INAA and RNAA), and in LINAC-based activation analysis using photons (PAA). In addition, the group has a unique capability in neutron beam analysis with both prompt gamma activation analysis (PGAA) and neutron depth profiling (NDP). The NDP technique utilizes prompt charged particle emission to determine elemental distributions within the first few micrometers of a surface while the PGAA technique utilizes prompt gamma-ray emission to measure the total amount of an element in a sample, regardless of its distribution. These techniques provide an arsenal of tools to address a wide variety of analytical problems in science and technology.

The activities of the past year have been highlighted by our involvement in the 7th International Conference on Modern Trends in Activation Analysis, new measurements carried out at other research facilities, and by a major renovation of our laboratory space in the Reactor Building. The MTAA-7 meeting, which was held in Cophenhagen in June, commemorated the fiftieth anniversary of the discovery of activation analysis by Hevesy and Levi. NBS scientists were authors of ten of the papers presented at this conference. The opportunity was also provided for visits to the laboratories of several of our European colleagues.

In addition to our ongoing use of the nearby reactors at the University of Maryland and the University of Virginia, primarily for fast and epithermal activation analysis, Group members carried out measurements on the neutron beam facilities at the new cold neutron source at Julich and the intense guided thermal neutron beams at Grenoble. The Julich work, which was reported at the MTAA-7, provided the first demonstration of the use of cold neutron beams for prompt gamma activation analysis. At the ILL reactor, which currently has the world's most intense thermal neutron beams, the neutron depth profiling facility was used to demonstrate the profiling of oxygen with the ^{17}O (n,a) ^{14}C implementation of NDP for oxygen must await the very intense beams of the proposed NBS Cold Neutron Facility to be practical.

The Group's contribution to the certification of Standard Reference Materials is illustrated by multielement measurements done on the following SRM's: Fly Ash, Flint Clay, Plastic Clay, Dolomitic Limestone, Rice Flour, and Wheat Flour. At major levels, the determination of silicon by fast neutron activation analysis has been demonstrated. Preliminary measurements of trace levels of lithium and boron in biological materials will be published using a thermal neutron irradiation followed by helium gas mass spectrometric determination for quantification.

Research into biomedical problems has again been strong this year centered around the activities of the joint NBS/NOAA/EPA Environmental Specimen Bank. A new stable isotope technique for the measurement of total blood volume in humans has been reported based on the NAA determination of the Cr-51/Fe-59 ration in samples spiked with Cr-50. The characterization of biological macromolecules by a combination of gel electrophoresis and neutron activation analysis is under development. A special large volume irradiation facility has been contructed for this purpose. A systematic effort has begun on the accurate and efficient measurement of trace elements in human serum, focused initially on zinc and selenium. The crucial step of valid sampling of biological materials was reviewed in a special issue of the Bureau's Journal of Research.[1]

The strong interaction with industrial scientists using neutron depth profiling, prompt gamma activation analysis, and neutron activation analysis has continued with a growing number of guest workers, research associates, and joint publications. The long-term NDP study of the mobility of helium in nickel has been completed. The measurement of distributions of lithium and boron in metals, glasses, and polymers continues to produce important results.

The joint NBS/FDA/USDA study of trace elements in human diet, sponsored by the International Atomic Energy Agency, has completed its second year. A total of 30 biologically important minor and trace elements have been measured on the total diet material, USDIET-I. A second composite diet material is being prepared for study and as a candidate for an NBS Reference Material.

During the coming year the Group will continue to improve the accuracy and sensitivity with which nuclear methods are applied to elemental measurement. This will address the problems of sample preparation, irradiation, and counting with the goal of reducing and quantifying the various sources of systematic error in analysis by nuclear methods.

---

1. Journal of Research of the National Bureau of Standards 91, No. 2, March 1986 Special Issue: Biomedical Sampling.

DETERMINATION OF ULTRATRACE LITHIUM AND BORON BY NEUTRON ACTIVATION AND MASS SPECTROMETRIC MEASUREMENT OF He-3 AND He-4

W. B. Clarke, M. Loekebakker, and R. D. Barr
(McMaster University, Hamilton, Ontario, Canada)

and

R. G. Downing and R. F. Fleming
(Center for Analytical Chemistry)

A technique for the analysis of lithium and boron at less than 10 nanograms per gram concentration levels was developed during the last year. The irradiation facilities and a noble gas mass spectrometer at McMaster University and the pneumatic irradiation facility at the thermal column of National Bureau of Standards Research Reactor were used in developing the technique.

The method takes advantage of the fact that Li-6 has a large cross section for the thermal neutron reaction Li-6 (n,H-3) He-4. The minute quantity of tritium produced during thermal neutron irradiation of nanogram quantities of lithium is contained in the irradiation vial. Samples are irradiated to a total thermal neutron fluence of approximately 3×10^{16} n/cm^2 and then allowed to decay for a period of a few days. The sensitivity of a statically operated mass spectrometer previously developed for oceanographic studies of helium isotopes and tritium is capable of quantifying the He-3 from the decay of H-3 ($t_{(1/2)}$ = 12.35 years). Furthermore, in the development stage of the technique it became apparent that boron could be reliably determined in the same sample by mass spectrometric assay of the He-4 produced by way of the thermal neutron reaction B-10 (n,He-4) Li-7.

In brief, the sample preparation consists of freeze drying a sample in a liner made of ultra-pure polyethylene. The liner and sample are then placed in a lead tube which has been pinched sealed at one end. The other end of the lead tube is attached to a high vacuum line, evacuated to completely remove atmospheric helium dissolved in the sample and liner, and then pinched off from the vacuum manifold to form a leak-tight container for subsequent irradiation. The vacuum is about 10^{-7} torr inside of the sealed lead capsule. The dimensions of the sealed tube are about 1 cm in diameter and about 6 - 7 cm long. This allows 4 tubes, 2 samples, and 2 standards, to fit side-by-side in an NBS polyethylene pneumatic irradiation rabbit. The lead container is quite rugged and has excellent integrity in the sense of inward leakage of atmospheric helium or outward loss of the reaction products.

One attractive aspect of this procedure is that the only chemical treatment of the sample consists of removal of water and other volatiles during freeze drying.

Repeated analysis of blanks carried through the entire process show that sporadic contamination is less than 0.02 ng for lithium and less than 0.5 ng for boron from all sources.

The liner acts as a catcher foil for the tritons and alpha particles emitted from the outer edge of the enclosed sample. The resulting gas atoms will rapidly diffuse out of the polyethylene during analysis. If the sample were instead residing against the lead tubing an unknown quantity of the He-4 and H-3 would become permanently embedded at the inside wall of the lead container. For very small samples this "lost" material would make for a significant loss of product during the mass spectrometric analysis.

The first samples analyzed were blood and separated components of blood because of the observation that lithium may contribute to the regulation of blood cell formation. In the past, a major difficulty in determining pathways of lithium and boron in biological systems has been that analytical methods described in the literature are difficult and often unreliable at such natural ultratrace levels.

Initially, irradiations were performed at the McMaster reactor in Hamilton, Ontario. This proved unsatisfactory for two major reasons. First, irradiation times longer than 10 hours sometimes caused the rupture of the lead containers due to excess pressure built up, mostly hydrogen, produced by gamma ray decomposition of the sample and of the polytheylene liner. Second, a large fraction of the neutrons at the irradiation position were of sufficient energy to induce the interfering reactions N-14(n,H-3),C-14, C-12(n,He-4)Be-9, O-16(n,He-4)C-13, and N-14(n,He-4)B-11. Each of these is a potentially serious interference in a biological material. As a result, the NBS research reactor was selected as the site for irradiation because of highly thermalized flux of neutrons avalilable in the thermal column of the 20 MW research reactor. Helium and triton forming interferences, from thermal neutron capture on H-2, S-32, S-33, O-17, K-39, Cl-35, and Ca-40, have been evaluated for each of the samples under investigation.

Table 1 gives some of the results obtained by the neutron activation - mass spectrometric technique on whole blood. Additional analyses on human blood, blood components, along with the possible medical implications are being submitted to the International Journal of Radiation and Isotopes. This more in-depth publication will also include results from analyses on other biological materials.

In the coming year, the technique will be further improved upon by better control on the irradiation conditions, and closer evaluation of the potential

Table 1. Lithium and boron in whole blood.

Donor	No. of samples	Lithium (ng g^{-1} wet wt.)	Boron (ng g^{-1} wet wt.)	wet wt./dry wt.
A	1	0.58 ± 0.09	16.3 ± 2.6	5.01
B	1	0.54 ± 0.09	16.2 ± 1.7	5.01
D	1	0.91 ± 0.12	28.4 ± 3.8	4.86
E	1	0.30 ± 0.06	15.3 ± 2.8	5.13
F	1	0.49 ± 0.08	20.3 ± 1.5	5.09
G	1	0.37 ± 0.10	17.9 ± 3.4	4.75
H	1	0.56 ± 0.10	23.7 ± 3.6	4.67
I	4	0.49 ± 0.06	19.5 ± 1.5	4.62
J	2	0.93 ± 0.05	79.5 ± 1.5	4.80
K	2	0.66 ± 0.08	30.6 ± 1.0	4.70
O	1	0.41 ± 0.03	21.7 ± 1.9	4.76
L	1	0.39 ± 0.03	48.4 ± 2.0	4.89
M	1	0.96 ± 0.04	63.0 ± 1.9	4.71
AVERAGE		0.58 ± 0.06	30.8 ± 5.6	

Notes: The first seven samples listed were irradiated in the McMaster reactor, and the others were irradiated in the NBS thermal column. Errors for individual values are estimates of analytical precision, and errors for average values are standard errors, i.e. one standard deviation of the means.

systematic errors present in the analysis. Inorganic materials are being prepared for determination of lithium and boron content as well.

DETERMINATION OF TOTAL ZINC AND SELENIUM IN HUMAN BLOOD SERUM

R. R. Greenberg and G. V. Iyengar

Establishment of precise and accurate analytical measurements for trace elements in various biomedical specimens is crucial in order to provide reliable reference values for various applications in environmental and health related investigations. In dealing with biological samples, it is not uncommon to experience contamination or other methodological problems for even such common elements as Cu, Fe and Zn which occur at relatively high concentration levels in many samples, such as blood serum, milk and urine. Other, more analytically difficult elements, e.g., Cr, Mo, Mn and Se in blood serum, present considerable challenges in obtaining meaningful analytical output. A comprehensive quality assurance (QA) program is an essential requirement for such studies, beginning with the biological and analytical validity of the sampled material, followed by chemical analysis using critically controlled analytical procedures. The requirement for QA is even more important if the analyzed specimen is intended to serve as a reference material. For such uses, it is not only desirable to generate a homogeneous materials, but the measurement process applied should be capable of keeping the analytical errors as low as possible, e.g., 1 - 2 %. Such a measurement capability has been demonstrated in our laboratory using instrumental neutron activation analysis (INAA) to determine Zn and Se in a pooled human serum sample.

It is of practical significance to note that real world clinical specimens are very precious, and often they are obtainable only in limited quantities, e.g. blood serum. Therefore, implicit confidence in the chosen analytical technique is necessary. There are currently many ongoing studies investigating the effects of Zn and Se as protective agents against various types of cancers and nutritional disorders. In view of the ubiquitous nature of Zn, it is often easy to contaminate samples with this element during the sample preparation steps prior to the actual determination step. Selenium is a particularly difficult element to determine in many biological materials in view of the volatility of a number of Se compounds, and the difficulty of decomposing some organo-selenium compounds. In this context, INAA offers a number of advantages compared to other analytical techniques including: high sensitivity; lack of matrix effects; minimal sample pretreatment, and non-destructive capability, which eliminates analytical problems due to sample dissolution and to volatility losses of Se. In addition the measurements can be repeated on the same samples, if necessary, utilizing the non-destructive nature of the technique.

Zinc and Se have been determined, using INAA, in seven replicates from a pooled human serum sample provided by the Organic Analytical Research Division. Care was taken in each step of the analysis to keep the total systematic error to one percent or less. Serum samples (approximately 500 mg each) were weighed into acid-washed, ultrapure quartz vials, lyophilized at -40° C, and sealed. A quartz vial containing 500 µL of high purity (subboiling-distilled) water was processed simultaneously with the samples as a blank, and two samples of Bovine Liver, SRM 1577 were prepared for use as control samples. A new standard solution was prepared gravimetrically containing both Zn and Se, and was deposited gravimetrically onto filter papers placed inside of quartz vials. A Se standard used in the certification analysis of Milk Powder, SRM 1549, was also prepared in the same manner as an additional check. The height of the filter papers in the quartz ampoules was exactly matched to that of the lyophilized serum samples to eliminate both irradiation and counting geometry effects. The samples, standards, controls and blank were irradiated together in two polyethylene irradiation containers (rabbits) for three hours in the RT-3 pneumatic tube facility of the NBS reactor. One month after irradiation, the samples were removed from the rabbits, washed in nitric acid to remove any surface contamination from the quartz vials, and counted at a distance of 5 cm from the gamma-ray detector, for approximately one day each. Zinc was quantitated using the 1115 keV gamma ray from Zn-65, and Se was quantitated using the 136, 265, and 400 keV gamma-rays from Se-75.

The results of this analysis are listed in Table 1 and are very encouraging. The observed precision (relative standard deviations) for the concentrations of both elements in the seven replicate samples was one percent, which was consistent with the counting statistics. The Se results obtained using each of the three different gamma-rays were in close agreement, and the observed concentrations in the Bovine Liver control samples were in close agreement with the certified values. The two Se standards agreed to within a few tenths of a percent, and this difference could be explained by the uncertainty due to counting statistics. The concentrations of both elements were in the reference range for "normal" individuals, indicating that this serum pool may be useful as a reference material. It may also be used as a research material for validating methodologies for analytical techniques whose systematic errors are less completely understood than are those of INAA.

In view of the closely bio-regulated concentration levels of many essential elements in tissues and body fluids, it may be necessary to achieve the level of precision and accuracy demonstrated in this investigation, to successfully identify

Table 1. Concentrations of Zn and Se Observed in Human Blood Serum - Pool 8642-TS (BM 28)

Sample	Zn (μg/g)	Se (ng/g)
HS-1	1.2373 ± 0.0066[1]	117.42 ± 0.81[1]
HS-2	1.2461 ± 0.0102	118.40 ± 1.26
HS-3	1.2438 ± 0.0095	114.72 ± 1.13
HS-4	1.2299 ± 0.0108	117.71 ± 1.24
HS-5	1.2243 ± 0.0095	116.74 ± 1.12
HS-7	1.2511 ± 0.0093	116.18 ± 1.06
HS-8	1.2313 ± 0.0063	116.87 ± 0.70
Mean ± 1s	1.2377 ± 0.0098	116.86 ± 1.19
Blank	0.0143 ± 0.0006	<0.2
Systematic error[2]	0.012	1.17
Recommended value[3]	1.223 ± 0.021	116.9 ± 2.3

---

[1] Uncertainties for individual measurements are 1 sigma counting statistics.

[2] Estimated total systematic error at 95% confidence level.

[3] Uncertainties are the estimated overall analytical uncertainty at the 95% confidence level.

subtle differences, if any, in specimens from normal individuals compared to those from pathological cases.

THE DETERMINATION OF CHROMIUM-50 IN HUMAN BLOOD AND ITS UTILIZATION FOR BLOOD VOLUME MEASUREMENTS

R. Zeisler
(Center for Analytical Chemistry)

and

I. Young
(National Institute of Health, Bethesda, MD)

Systematic studies involving the measurement of maternal blood volume increases are needed since subnormal increases have been associated with maternal complications and intrauterine growth retardation in a few instances. To establish a possible link, a new measurement procedure for the maternal blood volume is required that would be accurate enough to determine the 20 to 40% small difference between normal and subnormal increases during pregnancy.

Currently, only the radioisotope dilution technique employing chromium-51 (Cr-51) as a label for red blood cells can provide results with a standard error smaller than 5%. However, this technique cannot be used with pregnant women and also would impose severe restrictions on a large scale field study because of the radioisotope involved. Therefore, the Cr-51 radioisotope technique should be replaced by a dilution technique that utilizes enriched chromium-50 (Cr-50) as a label. The Cr-50 can then be determined by instrumenatal neutron activation analysis or mass spectrometry.

The current investigations focus on the development of an INAA procedure for the determination of red cell blood volumes (RCBV) via Cr-50 isotope dilution. Although INAA procedures were introduced in the 1970's to measure the stable isotope tracer Cr-50 in several clinical applications, the procedure was not routinely implemented for RCBV determinations. A possible reason for this may be the fact that low level determinations of Cr-50 (a 4.35% abundant isotope of natural chromium) are needed for reliable results. These were unavailable at the time. Only recently the knowledge about sources of contamination and the experience in contamination control has enabled us to determine chromium at naturally occuring low levels in such difficult samples as blood, serum, etc.

Besides the establishment of validated sampling procedures for the clinical blood samples, additional precautions were needed for the stable isotope technique with INAA because of interfering activation reactions and small activities produced. These were resolved with irradiations in highly thermalized neutron fields and background reduction during counting by Compton suppression. The application of the procedures to the measurement of natural chromium in total blood yielded the first

Table 1. RCBV Measurements on Blood Bank Units and Monkeys

Sample		Cr-50/Fe-59 Ratios			Volumes [g][a]		
		A_i	A_m	A_b	V_i	V_{Cr-50}	$V_{grav/Cr-51}$
			Blood Bank Units				
#B66371	A	1.93	1.38E-2[b]	6.6E-4	2.99	467	526
	B	1.92	1.17E-2	9.3E-4		532	
#PL 146	A	4.28	1.98E-2	11.1E-4	2.43	556	547
	B	4.30	2.03E-2	8.2E-4		536	
			Monkeys				
#497	A	2.76	3.52E-2	5.4E-4	3.79	302	294
	B	2.76	3.08E-2	4.0E-4		344	283
#499	A	2.85	3.17E-2	3.3E-4	3.84	349	354
	B	2.88	3.26E-2	2.2E-4		350	343
#512	A	2.53	2.69E-2		3.59	338	356
	B	2.55	2.74E-2			334	355

[a] Volumes are given in mass units because V_i was determined by weight.

The measurement of the red cell blood volume (RCBV) with chromium labeled erythrocytes is based on the simple principles of mass balance in a dilution experiment. A known amount of labeled blood is injectd into the cardiovascular system. From its dilution the volume is calculated. Considering background, the following equation applies:

$$RCBV \sim V_x = \frac{A_i \quad V_i}{A_m - A_b}$$

where:

A_b = background of natural chromium in blood
A_i = specific activity or concentration in labeled blood
V_i = volume of the injected labeled blood sample
A_m = measured specific activity or concentration after dilution
V_x = unknown blood volume.

results reported by INAA at a consistent low level of <2.5 ng/mL (0.3 to 2.5 ng/ml) in samples from human volunteers and rhesus monkeys.

Based on the INAA procedure, a new approach to the blood volume measurement via Cr-50 isotope dilution has been developed. It utilizes the ratios of the induced activities of Cr-51 to the iron-59 (Fe-59) instead of the calculation of specific activities or concentrations since the iron concentration in the blood cells remains unchanged during the dilution experiment. This makes the method independent of sample size and irradiation and counting parameters that may add to the uncertainty of the measurements. Only the volume or mass of the labeled blood which is injected into the subject's blood stream for dilution must be known exactly. The dilution factor is then determined on a second blood sample and the volume can be calculated.

Prior to a study with human volunteers, two RCBV measurement experiments were carried out to test the validity of the newly developed approach. One experiment involved two blood bank units, where the amount of blood could be easily determined to check the results. The second experiment involved three monkeys (rhesus macaca mulatta), where the RCBV was determined via the traditional Cr-51 radioisotope technique in addition to the Cr-50 stable isotope experiment. The results are summarized in Table 1.

The estimated uncertainty for the new procedure is not exceeding several percent and results may be more reliable than with the classical Cr-51 procedure. The first comparison of the two techniques confirmed this estimate. However, three measured values did not agree with the actual amounts or the results of the other technique. This may be due to the experimental circumstances where either contamination could have occurred or it could not be assured that the labeled blood had been completely injected into the cardiovascular system. If such shortcomings can be avoided, this novel approach is well suited as a clinical tool to study problems associated to the maternal blood volume due to its simplicity and inherent accuracy and precision.

EVALUATION OF USDIET-I TOTAL HUMAN DIET SAMPLES FOR NUTRITIONAL CONSTITUENTS

V. Iyengar
(Center for Analytical Chemistry)

A multination study, sponsored by the International Atomic Energy Agency, is aimed at obtaining comparative data on dietary intakes of 25 biologically important minor and trace elements in a variety of developed and developing countries. Three Federal Agencies, namely the National Bureau of Standards (NBS), the Food and Drug Administration (FDA) and the U.S. Department of Agriculture (USDA) are participating in this study. The scope of the study provides an unique opportunity to develop a coordinated approach by the collaborators of these 3 agencies for the U.S. part of the study.

The combined expertise of the participants is aimed towards the needed developments and improvements of analytical methodology for the accurate assessment of the dietary intakes of trace elements. Aspects of quality assurance in sampling, sample preparation, analysis and data evaluation have been addressed by intercomparison studies of minor and trace elements in dietary reference materials (NBS rice flour SRM 1568a, NBS wheat flour SRM 1567a and two mixed diet samples, namely IAEA-H9 and TDD-1D) using different analytical techniques. Precision and accuracy aspects related to Flame Atomic Absorption Spectrophotometry, Atomic Emission Spectrophotometry with an inductively coupled plasma source and Neutron Activation Analysis were evaluated by analyzing the same test materials by all the three methods.

As a contribution to this project a benchmark mixed U.S. diet research materials using 201 different foods from the FDA Total Diet Study (TDS) has been prepared. According to the FDA-TDS study, a 25-30 year old male consumes daily a total of 3075 g from these 201 foods. This represents the group with highest caloric intake per day and has been used as a basis for all the calculations in the present study. The first batch comprises of about 10 kgs of mixed diet.

Proximate analysis has been carried out on USDIET-I (fresh material) and the following results were obtained; total volatiles = 83.8 %, ash content 0.66 %, fat = 2.92 %, protein = 3.42 %, carbohydrates = 9.2 % and total caloric energy (kcal/100g) = 76.76.

Over 30 minor and trace elements have been characterized in USDIET-I using a combination of analytical techniques. A comparison of the daily intakes of Ca, Cu, Fe, Mg, Mn, Na, P and Zn from this total diet material with those of FDA-TDS figures calculated from single food analysis results showed that the mixed diet concept is a viable approach. The daily intakes from USDIET-I were also compared with the Recommended Daily Dietary Allowances suggested by the National Academy of Sciences. The agreements were generally very good. However, analysis for a number of elements such as Cd, Cr, Hg and Mo that occur at low concentration levels in individual foods, demonstrated the feasibility of a reliable assessment of their daily intake by use of a total diet material, e.g., USDIET-I.

A number of organic nutrients have also been determined in USDIET-I, and their stability during storage is being evaluated. The initial findings suggest that USDIET-I may also be useful to develop reference materials for organic nutrients. There is a great need for these types of reference materials. Thus it may pave the way for considering production of a single SRM certified for both organic and inorganic nutrients.

Simultaneously, the long-term implications of biomonitoring of foods is being studied by storing about 3 kgs of USDIET-I as originally composited. Dietary collections from different regions of the U.S. are currently underway. Representative portions of these total diets from future collections will also be preserved in the Biomonitoring Specimen Bank.

DETERMINATION OF SILICON BY FAST NEUTRON ACTIVATION ANALYSIS

D. A. Becker

An instrumental neutron activation analysis method has been developed for the determination of silicon in a variety of matrices, utilizing fast neutrons. This method has been applied to the certification of silicon in SRM 1632 b, Trace Elements in (Bituminous) Coal, and in the determination of silicon in a number of marine sediments.

The nuclear reaction used for the analysis is the silicon-29(n,p) aluminum-29 reaction, with counting of the 1273 Kev gamma ray (half-life is 6.5 minutes). A boron nitride capsule is used to hold the sample, which absorbs the thermal neutrons while passing the fast neutrons. This substantially lowers the overall radioactivity of the sample, while not affecting the analysis for silicon. In particular, the BN reduces the interference due to production of aluminum-28 by thermal neutrons,

The University of Maryland nuclear reactor was used for the irradiations, since its design (light water cooled and moderated) provides a greater intensity of fast neutrons than the NBS reactor, even though the thermal neutron intensity is less than 3% of the NBSR (which was designed specifically to provide a maximum intensity of thermal neutrons). Irradiation times ranged from one to six minutes, depending on the silicon concentration in the samples.

For the coal analysis, four bottles were analyzed in duplicate, with sample sizes ranging from 0.58 to 0.75 gram. The silicon concentration found was 1.35 ± 0.03% (S.D.; 1s). Good agreement was obtained between all four bottles.

For the sediment analysis (made as part of a series of specimen bank samples for NOAA and described elsewhere in this report) silicon concentration ranged from 23 to 31%. Excellent agreement was obtained for check samples of NBS SRM 1646 (Estuarine sediment), the IAEA sediment samples, and NRC-Canada reference sediments, although none of these are known to a high degree of accuracy.

From the above data it is estimated that analysis for silicon using aluminum-29 can be made for 2 mg of silicon with approximately 3 percent counting statistics, or 0.2 percent silicon in a one gram sample. Further, if no aluminum or phosphorus is present in the sample, this level could most likely be lowered to 0.02 percent, through use of the aluminum-28 isotope. Work is continuing on additional types of samples and to establish experimental detection limits for silicon.

SPECIMEN BANKING AND ANALYSIS IN THE NATIONAL STATUS AND TRENDS PROGRAM

R. Zeisler, S. F. Stone, B. J. Koster, D. A. Becker, and M. P. M. Tillekeratne

Recently, environmental monitoring has been complemented by programs for systematic and controlled long term storage of environmental samples, i.e. environmental specimen banking (ESB). The necessity, usefulness and importance of ESB has been demonstrated for current monitoring as well as for preserving the representation of the past for examination in future years. In 1984, the National Oceanic and Atmospheric Administration (NOAA) has initiated a specimen bank for estuarine and coastal samples, as part of its National Status and Trends (NS&T) Program. This specimen bank has been incorporated in the research activities of the Pilot Environmental specimen Bank which is housed at NBS. The research includes all steps of the ESB operation with special emphasis on quality assurance in the selection, collection, preparation, storage, and analysis of marine samples according to validated procedures.

The NS&T program is sponsoring two monitoring projects for the U.S. coastal waters: the Mussel Watch with 154 collection sites and the Benthic Surveillance with 50 collection sites. The mussel watch collects bivalves and sediments from tidal sites whereas the Benthic Surveillance collects bottom feeding fish and sediments from estuarine and continental shelf sites. Over 40 sites nationwide are now included in the ESB. The sampling techniques applied in these programs have been refined and modified in cooperation with the field scientists to fulfill the requirements of the ESB and to ensure comparability between the samples used in realtime monitoring and the baked samples. Protocols have been developed for the sampling and preparation of the specimens that greatly reduce the risk of contamination. Special tools and implements, chiefly made from titanium and Teflon, are used to prepare the samples for transport and storage at liquid nitrogen temperature. The samples are prepared for analysis in a clean-room by contamination free blending (sediments) or cryogenic homogenization (tissues) in Teflon disk mills.

A unique sequence of instrumental analytical methods involving X-ray fluorescence and neutron activation analysis procedures has been employed for the determination of 44 elements in marine bivalves. The individual procedures are a X-ray fluorescence method based on backscatter with fundamental parameter corrections, prompt gamma activation analysis, and neutron activation analysis with instrumental and radiochemical procedures. This analytical approach has been expanded to include the analysis of sediments and fish tissues. It is possible to use a single subsample of about 250 mg and follow it through three instrumental

Table 1. Results for the Determination of Selected Elements in Sediment Samples from the Benthic Surveillance Program (μg/g except as noted)

Element	S001A[a] DP	S010A EB	S013A NR	S019A MRD	S022A CC	S028A CB	Error
Al %	6.60	7.70	7.45	4.18	6.86	6.47	0.03 - 0.04
	6.64	7.74	7.50	4.16	6.80		
Si %	30.81	20.55	26.33	36.56	23.56	24.45	
	30.49	20.55	26.53	34.79	22.23	25.66	
V	61.5	110.1	89.8	42.5	93.0	115.2	2.9 - 5.0
	55.1	106.0	94.2	46.6	97.4	110.1	
Cr	35.2	105.5	28.1	39.4	52.4	111.2	2.5 - 3.5
	38.1	81.5	34.6	39.4	55.5	113.1	
Mn	366	631	662	277	550	1020	4.0 - 10.0
	419	608	667	277	553	1083	
Fe %	1.85	4.11	2.99	1.440	3.21	4.94	0.01 - 0.03
	1.88	4.46	3.32	1.542	3.61	5.29	
Zn	51.9	145.9	67.5	48.1	134.2	350.2	1.2 - 4.0
	51.5	160.3	67.8	51.2	146.7	353.9	
As	5.21	18.1	<3.2	6.51	10.7	23.9	0.3 - 1.2
	3.27	16.1	2.6	7.18	10.1	22.3	
Sb	0.50	3.42	<0.2	0.38	0.70	1.30	0.04 - 0.13
	0.49	2.95	<0.2	0.47	0.71	1.46	
Hg	<0.3	<0.5	<0.4	<0.3	<0.4	<0.6	
	<0.3	0.54	<0.4	<0.3	<0.4	<0.6	0.01

[a] DP - Dana Point, CA
EB - Elliott Bay, WA
NR - Nisqually Reach, WA
CC - Corpus Christi, TX
CB - Chesapeake Bay, MD
MRD - Mississippi River Delta, LA

Table 2. Determination of Selected Elements in Two Reference Materials Using INAA (µg/g except as noted)

Element	SRM 1646		IAEA SD-N-1/2	
	This Work	Certified Mean ± 2s	This Work	Certified Mean (C.I.)
Al %	5.91 ± 0.04 5.97 ± 0.03	6.25 ± 0.20	3.66 ± 0.02	(3.58 - 3.85)
Si %	31.61	(31)	28.16	(26.1 - 29.2)
V	92.2 ± 4.4 93.0 ± 2.9	88.0 ± 10.0	77.7 ± 3.2	77.7(65.0 - 80.7)
Cr	80.1 ± 0.8	76.0 ± 3.0	144.3 ± 1.1	149(125.0 - 161.0)
Mn	360.5 ± 5.7 369.7 ± 5.7	375.0 ± 20.0	809.9 ± 9.2	777(728.0 - 801.0)
Fe %	3.456 ± 0.027	3.35 ± 0.1	3.456 ± 0.027	(3.53 - 3.78)
Cu	<390	(3.7)	<300	72.2(68.1 - 75.2)
Zn	137.4 ± 2.0	136.0 ± 6.0	423.2 ± 3.9	439(423.0 - 452.0)
As	11.95 ± 0.27 10.85 ± 0.44	11.6 ± 1.3	65.03 ± 0.92 64.40 ± 0.88	50(42.4 - 60.0)
Cd	<6.3 <11	0.36 ± 0.07	11.8 ± 1.3 9.1 ± 1.5	11.0(10.0 - 12.0)
Ag			2.14 ± 0.23	2.3(2.0 - 3.2)
Sb	0.43 ± 0.08	(0.4)	3.48 ± 0.10	3.62(3.20 -3.95)
Hg	<0.4	0.063 ± 0.012	2.65 ± 0.15	(0.06 - 1.72)

analyses, nondestructively, and a final radiochemical procedure, which consumes the sample. The advantage of this approach is obviously the reduced sample preparation which minimizes contamination or loss and assures the true correlation of elements since all results are based on the same subsample, i.e., eliminating uncertainties due to sample to sample variations.

Analytical quality assurance has been accomplished by two means: First, the sequential analytical procedure allows for the independent determination of up to twenty elements by the two or three techniques involved. Since the same subsample is used by all techniques, any deviation of the results would indicate a possible bias of one technique. Secondly, a sufficient number of certified reference materials has been analyzed in parallel with the monitoring samples. Good agreement of the analytical results with the certified values will allow conclusions on the accuracy of the results obtained for the monitoring samples.

Analytical data have been obtained for tissue samples from earlier bivalves specimens[3] and from sediment samples collected during the 1985 NS&T project year. Results for selected elements in six NS&T sediment samples using instrumental neutron activation analysis are shown in table 1. Due to the limited number of individual samples that were available, no assessment of environmental status can be made at this time. However, the primary emphasis of this work is on high quality multielement determinations. The results obtained on referencce materials (table 2) confirm that the applied analytical approach is in control.

---

1. S. A. Wise and R. Zeisler, Eds., International Review of Environmental Specimen Banking, NBS Spec. Publ. 706, U.S. Government Printing Office, Washington (1985).

2. S. A. Wise, R. Zeisler, Environ. Sci. Technol., 18, 302A (1984).

3. S. F. Stone, R. Zeisler, Proc. 5th Conf. on Nuclear Methods in Environment and Energy Technology, J. R. Vogt, ed. NTIS U.S. Dept. of Commerce, Springfield, VA, CONF-840408 (1984).

ACTIVATION ANALYSIS OPPORTUNITIES USING COLD NEUTRON BEAMS

R. M. Lindstrom and R. Zeisler
and
M. Rossbach
(Nuclear Research Center (KFA) Jülich, F. R. Germany)

The application of neutron-capture prompt gamma-ray activation analysis (PGAA) has been pursued to date at only a few laboratories on a full-time basis, only partly because of the need for continuing access to a reactor neutron beam. Irradiation times of several hours are required for most samples in which many elements are to be measured, hence the throughput is low because only one sample can be irradiated and measured at a time.

The low sensitivity is not due to a low neutron capture rate, but to a low detection efficiency for the resulting gamma rays, because of the necessary bulk of active and passive shielding around the detector. Simply moving the detector closer to the sample increases the efficiency, but at the cost of higher backgrounds and other consequences of operating instruments in high radiation areas. Isenhour and Morrison have concluded that, for equal neutron fluence rates, PGAA is superior to conventional (delayed) NAA in the intensity of gamma-ray emission for 61 out of 63 elements considered.[1] The comparison fails, of course, when the fluence rate in an internal irradiation position is compared with that in an external beam. In general, beams provide only about 10^{-5} of the thermal neutron fluence rate of an in-core irradiation position. Further limitations are imposed on the technique by the inferior signal to background ratios in a PGAA facility as compared to a shielded gamma spectrometer used for delayed counting. In existing PGAA facilities, the baseline under the desired spectral peaks has several components:

1. The Compton continuum from high-energy gamma rays in the sample spectrum.

2. A continuum of scattered gamma rays from the neutron source. Despite the low scattering probability for photons at high angles, in an unfiltered beam the utility of low-energy capture lines is impaired.

3. Lines and continuum from neutron capture in the sample support, beam tube, beam stop, shielding, and detectors. This may come from a penumbra of thermal neutrons or from fast neutrons which travel several centimeters in low-Z materials before being absorbed. Radiations from H, B, C, Al, and Fe are

commonly present in background spectra, as is N from liquid nitrogen vessels and from air in unevacuated beam tubes. This component increases with the neutron scattering power of the sample.

4. Environmental background, both continuum and discrete, from the reactor and from nearby experiments in the often crowded space of a reactor experimental hall. This includes decay radiation from neutron activation products of structural parts and shielding, as well as leakage of neutrons and gamma radiation from beam ports and spectrometers.

All except the first of these background components are much less important in a cold neutron facility.

From the point of view of chemical analysis, the ideal neutron field has the largest possible number of activating particles per $cm^2 \cdot s$ on the sample, and the smallest possible number of interfering particles at the detector. A narrow beam is desirable so that the gamma-ray detector can be moved near the sample and the size of the shielding may be minimized. For PGAA, unlike neutron scattering measurements, the beam need not be collimated parallel, but should be uniform across the target.

A guided beam of cold neutrons meets these requirements exactly.[2] The slowest neutrons from the reactor are reflected with high efficiency from the walls of the guide tube, while the fast neutrons and gamma rays decrease as $1/r^2$ with distance from the source. Therefore the signal to noise ratio is high. Since the apparatus is not near the reactor and other experiments, the background from these sources is low and there is room between experimental facilities to construct efficient shielding. The capture rate is also higher with cold than with thermal beams. Since capture cross sections for most target nuclei are inversely proportional to the neutron velocity, the same number of neutrons per $cm^2 \cdot s$ at 30 K gives three times the reaction rate as at 300 K.

The recently commissioned ELLA Neutron Guide Laboratory at the FRJ-2 (DIDO) reactor[3] of the Nuclear Research Center Jülich provides cold neutron beams with the aforementioned qualities. A new neutron guide has been constructed which extracts neutron beams of intensity 8.4×10^8 $n/cm^2 \cdot s$ from a hydrogen cold source through a 48-cm cooled Bi filter. The guide used for the PGAA experiments is straight and of 5 x 10 cm cross section. The irradiation position is 50 m from the cold source. The target - detector assembly and the signal processing circuitry are illustrated in figure 1.

Neutrons emerged from the guide through a thin aluminum window to irradiate the sample, suspended in air by 13 μm Teflon threads. The neutron beam was collimated to a diameter of 2 cm by two Li-6 aperture plates. Excess neutrons downstream from the sample were stopped in an open-ended box slightly larger than the beam, fabricated of metallic Li-6 pressed into slabs and encapsulated in aluminum foil. No gamma-ray shielding of the neutron beam itself was required; when the neutrons were experimentally removed by a Li-6 stop, the residual gamma radiation at the sample position was only 50 μSv/h (5 mR/h).

The detector used was an Ortec GAMMA-X Plus intrinsic germanium diode (22.6% efficiency, 1.72 keV resolution (fwhm) at 1.33 MeV) equipped with a small cryostat with 24 h holding time. The front face of the detector can was placed 23 cm from the sample. The detector was surrounded by Pb shielding to reduce the background from neutron capture in the aluminum window. A collimating aperture 2 cm in diameter by 20 cm long admitted gamma rays from the sample, illuminating 60% of the face of the detector crystal. A transistor reset charge-sensitive pramplifier was used in connection with an Ortec 673 main amplifier and gated integrator to allow good throughput at high count rate. The signals were collected with a Nuclear Data 581 ADC (10 μs conversion time into 16384 channels) and a Nuclear Data Micro-Multichannel Analyzer connected to a VAX 11/750 computer. An Ortec ADCAM multichannel analyzer, connected to a personal computer, collected 8192-channel data in parallel and provided live spectral display. The application of loss-free counting circuits is being tested for the measurement of rapidly decaying nuclides after stopping the beam in front of the target.

Samples examined include Standard Reference Materials, industrial, biological, and environmental specimens, and air filters. Synthetic standards were irradiated to study the systematic errors in hydrogen containing matrices and other limitations on accuracy with existing facilities.

The main advantages of cold neutron beams were verified in the experiments. The neutron intensity at the sample position was 2×10^8 n/cm^2•s, and the cadmium ratio (with 25 μm Au foil covered by 510 μm Cd) was 1.0×10^4. Autoradiography of indium foils exposed to the beam showed good uniformity, with barely visible striations parallel to the long walls of the guide. The PGAA sensitivity, expressed in counts/s•g, was a factor 4.5 higher than the present sensitivity at the UMd-NBS facility, and a factor 9 higher than the published sensitivities at the previous reactor power of 10 MW.[4] Except for the high gamma-ray field from the window (which had been designed to minimize scattering, not capture), the beam was clean and the backgrund low. The hydrogen background in the spectrum of a Teflon sample envelope was 100 µg, four times lower than the better of two major PGAA facilities.[5]

In the analysis of plant and animal tissue, the limiting factor for both the sensitivity and the accuracy of PGAA determinations is the amount of hydrogen in the sample. The strong hydrogen capture gamma ray at 2223.2 keV is accompanied by a high Compton continuum, making the capture lines of other elements below 1995 keV much less sensitive than they would otherwise be. Active Compton suppression can reduce this baseline substantially, but not eliminate it. Since the scattering cross section of bound ^{1}H is much larger for cold than for thermal neutrons, large quantities of hydrogen in the analytical matrix lead to a smaller signal from the elements of interest, and therefore the maximum sample size is limited. A rigorous experimental and theoretical study of this problem remains to be done.

With the high gamma-ray detection efficiency possible with cold neutron beams, the practical limitation on the analytical usefulness of PGAA will be the ability to collect data at high counting rates without distortion. Recent advances in active collimation[6,7] and in loss-free acquisition techniques[8] make it likely that the collection time for electrons in germanium may become the rate-limiting step. With large Ge detectors coupled with compact high-Z gating detectors, Ge-Ge coincidence counting can be done with profit. Multiparameter counting offers a clean resolution of the problem of interfering lines in a crowded spectrum.

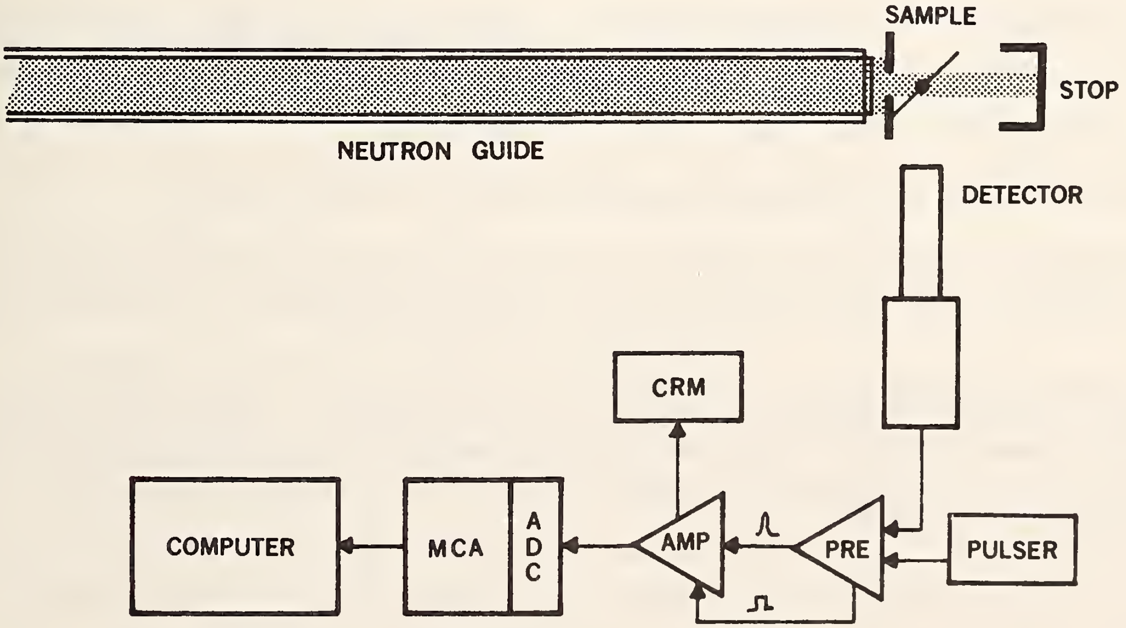

Figure 1. Experimental Arrangement

Further enhancement in sensitivity is possible since neutron optics may be used to focus cold neutrons onto a small area.[9] If a 10 cm x 10 cm beam of 10^9 n/cm^2·s could be focused on a 1 x 1 mm area by a shaped supermirror or a zone plate, the fluence rate would become a highly attractive 10^{13} n/cm^2·s. The techniques already developed for the micro-scale electron- and ion-probe analogs of this situation are directly applicable for the formation of two-dimensional images, with millimeter resolution, of the elements which produce prompt radiations under neutron bombardment.

---

1. T. L. Isenhour and G. H. Morrison, Anal. Chem. 38 (1966), 162.

2. H. Maier-Leibnitz and T. Springer, J. Nucl. Energy 17 (1963), 217.

3. K. Werner, T. Springer, and J. Duppich, in O. Harling, L. Clark, Jr., and P. von der Hardt (eds) "Use and Development of Low and Medium Flux Research Reactors" Munich: Karl Thiemig (1984), p. 783.

4. R. M. Lindstrom and D. L. Anderson, in S. Raman (ed) "Capture Gamma-Ray Spectroscopy and Related Topics - 1984" New York: Am. Inst. Physics, (1985), p. 810.

5. D. L. Anderson, W. H. Zoller, G. E. Gordon, W. B. Walters, and R. M. Lindstrom, in T. von Egidy, F. Gonnenwein, and B. Maier (eds) "Neutron-Capture Gamma-Ray Spectroscopy and Related Topics", London: Institute of Physics (1982), p. 655.

6. R. M. Lieder, H. Jäger, A. Neskakis, T. Venkova, and C. Michel, Nucl. Inst. Methods Phys. Res. 220 (1984), 363.

7. N. R. Johnson, C. Baktash, and I. Y. Lee, IEEE Trans. Nucl. Sci. NS31 (1984), 243.

8. G. P. Westphal, J. Radioanal. Chem. 70 (1982), 387.

9. A. G. Klein and S. A. Werner, Rep. Prog. Phys. 46 (1983), 259.

Acknowledgments: We thank K. Werner and J. Duppich for generously making available the facilities of the ELLA guide hall, R. Thomas for computer assistance, and P. Giesen (EG&G GmbH) for the loan of equipment and software.

NEUTRON DOSIMETRY GROUP: OVERVIEW

J. Grundl

The Neutron Dosimetry Group of the Center for Radiation Research (CRR) is engaged in the development and application of standard and reference neutron fields as permanent facilities for neutron dosimetry standardization, for neutron detector calibrations, and for reaction rate cross section measurements. Strong interactions with outside organizations, both in the federal and private sector, are important programmatic characteristics. A substantial component of the Groups activities involve the use of the NBS Research Reactor thermal column and tangential beams where facilities designed and built by the Neutron Dosimetry Group are in operation.

1. Dosimetry for Materials Performance Assessment

(a) First time ever production of neutron fluence standards with 30-year Cs-137 activity occurred this year. Neutron fluence standards are neutron sensors (activation foils generally) in which a radioactive species relevant for dosimetry is induced by irradiation in a standard neutron field. The NBS Cavity Fission Source was used to expose U-238 to a certified neutron fluence of about 2×10^{16} n/cm^2 which is sufficient to produce a measurable 30-year Cs-137 fission-product activity. These fluence standards are used to verify commercial neutron fluence measurements made with similar uranium foil dosimeters, such as are used in reactor pressure vessel surveillance.

(b) Quality assurance measurements of tantalum impurity in niobium were performed for several commercial and government laboratories using the thermal neutron irradiation facility at the reactor. The ^{92}Nb(n,n')^{92m}Nb reaction for fast-neutron dosimetry results in an X-ray emitting state with a 16-year half-life. If significant quantities (>20 ppm) of tantalum are generated in a neutron field with an appreciable slow neutron component, the tantalum becomes radioactive and decays with emission of the same energy X-ray as the Nb-92m.

2. Integral Neutron Cross Section Measurements

(a) The Department of Energy (DOE) is sponsoring a multi-laboratory effort to measure fission-spectrum-averaged cross sections of a relatively new reaction of interest for high fluence ($>10^{16}$ n/cm^2) neutron dosimetry. The reaction is ^{92}Nb(n,n')^{92m}Nb with a 16-year half-life. Many laboratories are involved because high fluence, standard-neutron-field irradiations are required and because the Nb-92m is an X-ray emitter which complicates the activity determination. NBS has completed a 30-day, 10^{17} n/cm^2 irradiation in the Cavity Fission Source for this project. The NBS Radioactivity Section will participate in the X-ray activity determinations together with the INEL Laboratory in Idaho, the University of Arkansas, and Harwell Laboratory in England. The 30-day irradiation in the NBS Facity Fission Source, an essential component of the measurement,was six times longer than any previously performed with this source. A notable goal of the irradiation was successfully achieved: The U-235 fission disks were handled with minimal personnel radiation exposure.

(b) Our productive and pleasant collaboration with the University of Virginia Department of Nuclear Engineering and Engineering Physics is continuing. Professor T. Williamson is presently analyzing data taken at NBS during his sabbatical year. A paper on the measurement of photofission cross sections in the NBS neutron driven gamma ray field will be presented at the 6th ASTM-Euratom Symposium on Reactor Dosimetry. Photofission cross sections of Np-237, U-235, U-238, and Th-232 were measured in both iron and cadmium capture gamma ray fields. These cross sections are important for correcting the neutron response of fission dosimeters used in all areas of materials performance assessment under stress of radiation. Professor Williamson and his students have also continued their analysis of data on the Nb-93(n,n') spectrum-averaged cross section for U-235 fission neutrons. Niobium foil materials were irradiated in the Cavity Fission Source of the NBS Reactor in exposures of six and four days duration. The activity of each foil is measured by comparing the number of counts with the counts from NBS SRM 4267-8, a Nb-93m activity standard. Preliminary results indicate an overall 3 percent uncertainty. Final results will be presented at the 6th ASTM-Euratom Symposium on Reactor Dosimetry.

(c) Integral tests of 10-100 keV-range neutron activation cross sections for Au, In, and Cu have been begun at the Intermediate Energy Standard Neutron Field (ISNF) facility at the reactor thermal column. In these tests, the neutron fluence rate is determined by a Pu-239 fission chamber monitor. Subsidiary measurements are being made to check for suspected problems of epi-thermal neutron leakage through the penetration for the monitor chamber stem. The neutron field near the penetration has been mapped by exposing of activation foils in the region of the penetration and comparing the results with foils activated in the ISNF with the penetration closed. The ISNF is ideally suited to cross section tests in this 10-100 keV region, and these tests may contribute to understanding the inconsistencies in the B-10 cross section in this energy range.

(d) The spectrum integrated helium generation cross section for B-10 in the NBS Intermediate-Energy Standard Neutron Field (ISNF) was measured by the HAFM technique some time ago and found to be discrepant with prediction by a surprising 10 percent. A paper was presented last year which investigated this discrepancy and others related to it. Since then some preparations have been made to make an independent measurement of this cross section in ISNF with the NBS double fission chamber. Such an active measurement in the high-intensity gamma fields within the NBS reactor thermal column poses severe experimental problems. The reaction products (Li-7 recoil and alpha particle) which can be nicely resolved in a thermal beam outside of the thermal column cannot yet be adequately discerned in the ISNF arrangement inside of the thermal column. It may be necessary to use a Cf fission neutron source to drive the ISNF geometry in order to perform this measurement. There is good reason to carry out this measurement, if at all possible, because of the basic importance of the B-10 reaction as a standard against which many other cross sections are measured and the confidence which exists concerning the 1/v shape of the reaction cross section.

3. Smaller Projects

(a) Several man months of effort were spent this year in documenting the calibration services offered in association with the NBS Fission Neutron Irradiation Facilities. Two documents, now in the NBS review process, will be published as NBS Internal Reports. They describe two services: Activation Foil Irradiations-Californium Fission Sources (44080C) and Activation Foil Irradiation-Cavity Fission Sources (44090C). The documents describe the characteristics, theory and operation of these benchmark neutron fields, including the traceability of their calibration to NBS-I. Available neutron fluences are given along with the uncertainty of relevant exposure parameters. The documents also detail operating procedure for performing irradiations in the hope of establishing some institutional memory.

(b.) Preliminary work in support of a proposed neutron life-time experiment has begun. The responsibility of the Neutron Dosimetry Group in the proposed experiment would be the determination of the average linear density of neutrons in the neutron beam, downstream from an electromagnetic proton trap. A detachable neutron detector would be absolutely calibrated in a series of subsidiary measurements employing both cold neutron beams and thermal neutron beams. The active neutron detector will consist of a thin B-10 deposit, viewed by four surface barrier detectors. A study of possible materials for the backing of the B-10 deposit has been made, and thin (0.38 mm) crystalline silicon wafers have been chosen as the backing material. These single-crystal backings will scatter thermal neutrons less than half as much as would the thinnest possible Al backing (0.13 mm). Furthermore, these crystal wafers are extremely smooth, flat, and rigid, so that good solid angle reproducibility and stability can be maintained.

(c) Prototype fission-scintillation counters developed by Lawrence Livermore National Laboratory (LLNL) were calibrated in tests at the reactor thermal column. The neutron sensitivity data provided by these tests was used by LLNL scientists to make crucial settings of the recording oscilloscopes prior to weapons tests at the Nevada site in March, 1985. These data are also being used in interpretation of the test results.

ATMOSPHERIC AND ENVIRONMENTAL STUDIES BY INSTRUMENTAL AND NEUTRON-CAPTURE PROMPT γ-RAY ACTIVATION ANALYSIS

G. E. Gordon, D. L. Anderson and J. M. Ondov
(University of Maryland, College Park, MD)

We continue to make extensive use of instrumental neutron activation analysis (INAA) and neutron-capture prompt γ-ray activation analysis (PGAA) for continued development and testing of the methods themselves and to determine concentrations of about 40 elements in particles, gases, rain and fog from the atmosphere, in related source materials such as crustal dust and coal fly ash, and in standards appropriate for use in this field. By measuring concentrations of such a large number of species, we are able to identify contributions from certain types of air-pollution sources to the atmospheric burden at ambient sampling sites, a technique now known as "receptor modeling". Examples of these studies are briefly discussed in the following sections.

1. Rare Earth Elements in Zeolite Catalysts and Rare Earth Source Materials

Since last year's report, Olmez and Gordon[1] published a paper in which they showed that refineries using zeolite catalysts and, to a lesser extent, oil-fired power plants are often strong sources of airborne rare earths. Furthermore, the rare earths released by these sources are borne by fine particles and have a pattern different from the crustal abundance pattern, being richer in light rare earths (e.g., La/Sm >20 vs. La/Sm of 5-6 for crust). To investigate the reasons for the unusual rare earth pattern, M. Kitto has been using both INAA and PGAA to analyze about a dozen types of catalysts and several ores and products from the principal U.S. supplier, MolyCorp. The analyses are not yet in final form, but major results

Table 1. Summary of results from Analyses of 13 Zeolite Catalysts

	Avg	Sigma	Max	Min	No. pts.	Crustal Values	
						Wedepohl[2]	Taylor[3]
La/Sm	61	76	305	8.43	13	6.7	4.9
La/Ce	2.21	1.79	5.16	0.36	13	0.58	0.49
La/Nd	1.80	0.54	2.61	1.11	10	1.47	1.06
La/Gd	530	681	2468	2.38	11	5.6	5.5
Al/Si	0.86	0.42	2.02	0.46	13	0.26	0.29

to date are shown in table 1. Indeed, we see that the light rare earths (La, Cd, Nd) in the catalysts have about the same ratios among themselves as the crustal values, but that, in many of the catalysts, the light rare earths (e.g., La) are vastly enriched relative to heavy rare earths (Gd, Sm). We intend to publish a full paper on this study in the near future.

2. Compositions of Airborne Particles at Mauna Loa Observatory, Hawaii

Since 1979, our group has collected weekly samples almost continuously at Mauna Loa Observatory (MLO) in Hawaii to monitor long-term trends and identify the sources of particles in that area of the Pacific. A fairly complete set of data has existed for some time up to Jan., 1983, when eruptions of Kilauea and, later, Mauna Loa, volcanoes interrupted sample collection and analysis. During the past year, Diane Hermann has been analyzing the vast number of samples collected since that time. The

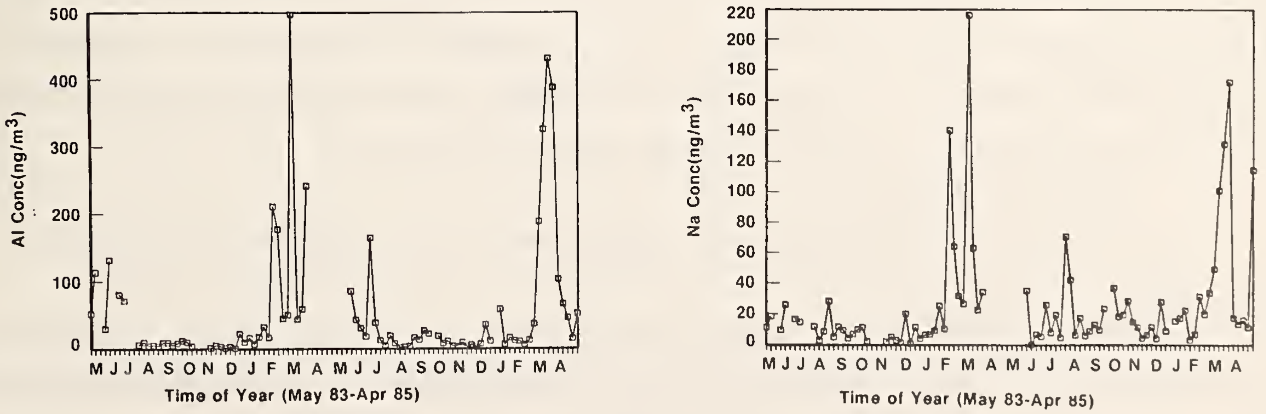

Figure 1. Atmospheric Particulate Concentrations of Al and Na at Mauna Loa Observatory, May 1983 - April 1985.

data from "shorts" INAA are now rather complete and the "longs" INAA measurements are now being made. Examples of the trends for Al and Na observed in shorts INAA are shown in figure 1. Aluminum is a good indicator of crustal dust, which shows huge increases each spring because of the transport of Asian dust from deserts in China. Sodium is a good indicator of marine aerosol. Its fluctuations are probably due to storms in the ocean. There are a number of missing values because the frequent volcanic eruptions since Jan., 1983 caused interruptions of sampling due to power outages, etc.

3. Compositions of Emissions from Volcanoes

In projects initiated by Prof. W. H. Zoller, who has moved to the University of Washington, the group has studied emissions from volcanoes for a number of years. During the past year, Olmez et al.[4] published results of their study of Kilauea volcano, for which the following is the abstract:

"During May 1983, gas and particulate samples were collected at the cooling vents of Kilauea volcano in Hawaii. Three vents on the southeast rift zone were sampled using base-treated filter packs to absorb acidic gases and Teflon filters for particles. The samples were analyzed for 40 elements by nondestructive neutron activation analysis. As with other volcanoes, the chalcophilic and volatile elements were enriched by up to seven orders of magnitude relative to erupted basalt. Unlike the case of other volcanoes, iridium was observed to be highly enriched (10^5 fold) at the two higher temperature vents, and the degree of enrichment appears to be related to both high temperatures and high fluorine content of the gases. Estimates of the emission rates of Ir during eruptions of Kilauea based on the measurements reported here and those of the Hawaiian Volcano Observatory yield an emission rate of about 3 g Ir per 10^6 m^3 of magma. This rate amounts to only about 0.3 % of the Ir present in the magma that is being released by the volcano. This previously unidentified Ir source to the atmosphere and ocean may have a significant influence on the geochemical cycle of Ir on the earth. The uniqueness of Kilauea in its emissions of Ir is probably related to the deep source of magma, which contains significant levels of Ir (0.32 ppb) and high levels of the halogens F and Cl."

4. South Pole Aerosol

The following is the abstract of a paper about to be submitted to Science by G. Tuncel and W. H. Zoller:[5]

"The average particle-borne Ir concentration in the South Pole atmosphere is $(7.3 \pm 3.1) \times 10^{-17}$ g/m^3. From this value, it is shown that the concentration of extraterrestrial material in the South Pole atmosphere is not large enough to explain the enrichments of anomalously enriched elements; however, meteoritic material contributes significantly to the observed concentrations of Co, Fe and Mn. The accretion rate for sporadic background extraterrestrial material is calculated as 11,000 tons/yr."

5. Regional Scale Receptor Modeling

The following is summarized from S. Tuncel's thesis:[6]

Samples of atmospheric particles were collected by the Environmental Protection Agency (EPA) from May, 1980 to Dec. 1981 at 3 rural sites in the Ohio River Valley (ORV): West site in KY, Center site in IN and East site in OH. All samples were analyzed by x-ray fluorescence (XRF) at EPA.[7] The XRF data and associated wind trajectories were used to select 200 of the ORV samples in the fine fraction for further analysis by INAA to provide data for about 40 species in each sample. A summary of the combined XRF/INAA data for selected elements in samples were collected from air masses arriving from the southwest is given in table 2.

Chemical mass balances (CMBs) were used to resolve elemental concentrations for each sample into 11 components: coal, oil and refuse combustion, soil and marine aerosol, emissions from refineries, motor vehicles, iron-and-steel plants, copper and cement plants, and regional sulfate. Oil emissions and soil were the least significant sources among the 11 in fine particle fractions from the ORV. On the average, 80% of the mass was explained, nearly all of it as regional sulfate. Coal emissions and regional sulfate contributed comparably to the As and Se concentrations. Of the fitted elements, Mn was the most severly underpredicted, especially at the West station. The problem is apparently caused by point sources of Mn (ferromanganese plants) at the west end of the Valley. Aside from Mn and, possibly, Mo and W, very few elements showed more than factor-of-two variations for different wind trajectory groups, ranging from those coming up the Valley to those coming from industrial cities around the Great Lakes.

During the summer of 1983, EPA, DOW and EPRI and their contractors collected ambient samples at a site near Deep Creek Lake, MD and in stacks and plumes of several coal-fired power plants upwind of the site. These samples have been subjected to XRF in other laboratories and are being analyzed by INAA by our group.

6. Analysis of Materials from the East Pacific Rise

Using INAA and PGAA we have analyzed over fifty smoker and worm tube samples from the 13° N and 21° N East Pacific Rise sites. With Dr. J. N. Valette-Silver (formerly with the Carnegie Institution of Washington and now with our group) and Dr. Jody Deming of the Chesapeake Bay Institute, the Johns Hopkins University, we have

Table 2. Concentrations of Selected Elements in Fine Fraction at Three ORV Sites in Air Masses with Southwest Back Trajectories

Element	Concentration (ng/m^3)*		
	West Site (n = 16)	Center Site (n = 14)	East Site (n = 23)
Na	110 ± 60	70 ± 40	90 ± 60
Al	180 ± 170	150 ± 120	110 ± 180
Si	570 ± 520	360 ± 240	230 ± 340
S	2500 ± 1400	4100 ± 1600	3400 ± 2600
Cl	30 ± 90	35 ± 21	50 ± 55
K	120 ± 50	115 ± 50	90 ± 65
Ca	105 ± 70	80 ± 30	55 ± 35
Sc	0.04 ± 0.04	0.03 ± 0.02	0.09 ± 0.14
V	1.4 ± 0.8	0.8 ± 0.5	0.8 ± 0.6
Mn	18 ± 17	4.7 ± 1.3	7 ± 8
Fe	140 ± 115	90 ± 50	120 ± 240
Zn	11 ± 6	14 ± 6	26 ± 19
As	0.9 ± 0.5	0.9 ± 0.4	1.4 ± 1.3
Se	1.9 ± 0.8	1.9 ± 0.7	2.0 ± 1.3
Br	4.1 ± 2.0	4.9 ± 1.5	6 ± 4
In	0.01 ± 0.009	0.01 ± 0.01	0.06 ± 0.2
Sb	0.6 ± 0.5	0.5 ± 0.2	0.6 ± 0.4
La	0.27 ± 0.25	0.2 ± 0.14	0.12 ± 0.11
Sm	0.03 ± 0.02	0.02 ± 0.01	0.014 ± 0.017
Pb	34 ± 15	53 ± 11	56 ± 22

*Uncertainties are standard deviations of a single observation

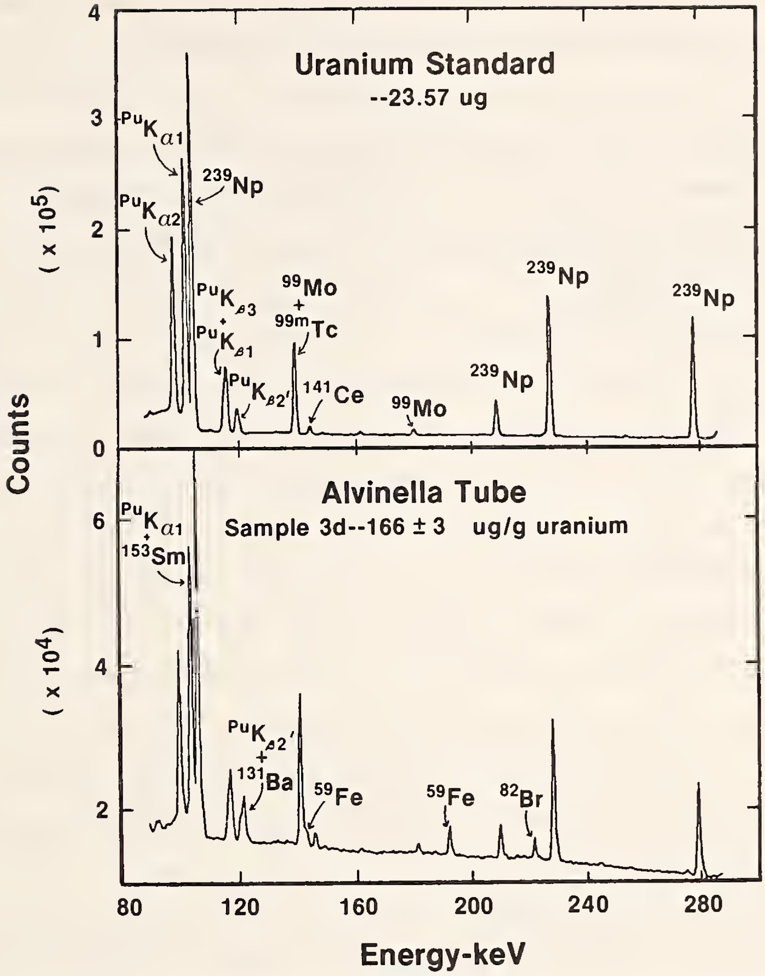

Figure 2. Gamma-Ray Spectra of (top) uranium standard and (bottom) 13°N East Pacific Rise worm tube sample following neutron irradiation.

reported[8] unusually high (up to 600 ppm) concentrations of uranium in the biogenic tube structure of Alvinella Pompejana Caudata, a small worm living in the vicinity of the hydrothermal chimneys. This enrichment may be due to either passive physical absorption or to active biochemical or microbial processes. In figure 2 are shown γ-ray spectra of one sample and a uranium standard following neutron activation. We are completing the full elemental analysis of these samples.

7. Comparison Study of Filters for Gas-Phase Sampling of the Atmosphere

We have recently completed the analysis of a series of atmospheric filter samples taken to evaluate the relative attributes of base-treated filters and activated charcoal-impregnated filters when used for gas-phase sampling. We found that the elements B, S, and As were strictly in the form of acidic species (most likely H_3Bo_3, SO_2, and As_2O_3, respectively), while Cl, Br, I, Se, Sb and Hg species were both acidic and non-acidic (organic or elemental) in nature. The charcoal filters had severe blank problems for most elements, and their large Mn content limited the INAA for short-lived irradiation products. The results of this experiment will be reported in a manuscript to be submitted to Atmospheric Environment. It is anticipated that these species may be important as "tracers of opportunity" for a number of natural or anthropogenic processes.

8. Boron and Selenium as Gaseous and Particle Tracer Elements for Coal-Fired Power Plant Emissions

As reported previously[9], gas-phase boron (as H_3BO_3) and particulate Se may be a useful tracer for SO_2 and SO_4^{2-} derived from coal-burning utilities. Figure 3 shows the correlation of these species over a period of two months at College Park, MD in 1984. Using simple input parameters (identical, evenly-spaced power plants burning "typical" coal[9,10]) and the modified (by GEG) Hybrid Receptor Model[11], we find remarkably good agreement between our data and the predicted B/SO_2, S/Se, and S(p)/S(g) ratios (table 3). We are working to refine the input parameters to better represent the coal-related emissions for the Ohio River Valley. We are also collecting particles, acidic gas-phase species, and rainfall at College Park, MD in order to complete a continuous year-long data set. We hope to use the data to unravel some of the details of the wet deposition of the sulfur species.

9. Ultrafine Particle Generation

In part of the work being done under funding from the Electric Power Research Institute, we (with Dr. Willliam R. Kelley of NBS) are experimenting with various techniques for generating ultrafine tracer particles to be used in source tagging experiments. In these experiments, ultrafine particles of K, Mn, and Nd are made

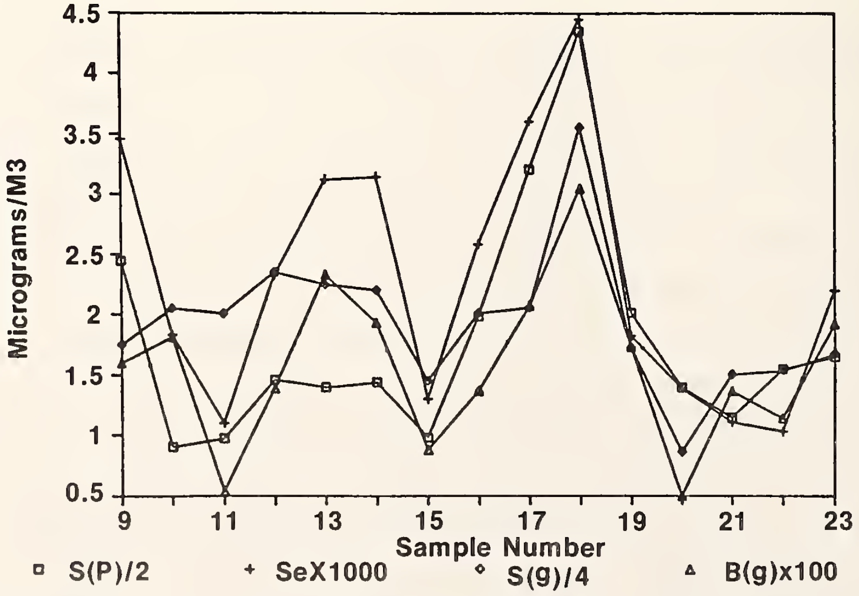

Figure 3. Concentrations of particulate S and Se and gas-phase S and B at College Park, MD.

Table 3. Comparison of Hybrid Receptor Model with Observed Concentrations at College Park, MD (CP) and Wallops Is., VA (WI).

	Concentration Predicted at Distance (km)				Observed CP (May and June)	Observed WI (July)
species	100	700	1000	1800	15 samples	12 samples
gases						
SO_2 ($\mu g/m^3$)	16	27	28	0.2	16 ± 5	8.1 ± 4.9
B ($\mu g/m^3$)	12	22	23	0.53	16 ± 7	70 ± 50
particles						
SO_4^{-2} ($\mu g/m^3$)	1.0	14	19	11	11 ± 5	13.2 ± 7.5
Se (ng/m^3)	0.7	2.5	3.0	1.0	2.3 ± 1.1	1.76 ± 0.91
ratios						
S(p)/S(g)	0.04	0.35	0.46	26.0	0.46 ± 0.21	1.20 ± 0.38
B(g)/SO_2 x 1000	0.75	0.81	0.82	1.80	1.00 ± 0.42	7.9 ± 2.7
S(p)/Se(p)	570	1900	2100	3100	1560 ± 680	3040 ± 770

either by combustion or by dispersing dilute solutions of the tracer materials with air atomizing nozzles. Size distributions of the residue aerosols are measured with a mobility analyzer. To provide a check on the mobility analyzer, we are using a five-sage micro-orifice impactor (MOI) with cut points at 1.03, 0.53, 0.142, 0.083, and 0.037 µm. Total tracer-particle mass is also being measured with a 47 mm filter sampler. Tracer particle mass on the filter and MOI samples is determined by measuring K, Mn, or Nd by INAA.

In table 4, we compare cumulative mass data obtained with the MOI with those inferred from the mobility measurements for a run in which a 3 ppm Mn solution in absolute methanol was aspirated into an air-atomizing nozzle at an air pressure of 1,585 kPag. About 66% of the mass was collected on the backup filter of the impactor and is, therefore, less than 37 nm. The mobility data, including the CNC measurement of particles less than 10 nm, suggest that at most 40% of the mass is accounted for by particle less than 37 nm. The data would agree if the average efficiency of the mobility analyzer for particles would account for 25% of the mass. This is quite likely since it is known that the mobility analyzer is only 3% efficient for 3 nm

Table 4. Comparison of cumulative mass distributions obtained with an MOI and DMPS system for the Sonicore and SSC-1 nozzles, percent less than stated size.

Sonicore nozzle				SSC-1 nozzle			
DMPS		MOI		DMPS		MOI	
diam. nm	mass <size, %	diam. nm	mass <size, %	diam. nm	mass <size, %	diam. nm	mass <size, %
10.49	6.2	37	66.2	10.49	5.0	37	65.5
11.49	7.0	83	67.6	11.49	5.6	83	67.2
12.96	7.8	142	90.4	12.96	6.4	142	97.7
15.43	9.1	530	98.2	15.43	7.7	530	99.5
17.97	11.2	1030	99.6	17.97	9.7	1030	-
20.45	14.1			20.45	12.4		
23.45	18.1			23.45	15.8		
26.93	23.3			26.93	20.2		
31.40	29.8			31.40	26.2		
36.41	38.2			36.41	34.7		
41.89	47.2			41.89	45.1		
48.37	56.9			48.37	58.6		
55.86	66.4			55.86	73.6		
64.81	74.1			64.81	85.7		
75.30	80.6			75.30	94.7		
86.79	85.7			86.79	99.5		
99.75	89.7			99.75	100.0		
115.19	92.6			115.19	100.0		
133.16	94.9			133.16	100.0		
153.61	96.9			153.61	100.0		
177.99	98.5			177.99	100.0		
205.99	100.0			205.99	100.0		
237.39	100.0			237.39	100.0		

particles. However, we are cautious in accepting the impactor data because of the possibility that the mass on the backup filter may include some larger particles as the result of particle bounce. Transmission electron microscopy measurements in progress may tell us whether or not particle bounce is important. However, we are making additional measurements with the impactor with He as a diluent to reduce the impaction cut points, and plan other measurements with a parallel diffusion battery. INAA is ideal for these studies because of its excellent sensitivity for the tracer elements.

---

1. I. Olmez and G. E. Gordon, Rare Earths: Atmospheric Signatures for Oil-Fired Power Plants and Refineries, Science 229, 966-968 (1985).

2. K. H. Wedepohl, in Origin and Distribution of the Elements, L. H. Ahrens, ed. (Pergamon Press, London, 1968) pp. 999-1016.

3. S. R. Taylor, Abundance of Chemical Elements in the Continental Crust: A New Table, Geochim. Cosmochim. Acta 28, 1273 (1972).

4. I. Olmez, D. L. Finnegan and W. H. Zoller, Iridium Emissions from Kilauea Volcano", J. Geophys. Res. 91, 653-663 (1986).

5. G. Tuncel and W. H. Zoller, Iridium Concentrations in the South Pole Aerosol: Estimation of Meteoritic Component, Science (to be submitted).

6. S. G. Tuncel, Regional Scale Receptor Modeling in the Northeast U.S., Ph.D. thesis, Department of Chemistry and Biochemistry, University of Maryland, College Park, MD 20742.

7. R. W. Shaw, Jr. and R. J. Paur, Atmos. Environ. 17, 2031 (1983).

8. J. N. Valette-Silver, A. Bates, D. Anderson, J. Deming, and W. H. Zoller, Uranium Enrichments in Smoker Material Collected for the East Pacific Rise, 1985 Annual Meeting, American Geophysical Union, Seattle, WA.

9. M. E. Kitto and D. L. Anderson, Simultaneous Collection of Particles and Gases from Coal-Fired Power Plants, National Meeting of the American Chemical Society, New York, NY (1986).

10. G. E. Gordon and I. Olmez, in APCA Specialty Conference on Receptor Methods for Source Apportionment: Real World Issues and Applications, Williamsburg, VA 1985.

11. C. W. Lewis and R. K. Stevens, Atmos. Environ. 19, 917 (1985).

PRECISION IN ROUTINE I.N.A.A. OVER A TWO YEAR PERIOD AT THE NBSR

M. J. Blackman
(Smithsonian Institution, Washington, D.C.)

Beginning in June 1984 and continuing to date, alliquots of SRM 679 - Brick Clay have been included as a check standard in 61 separate irradiations of archaeological ceramics. The goals of the analysis of the ceramics were to routinely analyze a large number of samples (1100) for as many elements as possible (32 sought) with as much precision as possible. Working within these constraints, irradiations and counting times could not be tailored to specific elements.

The irradiations were carried out with reactor power at 10 MW in the RT-3 pneumatic facility and with reactor power at 20 MW in the RT-1 and RT-4 pneumatic facilities. The length of the irradiations were varied in accordance with the neutron flux in each facility so that the fluence was approximately the same. Samples and standards, in .5 ml polyethylene microcentrifuge tubes, were packed in a single band in the "rabbit" to minimize linear flux gradients. No special attention was given to the placement of standards or check standards within the band, and therefore any radial flux variation was not controlled. The gamma counting was carried out on two different detectors with similar resolution, but quite different counting efficiencies (8.3% vs. 34.8%). Two different automated sample changers were used, one with a fixed geometry of 10 cm and the other with variable geometry. Each sample was counted twice, the first count after a 5 day decay and the second after at least a 30 day decay. The counting times were varied according to the detector efficiency and the sample to detector geometry so that the counting statistics were approximately equal for each element determined in each aliquots.

Initially about 10 grams of SRM 679 was dried for 24 hours at 110° C and cooled and stored in a dessicator. Fifty four nominal 100 mg. aliquots were weighed as needed over the two year period, in addition, seven nominal 40 mg. alloquits were also analyzed in separate irradiations. The initial stock of SRM 679 was periodically redried. During this period at least three different balances were used for weighing.

SRM 1633 (coal flyash) was the comparitor standard used to quantify 23 elements in SRM 679. Table 1. lists the elements sought, their radionuclides, associated gamma energies, and the concentration values used for the standard. Commercially available computer software was used to process the gamma ray data with several upgrades and a shift in computer systems occurring during the duration of the experiment. In summary, while the requisite care in accordance with good analytical

Table 1. Experimental Parameters

Elements	Nuclide	Gamma Ray Energy (keV)	Concentrations in SRM1633 Standard	Count
Na	Na-24	1369	0.32% *	1
K	K -42	1525	1.61% *	1
Ca	Ca-46	1296	4.70% *	1
Sc	Sc-46	889	27.0 ppm *	2
Cr	Cr-51	320	131 ppm #	2
Fe	Fe-58	1099 & 1292	6.20% *	2
Co	Co-60	1173 & 1333	41.5 ppm *	2
Zn	Zn-65	1115	213 ppm	2
As	As-76	559	61.0 ppm #	1
Rb	Rb-86	1077	125 ppm *	2
Sb	Sb-122	564	6.9 ppm *	1
Cs	Cs-134	796	8.6 ppm *	2
Ba	Ba-131	496	2700 ppm *	1
La	La-140	1596	82.0 ppm *	1
Ce	Ce-141	145	146 ppm *	2
Sm	Sm-153	103	12.9 ppm	1
Eu	Eu-152	1408	2.5 ppm *	2
Tb	Tb-160	879	1.9 ppm *	2
Yb	Yb-175	396	6.4 ppm	1
Lu	Lu-177	208	1.0 ppm *	1
Hf	Hf-181	482	7.9 ppm *	2
Ta	Ta-182	1221	1.8 ppm *	2
Th	Pa-233	312	24.8 ppm *	2
U	Np-239	106	11.6 ppm #	1

* Ondov, J.M., Zoller, W.H., Olmez, I., Aras, N.K., and Gordon, G.E. Analytical Chemistry, vol 47, pp. 1102-1109, 1975.

\# Certificate of Analysis, SRMs 1632 and 1633, OSRM, National Bureau of Standards, Department of Commerce, Washington, D.C. 20234.

Table 2. SRM679 BRICK CLAY: NOMINAL 100 MILLIGRAM SAMPLES

	Na PCT	K PCT	Sc PPM	Cr PPM	Fe PCT	Co PPM	Zn PPM	As PPM
Number Averaged	54	52	54	54	54	54	53	54
Mean Conc.	0.135	2.28	22.8	108	8.91	26.5	129	9.80
Group Sigma (%)	2.4	8.3	1.4	3.0	2.9	1.6	3.3	6.0
Counting Error (%) (single sample)	0.8	3.5	0.1	1.8	0.2	0.5	2.7	4.3
Upper 95% Limit	0.142	2.66	23.5	114	9.42	27.3	138	11.0
Lower 95% Limit	0.129	1.90	22.2	101	8.40	25.6	121	8.6

	Rb PPM	Sb PPM	Cs PPM	Ba PPM	La PPM	Ce PPM	Sm PPM	Eu PPM
Number Averaged	54	54	54	54	54	54	54	54
Mean Conc.	225	0.97	9.63	454	56.4	102	9.06	1.68
Group Sigma (%)	9.3	9.9	2.7	12.9	1.4	1.9	1.6	2.1
Counting Error (%) (single sample)	5.0	8.2	1.9	10.5	0.3	1.2	0.3	1.4
Upper 95% Limit	267	1.16	10.2	572	57.9	106	9.35	1.75
Lower 95% Limit	184	0.78	9.1	337	54.8	99	9.77	1.61

	Tb PPM	Yb PPM	Lu PPM	Hf PPM	Ta PPM	Th PPM	U PPM
Number Averaged	53	54	54	54	53	54	53
Mean Conc.	1.21	4.07	0.62	4.59	1.21	14.3	2.25
Group Sigma (%)	13.0	4.8	6.6	3.5	6.8	2.2	15.9
Counting Error (%) (single sample)	10.0	3.2	4.8	2.7	6.4	1.6	13.3
Upper 95% Limit	1.52	4.46	0.70	4.91	1.37	14.9	2.97
Lower 95% Limit	0.89	3.69	0.53	4.27	1.04	13.7	1.53

Table 3. SRM679 BRICK CLAY: NOMINAL 40 MILLIGRAM SAMPLES

	Na PCT	K PCT	Sc PPM	Cr PPM	Fe PCT	Co PPM	Zn PPM	As PPM
Number Averaged	7	7	7	7	7	7	7	7
Mean Conc.	0.138	2.38	23.2	108	9.17	26.9	130	9.69
Group Sigma (%)	1.9	12.4	2.4	2.4	3.0	3.4	4.2	6.6
Counting Error (%) (single sample)	2.9	15.6	0.1	1.4	0.2	0.4	2.2	12.8
Upper 95% Limit	0.144	3.10	24.6	114	9.84	29.1	143	11.3
Lower 95% Limit	0.131	1.66	21.9	102	8.49	24.6	116	8.11

	Rb PPM	Sb PPM	Cs PPM	Ba PPM	La PPM	Ce PPM	Sm PPM	Eu PPM
Number Averaged	7	7	7	7	7	7	7	7
Mean Conc.	214	0.93	9.70	468	56.2	105	9.09	1.71
Group Sigma (%)	10.5	10.6	4.0	11.4	1.2	2.2	1.1	1.7
Counting Error (%) (single sample)	5.1	2.8	1.4	6.3	0.4	0.7	0.6	1.4
Upper 95% Limit	269	1.18	10.6	599	57.8	110	9.33	1.78
Lower 95% Limit	159	0.69	8.7	337	54.6	99	8.85	1.64

	Tb PPM	Yb PPM	Lu PPM	Hf PPM	Ta PPM	Th PPM	U PPM
Number Averaged	7	7	7	7	7	7	6
Mean Conc.	1.22	4.29	0.61	4.63	1.30	14.7	2.13
Group Sigma (%)	11.3	8.3	9.0	3.9	7.7	2.9	21.5
Counting Error (%) (single sample)	8.2	4.3	8.0	2.3	7.0	1.3	7.6
Upper 95% Limit	1.56	5.17	0.75	5.07	1.55	15.8	3.30
Lower 95% Limit	0.89	3.42	0.48	4.19	1.06	13.7	0.95

procedures was taken for each analysis, there was a great deal of variability in irradiation facilities, counting equipment, and processing software. The data set for SRM 679 ought then to provide a baseline for analytical precision in instrumental neutron activation analysis over time at a single facility.

Table 2. shows the results of 54 analyses of nominal 100 mg. samples. Of the 23 elements quantified in SRM 679, over half (14) have a precision of better than 5% (1 standard deviation), with five elements better than 2% precision. Only three elements had precisions worse than 10% Ba - 12.9%, Tb - 13.0%, and U - 15.9%. Typical counting statistics for each of these elements in SRM 679 are: Ba - 10.5%; Tb - 10.0%; and U - 13.3%. For these three elements all but about 2 to 3 % of the sample variance can be attributed counting error. When the elements with very low counting errors (Sc, Co, La, and Sm) are examined, the sample variance not attributed to counting error is 1 to 1.5%. All random and systematic errors, exclusive of counting error, appear therfore, to contribute only about 1.5% to the sample variance, this includes potential sample inhomogeneity.

Table 3. shows the results of the 7 analyses of nominal 40 mg. samples. When these results are compared to those for the nominal 100 mg samples, the concentrations for all 23 elements fall within 1 standard deviation in the two sets. The implication is that to within about 1.5% to 2.0%, 40 mg. aliquots of SRM 679 and the standard SRM 1633 are both homogeneous and directly comparable to 100 mg. aliquots.

Examination of these two data sets shows that for a large number of elements instrumental neutron activation analysis can routinely achieve better than 5% precision regardless of changes in irradiation facilities, instrumentation, and computer processing software. With some special effort at tailoring irradiation and counting times to the nuclides displaying less precision, precision of better than 5% could be achieved routinely for all 23 elemental concentrations reported here.

NEUTRON DEPTH PROFILING AT NBS

R. G. Downing J. T. Maki, and R. F. Fleming
(Center for Analytical Chemistry)

The neutron depth profiling facility has been involved in a number of industrial and basic science activities over the last year. Over twenty academic and industrial scientists are collaborating with NBS through the use of NDP on modern material problems of mutual interest. Several of the companies have established direct computer links with our computers to facilitate the analysis of data.

Oxygen was nondestructively and quantitively profiled by NDP in a thin metal oxide film for the first time this year. Scientists from Eastman Kodak prepared the film from enriched oxygen-17 gas. Oxygen-17 has a relatively small neutron cross section for the emission of an energetic alpha particle, making it particularly difficult to profile. Elements such as oxygen, chlorine, and nitrogen would be profiled more routinely with the installation of the proposed cold neutron guide hall.

The metal oxide film and several thin boron implanted glass films were taken to the Institute Max von Laue-Paul Langevin (ILL) for study during the summer. Working with R. Henkelmann of Garching, Germany, the ILL depth profiling facility and the NBS facility have been cross calibrated. The ILL NDP facility is stationed on a thermal guide tube and consequently has significantly lower background than the NBS thermal beam. As a result, experiments were carried out at ILL to look at deeper elemental profiles as well as at elements which have lower-energy, charged particle emission.

Other work includes the completion of a study of helium release from single crystal nickel. This project culminates the thesis research work of J. T. Maki from the Nuclear Engineering Department at the University of Michigan, Ann Arbor. Two research papers are being submitted from work on boron implantation and diffusion in infrared detector materials. This research is through a joint project with Aerospace Corp., Los Angeles, CA. Also, the first profiles of lithium diffusion on a few minute time scale were made during the last year. Diffusion constants were derived for several compositions of polymer films without the typical destructive analysis. The polymer work has been carried out at the initiation of scientists from the Polymers Division at NBS.

Finally, the facility itself is evolving to meet the increasing work load. A turbomolecular vacuum pump was installed to increase system reliability and to reduce down time between samples. Two rotational sample stages were acquired which will be installed in the NDP target chamber. The stages will allow precise alignment of sample-to-detector geometry. This in turn will result in increased depth resolution in the profiles of certain types of samples. Further improvements in the facility are being developed to handle the increasing variety of measurements and experiments performed by NDP.

CALIBRATION OF A NEUTRON DRIVEN GAMMA RAY SOURCE

T. G. Williamson
(University of Virginia, Charlottesville, Virginia)

and

G. P. Lamaze, D. M. Gilliam and C. Eisenhauer
(Center for Radiation Research)

Cadmium and iron cylinders in the thermal column cavity of the National Bureau of Standards Reactor (NBSR) provide intense sources of capture gamma rays. The neutron and gamma ray fields in these cylinders have been measured and the fields used for photofission measurements. The thermal column cavity is a 0.3 m diameter spherical cavity in the graphite thermal column of the NBSR. The capture gamma ray sources are horizontal cylinders located so that the cylinder center is near the center of the cavity.

The cadmium capture gamma ray source is an extruded cadmium cylinder 1 mm thick and 55 mm diameter with a 1 mm thick cadmium cap on the end closest to the reactor. The cadmium cylinders can be enclosed in a 6.4 mm sheath of lithium glass to eliminate the cadmium capture gamma rays and to measure the background of gamma rays from the core and from neutron capture in the surrounding graphite. A lithium glass labyrinth in the cylinder away from the core minimizes streaming from scattered radiation.

The iron cylinder was machined from carbon steel containing 0.2% carbon. Other constituents measured by NAA include manganese, 0.7%, chromium 0.08%, arsenic, 0.005%, copper, 0.012%, and antimony, 0.0017%. The cylinder was tapered to fit in the spherical cavity with the following dimensions:

Inner radius	37.5 mm
Outer radius	47.0 mm
Length	
maximum	234 mm
miminum	215 mm

Eight 3 mm diameter aluminum rods were fastened to the iron to support it in the graphite cavity. During irradiations a 3 mm aluminum sleeve and 6.4 mm of lithium glass fit inside the cylinder to minimize the thermal neutron fluence in the cylinder (figure 1). The lithium glass cylinder has a lithium glass end cap on the reactor end and a labyrinth in the cylinder away from the core to minimize streaming of scattered neutrons.

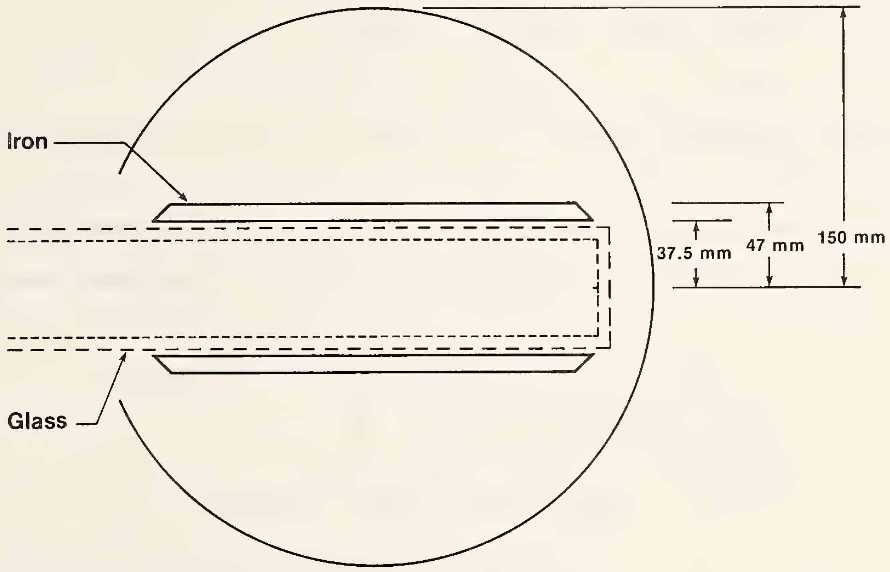

Figure 1. Iron cylinder in thermal column cavity

The neutron fluence at the surface of the cylinders was measured by exposing dilute gold foils on the exterior of the cylinders and also by direct counting of the activated cylinders in collimated geometry. Foils were taped to the outer radius of each cylinder equally spaced around the circumference at the center and at each of the ends. The foil activities were measured with a calibrated germanium detector. For both cylinders the top to bottom variation at each of the three axial positions was less than 10% and the right-to-left variation less than 3%. The ratio of the foil activity at the end away from the reactor to that at the end nearest to the reactor was 0.67 for both cylinders. The thermal neutron fluence rate at the outer radius and axial center of the iron cylinder is 1.42×10^{11} n/cm^2-s and on the cadmium cylinder 4.83×10^{10} n/cm^2-s.

The gamma ray distribution along the axis is calculated for a cylindrical shell source. For a source distribution which varies linearly along the cylindrical axis, z, the source term is

$$S(z) = S(1 + az)$$

S is the gamma ray source - photons/cm^2-s

a is the slope of the distribution.

With the origin of the z axis at the center of the cylinder and S the source strength at $z = 0$, the distribution is the following

$$\Phi/S = 1/2 \{ARCTAN(Z1/R) + ARCTAN(Z2/R)\} \text{ for the constant term}$$

and

$$\Phi/S = (Ra/4)\ LN\ \{(Z1^2 + R^2)/(Z2^2 + R^2)\} \text{ for the linear term,}$$

where $Z1 + Z2 = L$, the cylinder length, and R is the cylinder radius.

With attenuation of photons in the cylinder the uniform term becomes

$$\Phi/S = (1/2)\ EXP(-b)\ \{K(\Theta1,b) + K(\Theta2,b)\}$$

b is attenuation length - μt

K line source attenuation function

$\Theta1$ and $\Theta2$ angles from a point on axis to the cylinder ends.

The cadmium cylinder has a cadmium cap on the end nearest to the reactor which provides an additional gamma ray source. The axial distribution of gamma rays from this source is

$$\Phi/S1 = (1/4)\ LN\ \{1 + (R^2/Z3^2)\}$$

S1 is source at the end cap - photons/cm^2-s

Z3 is the distance from the end.

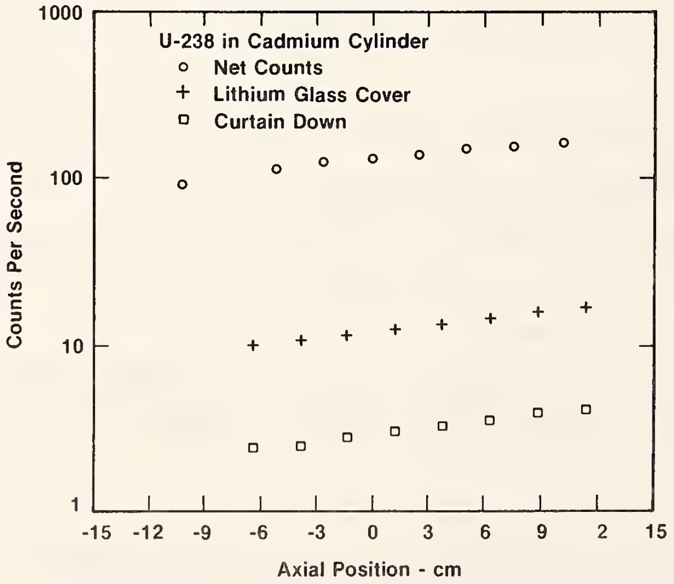

Figure 2. U-238 in cadmium cylinder

For cadmium the axial gamma ray distribution was calculated by approximating the gamma ray source as a cylinder at the outer cadmium surface with no attenuation of the photons through the cadmium or the aluminum support cylinder.

For iron a one dimensional radiation transport calculation in cylindrical geometry (ANISN) was done to obtain the radial distribution of thermal neutrons and of capture photons. The location of the radial averaged thermal neutron fluence was chosen as the location of a shell source of photons and the photons were attenuated by material between this shell and the center of the cylinder. The iron capture gamma ray spectrum contains photons at all energies up 9 Mev, however, about 35% of the gamma rays are in the energy interval from 7 to 8 Mev. The threshold for photofission in the isotopes in this investigation is about 6 Mev. Thus the attenuation coefficient for this calculation was that at 7.0 Mev for iron, aluminum and pyrex glass. The attenuation length from a shell at 43 mm, the location of the average thermal neutron fluence, to the cylinder center is $\mu t = 0.2$. Of this attenuation length, 67% is in iron, 22% in glass and 11% in aluminum. These values were used to calculate the distribution of the capture gamma ray intensity along the cylindrical axis relative to the photon source strength.

Photofission measurements were made with NBS miniature fission chambers. Paired fission chambers were placed in the cylinders so that fission count rates could be taken at various positions along the cylindrical axis. The chamber designations and material masses are tabulated below:

Chamber	Designation	Mass
U-238	HD-5-2	691.1 ± 1.3% μg
U-235	S-002-1	1.921 ± 0.6% μg
Th-232	L-5-2	603.5 ± 2.0% μg
Np-237	S-2-2	260.6 ± 1.2% μg

Measurements were taken with the boral curtain up and down, and for the cadmium cylinder, with and without the lithium glass cover. Data for U-238 in cadmium are shown in Figure 2. The response with the boral curtain down is about 2% of the response with the bare cadmium cylinder and the response with the lithium glass cover about 10%. The lithium glass data was used as background to obtain the net response to the cadmium capture photons.

The calculated and measured distributions for Th-232 is shown in Figure 3. The value of the parameter a, the slope of the linear term, was adjusted to give the best fit of the calculated distribution to the measured distribution for a span of 60 mm on either side of the center of the cylinder (the 5 measured points nearest the

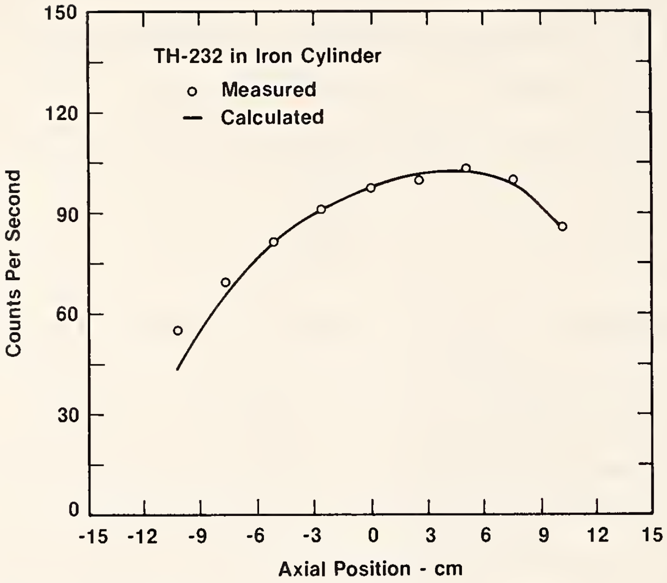

Figure 3. Th-232 in iron cylinder

center). The measured quantity is fissions per second (cps) per atom and the calculated quantity is the capture gamma ray fluence rate. The ratio of these values is photofission cross section. Cross sections calculated from the detector foil masses and the ratio of the measured to the calculated distributions averaged over the center five points are tabulated below:

	Photofission Cross Section - mb	
	Cadmium	Iron
U-238	0.28	2.90
Th-232	0.14	1.43
Np-237	0.66	7.47

These are spectrum averaged cross sections for the cadmium capture gamma ray spectrum and for the iron capture gamma ray spectrum respectively.

In the cadmium cylinder the photon fluence rate at the center is 2.4×10^{11} photons/cm^2-s and the dose rate 0.83 Mrads/h (8300 Gy/h) and in iron the photon fluence rate is 4.8×10^{10} photons/cm^2-s and dose rate 0.36 Mrads/h (3600 Gy/h). The fast neutron fluence rate at the center measured with Ni (n,p)Co is 2.3×10^{5} neutrons/cm^2-s.

C. REACTOR OPERATIONS AND SERVICES

REACTOR OPERATIONS AND SERVICES

T. Raby

The past year was the first full year of operation at the higher power level of 20 MW, double the previous power level. The new power level proved very successful and in general operations were routine and smooth.

1. Reactor Operations

Reactor operation was continuous over the last year except for periods of refueling and maintenance. A summary of the operating statistics for the period July 1, 1985 to June 30, 1986 is presented in the following table:

No. of days at 20 MW	285
On-line time at 20 MW	78%
Average U-235 burnup	64%
No. of Irradiations	2080
Hours of Irradiations	3577
Hours per Irradiation	1.7

2. Irradiation Services

Extensive irradiation services were provided to many users from within and outside NBS. In all, more than 2000 irradiations involving thousands of samples were performed.

ENGINEERING SERVICES

J. Nicklas

In addition to normal engineering and design services provided to reactor operations, experimenters and users, the engineering staff is involved in a continuing effort to upgrade the reactor instrumentation in addition to normal surveillance calibrations.

The shim arm test assembly used for testing shim arm mechanisms and clutch release assemblies is about finished and is available for spare parts for reactor shim arms.

Fifty fuel assemblies have been inspected and accepted from the DOE contractor by the NBSR staff. An additional 25 fuel assemblies have been fabricated and are awaiting acceptance. Fuel compacts now being made contain 350 gms per element, a change from 300 gm elements. The first 200 plates of the 350 gm elements will be radiographed to determine that the process is under control.

The full element handling tool heads have been modified slightly by adding another spring pin to the mounting block which bears on the lifting shaft to increase its resistance to rotation. This resistance will assure locking of the element to the upper grid and provide operators with a more positive feel when transferring fuel. A new tool for the transfer of fuel from the reactor core to the storage pool was made and tested.

A method has been developed to plug heat exchanger tubes with rubber plugs. The previous method of pounding metal plugs into the tubes required entry into the bonnet with subsequent high radiation exposure to personnel and was limited to personnel that could enter a 12 inch manhole.

A tool for pulling the fuel transfer arm bearings has been designed and fabricated. The original carbon steel bearings are causing an occasional sticking of the transfer arms which causes some loss of feel when transferring fuel.

The second tritium monitor has been installed, tested and completed. Two more modern design differential transmitters have been installed in the process demineralized water system.

The instrument group has also provided assistance to the experimental researchers with electronics repair, modification and interface designing. An uninterruptible power supply system was planned, purchased and installation is underway at this time. The UPS system will provide continuous clean power to the experimental computer and associated instrumentation during brief power interruption.

An instrumentation panel for monitoring the Cryogenics Bismuth Tip experiment facility is in the assembly and testing stage.

D. SERVICE PROGRAMS

NEUTRON ACTIVATION ANALYSIS AT THE FOOD AND DRUG ADMINISTRATION

W. C. Cunningham and W. B. Stroube, Jr.
(U.S. Food and Drug Administration, Washington, DC)

The Food and Drug Administration (FDA) maintains a neutron activation analysis (NAA) facility in the reactor building of the National Bureau of Standards (NBS). The NAA program at FDA includes analytical support for regulatory activities and special projects as well as applications research. NAA complements the other analytical techniques used at FDA and serves as a reference technique for quality assurance practices.

During the past year the NAA laboratory of FDA was involved in many areas including regulatory analysis, methods development and applications research. In regulatory work, both radiochemical and instrumental NAA were used as reference techniques, providing broad-based multielement information. Methods development and applications research were performed as part of an ongoing FDA effort to improve its ability to protect the public. In one area the FDA NAA facility applied its various procedures to the analysis of food supplements, mineral supplements and herbal products. This work will enable the FDA NAA facility to react more quickly when these products must be analyzed. Radiochemical research included tracer experiments designed to discover the mechanisms responsible for chromium losses that occur during various digestion procedures.

Epithermal neutron activation analysis (ENAA) applied to food matrices has been a joint ongoing project between the FDA Elemental Research Section and the NBS Nuclear Methods Group. Early work on applying ENAA to the determination of iodine in infant formula demonstrated the usefulness of the technique for food analysis.[1] As the scope of the project increased, two other research reactors, located at the University of Virginia and at the University of Maryland, were used to show the utility of the technique. This year ENAA studies were expanded to include a wide variety of food matrices. This work was presented at the 7th International Meeting on Modern Trends in Activation Analysis (MTAA)[2]. As evidenced by the high interest industry has shown in this procedure, the work has met a clear analytical need. Several small reactors are now offering ENAA services that are based on the methodology developed under this project.

---

1. W. B. Stroube, Jr. and G. J. Lutz, in Production, Regulation and Analysis of Infant Formula, Association of Official Analytical Chemist, Arlington, VA, 1985, p.424.

2. William B. Stroube, Jr. and George J. Lutz, Proceedings of the 7th MTAA, 1986, J. Radioanal. Chem., in press.

PURIFICATION OF REACTOR-PRODUCED FLUORINE-18 FLUORIDE USING HIGH PRESSURE ION CHROMATOGRAPHY

J. M. Bennett, M. A. Channing, and R. D. Finn
(National Institutes of Health, Bethesda, MD)

Reactor-produced F-18 labeled fluoride is an important alternative for facilities which do not have access to a particle accelerator. Fluorine-18 can be prepared via a two-step nuclear reaction:

$$^{6}\mathrm{Li}(n,\alpha)^{3}\mathrm{H} \text{ and } ^{16}\mathrm{O}(^{3}\mathrm{H},n)^{18}\mathrm{F}$$

In our experiments two quartz tubes (3 mm i.d. x 90 mm) containing 0.4 g of 95.56% enriched $^{6}Li_2CO_3$ have been irradiated for 2 hours at a thermal flux of 1.3 x 10^{14} n cm^{-2} sec^{-1} at the National Bureau of Standards Nuclear Reactor. Typically, 170 mCi of fluorine-18 is produced concurrently with 60 mCi of tritium (EOB). A method has been developed utilizing high performance ion chromatography (HPIC) to not only separate, but isolate and purify the fluorine-18 species as its tetramethylammonium salt. Potential sources of cationic and anionic contaminants have been identified and examined by analytical HPIC, while radionuclidic impurities have been determined using gamma spectroscopy and scintillation counting.

The reactivity of the final reagent fluoride was determined by monitoring its incorporation as fluorine-18 labeled 2-fluoro-2-deoxy-D-glucose upon reaction with methyl 4,6-O-benzylidene-2, 3-cyclic sulfato-β-D-mannopyranoside.

Radionuclide purity from gamma-emitting contaminants was ascertained by gamma spectrum analysis with a hyper-pure germanium detector in conjunction with a Nuclear Data 683 series programmable MCA/computer system. The product had no detectable gamma activity after purification other than the 511-KeV gamma peak of F-18.

Radionuclide purity from tritium and other beta-emitting contaminants was checked with a Beckman LS 5800 liquid scintillation counter after the decay of F-18 was virtually complete. The tritium activity in the final product represents an average of 14 ± 1.6 µCi in a final volume of 20 mL containing 6.1 ± 1.8 mCi of F-18 activity (Table 2). This value of ^3H is well within the maximum permissable body burden.

Conclusions

- Utilization of strong anion exchange (SAX) chromatography for trapping F-18-fluoride eliminated interfering cationic and anionic species and also lowered the tritium by-product to a permissable level.

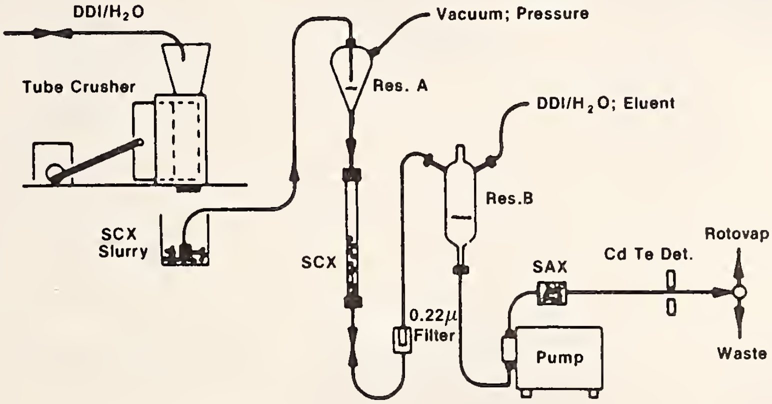

Figure 1. Reactor-produced F-18 fluoride purification apparatus.

- Although neutron bombardment of trace impurities present in lithium-6 enriched lithium carbonate ($^6Li_2CO_3$) may produce a variety of radionuclides, examination of the final reagent mixture by beta and gamma spectroscopy showed only the expected fluorine-18 and tritium to be present.
- Starting with approximatley 90 mCi of $^{18}F/^6Li_2CO_3$ and after a 70 min. purification typically, 40 mCi (uncorrected) of the TMAOH/TMAF ^{18}F-fluoride reagent was produced. This reagent effected incorporations of ≧ 95% upon reaction with methyl 4, 6-O-benzylidene-2, 3-cyclic sulfato-B-D-mannopyranoside.

E. PERSONNEL ROSTER

REACTOR RADIATION DIVISION

460

R. S. Carter, Chief
T. M. Raby, Deputy Chief
*E. C. Maxwell, Admin. Officer
*S. E. Tassey, Secretary
S. C. Shatzer, Clerk-Typist

Neutron Radiography
M. Ganoczy
#T. Cheng

Division Staff
R. Casella
B. Mozer
F. Shorten

Cold Neutron Program
J. M. Rowe (3/4)
#I. Anderson
C. Glinka (3/4)
+M. Kahn
P. Kopetka
I. Schroder
T. Udovic
R. Williams
*G. Greene
W. Knill (1/2)
#H. Stanley

REACTOR OPERATIONS
T. M. Raby, Chief
J. F. Torrence, Deputy Chief
C. Harrison, Secretary

Reactor Operators
R. Beasley
M. Bell
N. Bickford
J. Clark
F. Clark
H. Dilks
L. Lindstrom
M. McDonald
W. Mueller
T. Myers
J. Ring
R. Sprow
R. Stiber
A. Toth
D. Wilkison

ENGINEERING SERVICES
J. H. Nicklas, Chief
C. Harrison, Secretary

Mechanical Design
E. Guglielmo
J. Sturrock

Electronics
R. Conway
R. Hayes
L. Shuman

NEUTRON CONDENSED MATTER SCIENCE
J. J. Rush, Chief
M. Clark, Secretary
+L. Clutter, Secretary

Crystallography
E. Prince
A. Santoro
#C. Choi
#V. Himes
J. LaRock (1/2)
A. Mighell
W. Rymes (1/2)
#J. Soubeyroux
*J. Stalick
#F. Beech

Metal Hydrides and Molecular Materials
D. Fravel (1/2)
#H. Prask
J. Rowe (1/4)
W. Rymes (1/2)
#H. Savage
#S. Trevino
#J. Nicol

Magnetic and Amorphous Materials
J. Rhyne
#J. Fernandez-Baca
°R. Erwin
#T. Giebultowicz
*J. Lynn
#P. Mangin
#M. Spano
W. Knill (1/2)
#Y. Yu

Advanced Neutron Methods
N. Berk
D. Fravel (1/2)
C. Glinka (1/4)
J. Gotaas
#S. Krueger
J. LaRock (1/2)

*Part-time
+WAE, Coop, Intermittent
#Guest Scientist, research assoc. (Full Time)
°Post-doc

NON-RRD NBS STAFF LOCTED AT REACTOR

Division 354

D. Brown
C. Campbell
I. Jensen
F. Moore
J. Shubiak
J. Wang

Division 532

E. Boswell
C. Eisenhauer
D. Gilliam
J. Grundl
G. Lamaze
E. McGarry
R. Schwartz
V. Spiegel
A. Wasson

Division 551

D. Becker
S. Carpenter
G. Downing
K. Fitzpatrick
R. Fleming
R. Greenberg
J. Langland
R. Lindstrom
G. Lutz
J. Maki
B. Norman
S. Stone
R. Zeisler

GUEST WORKERS AND COLLABORATORS

Division 400

J. Cahn

Division 420

F. Brinckman
J. Blendell
T. Coyle
S. Frieman
K. Frase
E. Fuller
E. Lewes
K. Hardman-Rhyne
G. Olson
R. Roth
B. Steiner
W. Haller

Division 430

R. Fields

Division 440

B. Bauer
T. Davis
C. Han
C. Chiang
R. Waterstrat
W. Wu

Division 450

F. Biancanello
R. Reno
R. Shaefer
R. Shull

Division 520

G. Greene
E. Kessler

Division 533

R. Placious

Division 541

R. Cavanagh
R. Kelly
T. Madey

Division 543

R. Harrison
I. Weber
A. Wlodawer

Division 552

B. Koster
L. Sander
S. Wise

Division 553

C. Poston
H. Rook
J. Snell

Division 725

J. Ehrstein

Division 774

H. Hanbley
J. Straty

Aberdeen Proving Ground

C. Heimback

Armed Forces Institute of Pathology

D. Nagarajan

Army Armament Research and Development Command

C. Choi
H. Prask
S. Trevino

Federal Bureau of Investigation

R. Bilko
J. Haverkost
J. Kilty
P. Kostella
M. Moscop
C. Peters
J. Riley
P. Tangren
P. Thompson

Food and Drug Administration

W. Cunningham
W. Stroube, Jr.
J. Tanner

National Institutes of Health

J. Bennett
M. Channing
W. Eckelman
R. Finn
R. Frank
A. Katki
M. Neuder
H. Savage

Naval Research Laboratory

K. Grabowski
A. Imam
N. Koon

Naval Surface Weapnos Center

J. Cullen
G. Riel
M. Spano

Smithsonian Institution

R. Bishop
M. Blackman
T. Chase
Y. Cheng
J. Mishara
E. Myers
J. Olin
R. Wright

PERSONNEL ROSTER

Argonne National Laboratory

S. Susman

Battelle Pacific Northwest Laboratories

L. Brackenbush
F. Brauer
G. Endres
M. Failey
R. Sanders

Chalmers Institute of Technology

L. Sjolin

C.N.R.S. Grenoble, France

C. Chaillout
D. Gignoux
M. Marezio
J. Soubeyroux
D. Tranqai
G. Zaccai

CSURO - Australia

R. Hill

Institut Laue-Langevin Grenoble, France

A. Magerl
R. Pynn

Institute of Nuclear Sciences

R. Drascovic

KFA Jülich, Germany

R. Hempleman
D. Richter
M. Stoepler

Los Alamos National Laboratory

R. Robinson
J. Wilkerson

Max-Planck Institute

R. Huber
R. Kirchheim
E. Lukacevic
J. Walter

Oak Ridge National Laboratory

J. Hayter
F. Kam

Sandia National Laboratory

J. Schirber
D. Varsick

Alfred University

R. Snyder
R. Zhow

Cambridge University (U.K.)

J. Horton
G. Squire

Carnegie-Mellon University

E. Boltich
W. Wallace

Georgetown University

H. Mallek

Iowa State University

R. Shelton

Kyoto University (Japan)

H. Hasegawa
T. Hashimoto
Q. Trancong

McMaster University

W. Clarke

PERSONNEL ROSTER

Michigan State University

E. Case
Y. Fan
S. Solin

M.I.T.

S. Chen
J. Didiskein
M. Green
B. Wuensch

Northwestern University

H. Calderon
J. Ketterson
S. Kim
J. Weertman

Oregon State Graduate School

P. Davis

Purdue University

J. Furdyna
T. Giebultowicz
A. Overhauser

San Jose State University

A. Ling

State University of New York

H. Greenblatt
H. Herman

University of Annecy, (France)

J. Bouillot

University of Antwerp (Belgium)

K. Michel

University of California (Santa Barbara)

M. Eddy
C. Levii
R. Odette
G. Stucky

University of California (San Diego)

J. Arnold
K. Nishiizumi

University of Cincinneti

H. Jackson

University of Illinois

J. Borchers
S. Hardcastle
D. Heumann
P. Miceli
M. Salamon
S. Sinha
S. Youngquist
H. Zabel

University of Maryland

D. Anderson
I. Anderson
A. Bates
J. Dodd
S. Faller
J. Fernandez-Baca
A. Fiesel
G. Gordon
F. Guenther
M. Han
D. Herman
J. Hoff
M. Kitto
S. Krueger
Q. Li
J. Lynn
C. LeCompte
L. McCarthy
J. Nicol
J. Ondov
J. Robertson
A. Sheffield
P. Sheridan
H. Stanley
S. Stone
C. Thompson
G. Tuncel
S. Tuncel
J. Valette-Silver
W. Waters
Y. Yu
W. Zoller

University of Michigan

D. Vincent

Univrsity of Millan (Italy)

M. Zocchi

University of Missouri

W. Ching
W. James
T. Little
S. Werner

University of Muenster

F. Kemper

University of Nancy (France)

P. Mangin

University of New Hampshire

R. Blakemore

University of Notre Dame

R. Ricker

University of Rhode Island

D. Andrauskas
S. Hasanain
S. Pickart

University of Virginia

T. Williamson

University of Washington

K. Mottet
W. Zoller

University of Wisconsin

D. Huber

Aerospace Corporation

R. Bowman
J. Knudsen

Alcoa Technical Center

C. Jensen
R. Rioja

Allied Corporation

G. Fish
A. Maeland

Atomic Energy of Canada, LTD

W. Lennard

Baker Chemical Company

R. Ganapathy

Bell Laboratories

R. Cava
H. Chem
J. Mitchell
D. Murphy
J. Remeika
J. Riley

Bell-Northern Research Ltd.

F. Shepherd
W. Vandevorst

Directed Technologies, Inc.

N. Chesser

Eastman Kodak

T. Houssain
M. Landry
C. Swanson

E. I. DuPont de Nemours Co.

G. Jones
D. Corbin
c. Torardi

PERSONNEL ROSTER

Exxon

R. Busch
J. Dozier
J. Gethner
J. Huang
D. Lohse
S. Sinha

General Electric Co.

C. Austin
R. Bonnan
R. Darlia
L. Provo
A. Taub

W. R. Grace

M. Wax
R. Wormsbecker

GTE Laboratories

M. Downey
D. Oblas
G. Hamill

IBM (Yorktown Heights)

M. Schaefer
R. Gambino

Intel Corporation

N. Cox

Mobil Central Research Laboratory

D. Olsen

Motorola, Inc.

S. Wilson

Rockwell International

M. Brown

Southerwest Research Institute

R. Page

Westinghouse-Hanford Corp.

W. McElroy

F. PUBLICATIONS

COLLABORATIVE PROGRAMS

Anderson, I. S., Rush, J. J., Udovic, T. J., and Rowe, J. M., " Hydrogen Pairing and Anistropic Potential for Hydrogen Isotopes in Yttrium", Phys. Rev. Lett. (in press).

Berk, N. F., and Hardman-Rhyne, K. A., " Characterization of Alumina Powder Using Small Angle Scattering, I: Theory", J Appl. Cryst. 18 467 (1985).

Berk, N. F., and Hardman-Rhyne, K. A., "The Phase Shift and Multiple Scattering in Small Angle Neutron Scattering: Application to Beam Broadening from Ceramics", Proc. of the 1985 Santa Fe Intern. Conf. on Neutron Scattering: Physica 136, 218 (1986).

Berk, N. F., " Exact Properties of Model for Biocontinuous Structures", Phys. Rev. Lett., 1986 (in press).

Bonnet, J. E.; Rose, D. K., Faux, D. A., and Anderson, I. S., "Long Range and Short Range Ordering of H and D Atoms in Solid Solution in Yttrium", J. Less Common Metals (in press).

Bordet, P., Mchale, A., Santoro, A., and Roth, R. S, "Powder Neutron Diffraction Study of $ZrTiO_4$, $Zr_5Ti_7O_{24}$ and $FeNb_2O_6$", J. of Solid State Chem. 64; 30-46 (1986).

Bouillot, J., Rowe, J. M., and Rush, J. J., "Structure of $(KCN)_{.7}(KBr)_{.3}$ Mixed Crystal by Neutron Powder Diffraction", Phys. Rev. (in press).

Cava, R. J., Santoro, A., Murphy, D. W., Zahurale, S. M., Fleming, R. M., Marsh, P., and Roth, R. S, "The Structure of the Lithium Inserted Metal Oxide δ-LiV_2O_5", J. Solid State Chem. (in press).

Cavanagh, R. R., Rush, J. J., and Kelley, R. D., "Incoherent Inelastic Neutron Scattering: Vibrational Spectroscopy of Adsorbed Molecules on Surfaces. Methods of Surface Characterization, T. E. Madey and J. Yates, eds., Plenum, NY (1986).

Casella, R. C., "On the Theory of Coherent Neutrino Scattering from Crystals. IL Nuovo Cimento (in press).

Casella, R. C., "Coherent Scattering of Low Energy Neutrinos from Macroscopic Objects", American Institute of Physics Conference Proceedings (in press).

Chaillout, C., Remeika, J. P., Santoro A., and Marezio M., "Bismuth Valence Order-Disorder Study in $BaBiO_3$ by Powder Neutron Diffraction", Solid State Communications 56, 833 (1985).

Choi, C. S., George, C., Gilardi, R., Alippen-Anderson, J. L., Marchand, A. P., and Reddy, D. S., "Structure of 6,6,10,10-Tetranitropentacyclo $[5.30.0^{2.5}.0^{4,8}]$decane, $C_{10}H_8O_8$. Acta Cryst. C41 788-791 (1985).

Choi, C. S., and Prask, H. J, "Texture of Extruded Uranium Alloy by Neutron Diffraction", J. Appl. Cryst. 18, 413-418 (1985).

Didisheim, J. J., Prince, E., and Wuensch, B. J., "Neutron Rietveld Analysis of Structural Changes in Nasicon Solid Solutions $Na_{1+x}Zr_2Si_xP_{3-x}P_{3-x}O_{12}$ at Elevated

Temperatures: $x = 1.6$ and 2.0 at 320°C", Solid State Ionics 18-19, 944-958 (1986).

Eick, H., and Prince, E., "A Neutron Diffraction and Electron Microscopy Examination of $2BaBr2BaCl_2$", Acta. Cryst. C42, 915-917 (1986).

Erwin, R. W., Lynn, J. W., Rhyne, J. J., and Chen, H. S., "Spin Stiffness Anomaly in the Reentrant Spin-Glass $(Fe_{0.25}Ni_{0.75})_{0.75}P_{0.16}B_{0.06}Al_{0.03}$", J. Appl. Phys. 57 3473 (1985).

Erwin, R. W., Lynn, J. W., and Magerl, A., "The Reentrant Spin-Glass Order Parameter in $(Fe_{0.3}Ni_{0.7})_{75}P_{16}B_6Al_3$", Proc. of the International Conference on Magnetism 1985, North-Holland, Amsterdam, 101 (1985).

Fan, Y. B., Solin, S. A., Neumann, D., Zabel, H., and Rush, J. J., "Elastic Neutron Scattering Studies of the Structure of Graphite Interacalated with Potassium and Ammonia", Phys. Rev. B (in press).

Fernandez-Baca, J. A., Lynn, J. W., Rhyne, J. J., Fish, G. E., "Spin Dynamics of Amorphous $Fe_{0.86}B_{0.14}$", Physica 136B, 53 (1986).

Fernandex-Baca, J. A., Rhyne, J. J., and Fish, G. E., "Neutron Scattering Study of the Spin Dynamics of Amorphous $Fe_7Ni_2Zr_1$", J. Magnetism and Magnetic Materials 54-57, 289 (1986).

Fischer, R. X., Baur, W. H., Shannon, R. D., Staley, R. H., Vega, A. J., Abrams, L., and Prince, E., "Neutron Patterns from Tilings with Five-Fold Symmetry", J. Phys. Chem. (in press).

Fisher, R. X., Baur, W. H., Shannon, R. D., Staley, R. H., Vega, A. J., Abrams, L., and Prince. E., "Neutron Powder Diffraction Study and Physical Characterization of Zeolite D-rho", J. Phys. Chem. (in press).

Giebultowicz, T. M., "Monte Carlo Simulation of Dilute Magnetic Semiconductors for High Concentrations of the Magnetic Component", J. Magnetism and Magnetic Materials 54-57, 1287-1288 (1986).

Giebultowicz, T. M., Overhauser, A. W., and Werner, S. A., "Direct Observation of the Charge-Density Wave in Potassium by Neutron Diffraction", Phys. Rev. Letters 56, No. 14, 1485-1488 (1986).

Giebultowicz, T. M., Rhyne, J. J., Ching, W. Y., Huber, D. L., Galazka, R. R., "Static and Dynamic Spin Correlations and Exchange Interactions in $Cd_{1-x}Mn_xTe$", J. Magnetism and Magnetic Matls. 54-57, 1149 (1986).

Gignoux, D., and Rhyne, J. J., "Spin Excitations in $TbNi_5$ by Inelastic Neutron Scattering", J. Magnetism and Magnetic Matls. 54-57, 1179 (1986).

Glinka, C. J., Rowe, J. M., and LaRock, J. G., "The Small Angle Neutron Scattering Spectrometer at the National Bureau of Standards (in press).

Gotaas, J. A., Rhyne, J. J., Wenger, L. E., and Mydosh, J. A., "Long-Range Incommensurate Spin State in Dilute YGd Alloys", J. Magnetism and Magnetic Materials 54-57, 93 (1986).

Hardcastle, S. E., Neumann, D. A., Zabel, H., and Rush, J. J., "Critical Behavior of the Interlayer Shear Constant in Stage 2 K and Rb Graphite Intercalation Compounds", Synthetic Metals (in press).

Hardman-Rhyne, K. A., and Berk, N. F., "Characterization of Alumina Powder Using Small Angle Scattering, II: Experiment", J. Appl. Cryst. 18, 473 (1985).

Hardman-Rhyne, K. A., Frase, K. G., and Berk, N. F., "Applications of Multiple Small Angle Scattering to Studies of Ceramic Processing", Proc. of the 1985 Santa Fe Intern. Conf. on Neutron Scattering, Physica B 136B, 223 (1986).

Hardman-Rhyne, K. A., and Berk, N. F., "Ceramics Material Characterization Using Small Angle Neutron Scattering Techniques", Materials Characterization for Systems Performance and Reliability, eds. James W. McCauley and Volker Weiss, Plenum Press, New York, 257-269 (1986).

Hardman-Rhyne, K. A., Berk, N. F., "Small Angle Neutron Scattering Form Porosity in Sintered Alumina, Communication of the American Ceramic Society, 1986 (in Press).

Hemplemann, R., and Rush, J. J., "Neutron Vibrational Spectroscopy of Disordered Metal-Hydrogen Systems, Proceedings of NATO Workshop, Rhodes, Greece, Physica B (in press).

Himes, V. L., and Mighell, A. D., "NBS lattice - A Program to Analyze Lattice Relationships," NBS Tech. Note 1214, U. S. Dept. of Commerce NBS (1985).

Jin, L., James, W. J., Lemaire, R., and Rhyne, J., "Magnetic Structure of $DyCo_3$", J. Less-Common Metals. (in press).

Jin, L., James, W. J., Lemaire, R., and Rhyne, J. J., "Magnetic Structure of DyFe.", J. Less-Common Metals 118, 269 (1986).

Kircheim, R., Huang, H. Y., Carstanjen, H. D., Rush, J. J., and Udovic, T. J. "Inelastic Neutron Scattering and Resistivity of Hydrogen in Cold-Worked Palladium", J. Less Common Metals (in press).

Lukacevic, E., Rush, J. J., and Santoro, A., "Neutron Powder Diffraction and Inelastic Scattering Study of the Structures of Zr_2Pd, $Zr_2PdD_{1.70}$ and $Zr_2PdD_{1.96}$", Acta Cryst. (in press).

Lukacevic, E., Santoro, A., and Roth, R. S., "Neutron Powder Diffraction Study of the Structure of the Compound $Li_{0.3125}La_{0.5625}MoO_4$", Solid State Ionics 18-19, 922-928 (1986).

Lynn, J. W. "Helium Condensation Observed in Small Angle Neutron Scattering", Physica 136B, 117-119 (1986).

Lynn, J. W., and Rhyne, J. J., "Spin Dynamics of Amorphous Magnets", Chapter in Spin Waves and Magnetic Excitations, edited by S. K. Sinha and A. S. Borovik-Romanov, North Holland Physics Publishers (in press).

Magerl, A., Rush, J. J., and Rowe, J. M., "Local Modes in Dilute Metal-Hydrogen Alloys", Phys. Rev. B33, 4, 2093-2097 (1986).

PUBLICATIONS

Miceli, P. F., Youngquist, S. E., Neumann, D. A., Zable, H., Rush, J. J. and Rowe, J. M., "Neutron Scattering Study of the Vibrational Density of States in Icoshedral and Crystalline $Al_{0.80}Mn_{0.20}$", Phys. Rev. Lett. (in press).

Michel, K. H., and Rowe, J. M., "Molecular Symmetry and Translation-Rotation Coupling in Orientationally Disordered Crystals", Phys. Rev. B32, 9, 5818-5832 (1985).

Michel, K. H., and Rowe, J. M., "KCN, A Model System of Translation Rotation Coupling in Orientationally Disordered Crystals", J. Chimie Phys.. 82, 2-3, 199-204 (1985).

Mighell, A. D., and Himes, V. L., "Compound Identification and Characterization Using Lattice-Formula Matching Technqiues", Acta Crysta. A, 101-105 (1986).

Mozer, B, Gratias, D., and Shechtman, D., "Neutron Diffraction Studies of the Icosahedral Phase of Al-Mn Alloys", J. de Physique Collogue, No. 3, (in press).

Murphy, D. W., Cava, R. J., Rhyne, K., Roth, R. S., Santoro, A., Zahurak, S. M., and Dye, J. L., "Structural Aspects of Insertion Reactions of the Pyrochlore $KNbWO_6$", Solid State Ionics 18-19, 799-801 (1986).

Nossal, R., Glinka, C. J., and Chen, S. H., "SANS Studies of Concentrated Protein Solutions. I. Bovine Serum Albumin. Biopolymers", 25, 1157-1175 (1986).

Prask. H. J., and Choi, C. S., "Neutron Diffraction Characterization of Tungsten-Nickel-Iron Alloys", Technical Report AREAE-TR 85015, AD-E401, 461, ARC, Dover, NJ (1986).

Prask, H. J, and Choi, C. S., "Encyclopedia of Materials Science and Engineering, 7, 4095-97, edited by M. B. Bever, Pergamon Press, NY (1986).

Prask, H. J.and Choi, C. S., "Texture, NDE Characterization Encyclopedia of Materials Science and Engineering", 7, 4095, edited by M. B. Beuer, Pergamon Press, New York (1986).

Prask, H. J., and Choi, C. S.,"Sub-Surface Residual Stress Measurements by Means of Neutron Diffraction: Aluminum, Steel, and Depleted Uranium, Materials Characterization for Systems Performance and Reliability", edited by J. W. McCauley and W. Weiss, Plenum Press, NY and London (1986).

Prince, E., and Nicholson, W., "The Influence of Individual Reflections on the Precision of Parameter Estimates in Least Squares Refinement. Structure and Statistics in Crystallography, Ed. A. J. C. Wilson, Adenine Press, Guilderland, NY, 183-195 (1985).

Prince, E., "Precision and Accuracy in Structure Refinement by the Rietveld Method", Structure and Statistics in Crystallography, Ed. by A. J. C. Wilson, Adenine Press, Guilderland, NY, 93-103 (1985).

Rhyne, J. J., "Magnetic Properties of Amorphous Metals", Invited Paper, Research Opportunities in Amorphous Solids with Pulsed Neutron Sources Workshop, Argonne Natl. Lab., J. of Non-Crystalline Solids 76, 129 (1985).

Rhyne, J. J., "Effects of Random Field Interactions in Amorphous Rare Earth Alloys. Invited paper", INTERMAG Conf., St. Paul, MN, IEEE Trans. Mag. 21, 1990 (1985).

Rhyne, J. J., "Quenching of Long-Range Magnetic Order by Random Interactions in Amorphous Alloys", Invited paper, International Conference on Neutron Scattering, Santa Fe, NM, Physica 136B, 30 (1986).

Rhyne, J. J., Cooper, B. R., Huber, D. A., Koon, N. C., and O'Handley, R. C. editors, Proceedings of the International Conference on Magnetism ICM-85, J. Magnetism and Magnetic Materials North Holland 54-57 (1986).

Rhyne, J. J., Erwin, R. W., Salamon, M. B., Sinha, S., Cunningham, J. E., Borchers, J., and Flynn, C. P., "Long-Range Incommensurate Magnetic Order in Dy-Y Multilayers", Invited Paper, Seventeenth Rare Earth Research Conference, Hamilton, Canada, J. Less-Common Metls. (in press).

Richter, D., Hempelmann, R., Rush, J. J., Rowe, J. M., Eckert, J., Goldstone, J. A., and Tonks, D., "Localized Vibrations of Hydrogen in Metals", Physica B (in press).

Rowe, J. M., Bouillot, J., Rush, J. J., and Luty, F., "Structural Phase Diagram of Mixed $(ICN)_x(KA)_{1-x}$ Crystals by Means of Neutron Powder Diffraction", Physica B 136, 498-502 (1986).

Rowe, J. M., Rush, J. J., Schirber, J. E., and Mintz, J. M., "Isotope Effects in the PdH System - Lattice Dynamics of $PdT_{0.7}$", Phys. Rev. Lett. (in press).

Rowe, J. M., Rush, J. J., Michel, K. H., Comment on Dielectric Susceptibility Measurements in $(KCN)_x (KBr)_{1-x}$", Phys. Rev. Lett. (in press).

Rush, J. J., and Rowe, J. M., "Chemical Physics with Emphasis on Low Energy Excitations", Physica B137, 169-182 (1986).

Rush, J. J., Cavanagh, R. R., Kelly, R. D., and Rowe, J. M., Interaction of Vibrating H Atoms on the Surface of Platinum Particles by Isotope Dilution Neutron Spectroscopy", J. Chem. Phys. 83, 5339-5341 (1985).

Salamon, M. B., Sinha, S., Rhyne, J. J., Cunningham, J. E., Erwin, R. W., Borchers, J., and Flynn, C. P., "Long-Range Incommensurate Magnetic Order in a Dy-Y Multilayer", Phys. Rev. Lett. 56, 259 (1986).

Schioler, L. J., Wuensch, B. J., and Prince, E., "The Relation Between Structural Change and Fast Ion Conduction in the NASICON Solid Solution System. Solid State Ionics (in press).

Schroder, I. G., Linperi, Li, Gilliam, D. M., McGarry, E. D., Eisenhauer, C. M., "Measurement of Aboslute Fission Cross Sections for ^{252}Cf Spoutaneous Fission Neutrons", Trans. Amer. Nuc. Soc 50, 154 (1985).

Schroder, I. G., Gilliam, D. M., Carlson, A. D., and Bright, Hutchinson, J. M. R., "International ^{235}U Fission Foil Mass Intercomparison", Trans. Am. Nuc. Soc. (in press).

Smith, H. K., Rhyne, J. J., Hardman-Rhyne, K. A., and Wallace, W. E., "Thermodynamics of Hydrides and Deuterides of R_6Fe_{23} and R_6Mn_{23}", J. Less Common Metals (in press).

Spano, M. L., and Rhyne, J. J., "Effects of Applied Fields on the Magnetic Order of Amorphous Tb_xFe_{1-x} Alloys", Magnetism and Magnetic Matls. 54-57, 300 (1986).

Stalick, J. K., and Mighell, A. D., "Crystal Data Version 1.0 Database Specifications, NBS Tech. Note (in press).

Torardi, C. C., Reiff, W. M., Lazar, K., and Prince, E., "Structures and Low Temperature Magnetism of the New Lithium and Sodium Insertion Compounds: $LiFe(II)ClMoO_4$ and $NaFe(II)ClMoO_4$", J. Chem. Phys. Solids (in press).

Torardi, C. C., and Prince, E., "Structure of the Lithium Insertion Compound $Li_2Fe_2(MoO_4)3$ from Neutron Powder Diffraction Data", Materials Research Bulletin 21, 719-726 (1986).

Trevino, S. S., and Tsai, D. H., "The Simulation of Condensed Matter Chemistry and Destontion", Proceedings of the 1986 Army Science Conference, 1986 (in press).

Udovic, T. J., and Kelley, R. D., "Neutron Scattering Studies of Hydrogen in Catalysts. Hydrogen in Catalysis: Theoretical and Practical Aspects, Z Paal and P. G. Menon, eds., Marcel Dekker, Inc., NY (1986).

Wax, M. J., Cavanagh, R. R., Rush, J. J., Stucky, G. D., Abrams, L., and Corbin, D. A., Neutron Scattering Study of Zeolite Rho", Phys. Chem. 90, 532 (1986).

Weiss, G. H., Shmueli, U., and Prince, E., Discussion of Fourier Representations of Pdfs Arising in Crystallography", J. Res. NBS 90, 513-515 (1985).

Wenger, L. E., Hunter, G. W., Mydosh, J. A., Gotaas, J. A., and Rhyne, J. J., "Spin Density Wave Transition in Dilute YGd Single Crystal", Phys. Rev. Lett. 56, 1090 (1986).

Werner, S. A., Rhyne, J. J., and Gotaas, J. A., "Spin Density Wave Magnetism in Copper-Manganese Alloys", Solid State Commun. 56, 457 (1985).

Yu, H., Kitano, T., Kim, C. Y., Amis, E. J., Chang, T., Landry, M. R., Wesson, J. A., Han, C. C., Lodge, T. P., and Glinka, C. J., "Uniaxial Deformation of Rubber Network Chains by Small Angle Neutron Scattering", Macromolecules (in press).

INDEPENDENT PROGRAMS

Alberts, W. G., and Schwartz, R. B., "Comparison of the Filtered-Neutron Beams at the NBS and PTB Reactors by Calibrating a Spherical Remmeter, Proc. Fifth Symposium on Neutron Dosimetry, 17-21 Sept. 198, Munich, Germany, EUR 9762 EN Volume 1 (1985).

Anderson, D. L., Sun, Y, Failey, M. P., and Zoller, W. H., "Neutron-Capture Prompt Gamma-Ray Multielement Analysis of Twenty-Two Geochemical Reference Standards, Geostandards Newsletter 9, 219-228 (1985).

Becker, D. A., "The Role of Reactor Characterization in NAA Quality Assurance", J. Radioanal. Nucl. Chem. (in press).

PUBLICATIONS

Blackman, M. J., "The Provenience of Obsidian Artifacts from Late Chalcolithic Levels at Aphrodisias, Turkey", in Prehistoric Aphrodisias, ed. M. Joukowsky, (Archaeologia Transatlantica Vol. IV) Louvain-la-Neuve, Institut Superieur D'Archelogie et Histoire de L'Art Brown University (in press).

Blair, W., Olson, G., Brinckman, F., Paule, R., and Becker, D., An International Butyltin Measurement Methods Intercomparison: Sample Preparation and Results of Analysis, NBSIR 86-3321 (1986).

Carpenter, B. S., Gramlich, J. W., Greenberg, R. R., Machlan, L. A., DeVievre, P., Eschbach, H. L., Meyer, H., Van Audenhove, J. Connolly, V.E. Trahey, N. M., and Zook, A. C., "Standard Reference Materials: UranIUM-235 Isotope Abundance Standard Reference Materials for Gamma Spectrometry Measurements", NBS Spec. Publ. 260-96 (in press).

Carpenter, B. S., and Pilione, L. J., "The Use of Delayed Nuclear Track Counting for Determinging Bismuth", Journal of Radioanalytical and Nuclear Chemistry (in press).

Carpenter, B. S., Horvath, C., and Vogt, C. R., "The Production of Porous Microspheres by the Nuclear Track Techniques", Nuclear Tracks and Radiation Measurements (in press).

Bowman, R. C., Jr., Robertson, R. E., Knudsen, J. R., and Downing, R. G., "Studies of Boron Implantation Through Photochemically Deposited SiO_2 Films on $Hg_{1-x}Cd_xTe$", Proceedings of the International Conference on Optical and Optoelectronic Applied Sciences and Engineering, 1986 (in press).

Downing, R. G., Maki, J. T., and Fleming, R. F., "Application of Neutron Depth Profiling to Microelectronic Materials", ACS Symposium Series No. 295, L. A. Casper, ed., 163-180 (1984).

Downing, R. G., Maki, J.T., and Fleming, R. F., "Analytical Applications of Neutron Depth Profiling", Proceeding of the 1986 Modern Trends in Activation Analysis (in press).

Fleming, R. F., and Lindstrom, R. M., "Precise Determination of Aluminum by Instrumental Neutron Activation" (in press).

Garry, V. F., Pohlman, B. L., Wick, M. R., Garvey, J. S., Zeisler, R., "Chronic Cadmium Introxication: Tissure Response in an Occupationally Exposed Patient", Am., J. Indust. Med. (in press).

Gilliam, D. M., and Lamaze, G. P., "Absolute Neutron Flux Determination - A Problem for the Determination of τ_n, Proceedings of Workshop on The Investigation of Fundamental Interactions with Cold Neutrons, NBS-SP711 36 (1986).

Greenberg, R. S., "The Role of Neutron Activation Analysis in the Certification of NBS Standard Reference Materials", Proc.of the Seventh International Conference on Modern Trends in Activation Analysis (in press).

Greenberg, R. R., Fleming, R. F., and Linstrom, R. M., "Elemental Characterization of Four Coal Standard Reference Materials via Instrumental Neutron Activation Analysis and Neutron-Capture Prompt Gamma Activation Analysis" (in press).

Greenberg, R. R., "Elemental Characterization of the National Bureau of Standards Milk Powder Standard Reference Materials by Instrumental and Radiochemical Neutron Activation Analysis", Analy. Chem. (in press).

Grundl, J. A., Eisenhauer, C. M., "Compendium of Benchmark Neutron Fields for Reactor Dosimetry-Standard Neutron Fields Entries", NBSIR 85-3151 (1986).

Grundl, J. A., "Pursuing Public and Professional Perception of Nuclear Energy With the Smithsonian Lady Godiva Replica and Demonstration/Display", Proc. of Fast Burst Reactor Workshop, Albuquerque, NM (1986).

Han, C., Okada, Y., Murgoga, Y., McRackin, F. L., Bauer, B. J., and Tran-Cong, Q., "Static and Kinetic Studies of Polystene/Poly (vinylmethylether) Blends", Polymer Engineering and Science 26, No. 1 (1986).

Iyengar, G., v., and Tanner, J.T., "Biological and Dietary Reference Materials for Organic and Inorganic Nutrients", Food Laboratory Newsletter, No. 4, 20-25 (1985<).

Iyengar, G. V., "Sample Validity in Biological Trace Element Research Studies", J. Radioanal. Nucl. Chem. (in press).

Iyengar, G.V., Tanner, J. T., Wolf, W. R., and Zeisler, R., "Preparation and Characterization of Mixed Diet Composite USDIET-I: Determination of Energy, Phytic Acid and Elemental Concentration", IAEA Coordinated Research Programme on Human Daily Dietary Intakes of Nutritionally Important Trace Elements (in press).

Kitto, B. M. E. and Aanderson, D. L. "Simultaneous Collection of Particles and Gases from Coal-Fired Power Plants", Proc. of the National Meeting of the American Chemical Society, New York, NY (1986).

Kotra, J. P., and Zoller, W. H., "A High Volume, Aircraft-Based Filter Sampling System for the Collection of Atmospheric Particles and Reactive Gases (in press).

Lindstrom, R. M., Zeisler, R., and Rossbach, M., "Activation Analysis Opportunities Using Cold Neutron Beams", submitted to Proc. 7th MAA, Copenhagen (1986).

Lindstrom, R. M., "Activation Analysis of Semiconductor Materials, in L. A., Casper, ed., "Microelectronics Processing: Inorganic Materials Characterization", (ACS Symp. Ser. No. 295), Am Chem. Soc., Washington, 294-307 (1986).

Linidstom, R. M., and Anderson, D. L., "Analytical Neutron-Capture Gamma-Ray Spectroscopy: Status and Prospects", S. Raman, ed., Capture Gamma-Ray Spectroscopy and Related Topic - 1984 (AIP Conf. Proc. No. 125), Am. Inst. Physics. New York 810-819 (1985).

Lauenstein, G. G., Schantz., M. M. Wise, S. A., Zeisler, R., "Specimen Banking in the National Status and Trends Program: Development of Portocols and First Year Results", Proc. Oceans '86 (in press).

Maki, J. T., Fleming, R. F., and Vincent, D. H., "Deconvolution of Neutron Depth Profiling Spectra", Nuclear Instruments and Methods in Physics Research B17, 147 (1986).

Michel, R., Iyengar, G. V., and Zeisler, R., "Current Aspects of Multielements Analysis in the life Sciences, Instrumental Multielement Analysis, Sansoni, B., ed., VCH Publishers, Deerfield Beach, FL, 607-618 (1985).

Myers, E., "Chemical Composition of the Sackler Maiolica Ceramics, "Appendix in Forthcoming Catalogue on the Sackler Maiolica, Lois Katz. The Arthur M. Sackler Foundation, New York, NY (in press).

Myers, E., Blackman, J. J., "Conical Plates of the Hispano-Moresque Tradition from Islamic Osar es-Seghir: Petrographic and Chemical Analysis, "La Ceramica Medievale Nel Mediteraneo Occidental, 55-68, Edizioni All'Insegna Del Giglio, Florence, Italy (in press).

Olin, J. S., and Blackman, M. J., "The Proceedings of the 1984 Archaeometry Symposium Institutio Press, Washington, DC (in press).

Olmez, I. Gulovali, M.C. and Gordon, G. E., "Trace Element Concentrations in Lichens near a Coal-Fired Power Plant", Atmos. Environ. 19, 1663-1669 (1985).

Olmez, I. and Gordon, G. E., "Rare Earths: Atmospheric Signatures for Oil-Fired Power Plants and Refineries", Science 229, 966-968 (1985).

Olmez, I., Finnegan, D. L. and Zoller, W. H., Iridium Emissions from Kilauea Volcano, J. Geophys. Res. 91, 653-663 (1986).

Ondov, J. M. "Cascade Impactors in the Chemical and Physical Characterization of Coal-Combustion Aerosol Particles", in Fossil Fuels Utilization: Environmental Concerns, R. Markuszewski and B. Blaustein, ed., Am. Chem. Soc. (1986).

Riley, J. E., Jr., and Linstrom, R. M., "Determination of Boron in Borosilicate Glasses by Neutron Capture Prompt Gamma-Ray Activation Analysis (in press).

Schwartz, R., "Experiences in Calibration of Neutron Survey Instruments", Proc. Workshop on Radiation Survey Instruments and Calibrations (1985).

Stone, S. F., Hancock, D., and Zeisler, R., "Characterization of Bioligical Macromolecules by Electrophoresis and Neutron Activation," Journal of Radioanalytical and Nuclear Chemistry (in press).

Stroube, W. B., Jr., and Lutz, G. J., "Analysis of Foods for Iodine by Gp Thermal Neutron Activation Analysis", J. Radioanal. and Nucl. Chem. (in press).

Tanner, J. T., Smith, J. S., Angyal, G., Defibaugh, P. W., Villalobos, M. C., Bueno, M. P., Iyengar, G. V., Wolf, W. R., and Zeisler, R., "In Search of SRMs for Organic Nutrients", 2nd International Workshop on Biological Reference Materials, work, W. R. ed. (in press).

Tuncel, S. G., Olmez., I., Parrington, J. R., Gordon, G. E. and Stevens, R. K., "Trace Elements no Airborne article in Rural Areas: Development of Regional Sulfate Signatures, in Receptor Models for Source Apportionment: Real World Issues and Applictions, T. G. Pace, ed. (Air Pollution Control Assn., Pittsburgh, PA 116-126 (1985).

Tuncel, G. and Zoller, W. H., "Iridium Concentrations in the South Pole Atmosphere: Estimation of Meteroritic Component, Science (in press).

Yang, H., Stein, R. S., Han, C., Bauer, B., Kramer, E., "Compatibility of Hydrogenated and Deuterated Polystyene", Polymer Communications 27, 12 (198).

Wise, S. A. and Zeisler, R., "The U. S. Pilot Environmental Specimen Bank Program", NBS (US) Spec. Publ. 706, 34-45 (1985).

Wise, S. A. and Zeisler, R., eds., "International Review of Environmental Specimen Banking", NBS (US) Spec. Pub. 706, 62 (1985).

Zeisler, R., Stone, S. F., Fitzpatrick, K. A., Wise, S. A., "The Eighth U. S. - German Seminar of State and Planning on Environmental Specimen Banking and The International Review of Environmental Specimen Banking", NBS (US) Spec. Publ 706, 1-3 (1985).

Zeisler, R., "The Sampling and Analysis of Human Livers", NBS J. Res., 91, 75-85 (1986).

Zeisler, R., "Foreword: Symposium on Standardization f Collection and Preparation of Biomedical Samples for Trace Element Analysis," NBS J. Res., 91, 45-46 (1986).

Zeisler, R., and Young, I., "The Determination of Chromium-50 in Human Blood and Its Utilization for Blood Volume Measrement", J. Radioanal. Nucl. Chem. (in press).

NBS-114A (REV. 2-8C)

U.S. DEPT. OF COMM. **BIBLIOGRAPHIC DATA SHEET** *(See instructions)*	1. PUBLICATION OR REPORT NO. NBS/TN-1231	2. Performing Organ. Report No.	3. Publication Date December 1986

4. TITLE AND SUBTITLE

NBS Reactor: Summary of Activities July 1985 Through June 1986

5. AUTHOR(S)

F. J. Shorten, Ed.

6. PERFORMING ORGANIZATION *(If joint or other than NBS, see instructions)*

NATIONAL BUREAU OF STANDARDS
DEPARTMENT OF COMMERCE
Gaithersburg, MD 20899

7. Contract/Grant No.

8. Type of Report & Period Covered

July 1985 to June 1986

9. SPONSORING ORGANIZATION NAME AND COMPLETE ADDRESS *(Street, City, State, ZIP)*

Same as item 6.

10. SUPPLEMENTARY NOTES

☐ Document describes a computer program; SF-185, FIPS Software Summary, is attached.

11. ABSTRACT *(A 200-word or less factual summary of most significant information. If document includes a significant bibliography or literature survey, mention it here)*

This report summarizes all those programs which depend on the NBS reactor. It covers the period from July 1985 to June 1986. The programs range from the use of neutron beams to study the structure and dynamics of materials through nuclear physics and neutron standards to sample irradiations for aetivation analysis, isotope production, radiation effects studies, neutron radiography, and nondestructive evaluation.

12. KEY WORDS *(Six to twelve entries; alphabetical order; capitalize only proper names; and separate key words by semicolons)*

Activation analysis; crystal structure; diffraction; isotopes; molecular dynamics; neutron; neutron radiography; nondestructive evaluation; nuclear reactor; radiation.

13. AVAILABILITY

☒ Unlimited
☐ For Official Distribution. Do Not Release to NTIS
☒ Order From Superintendent of Documents, U.S. Government Printing Office, Washington, D.C. 20402.
☐ Order From National Technical Information Service (NTIS), Springfield, VA. 22161

14. NO. OF PRINTED PAGES

161

15. Price

* U.S. Government Printing Office: 1986 0-181-076 (40202)

NBS Technical Publications

Periodical

Journal of Research—The Journal of Research of the National Bureau of Standards reports NBS research and development in those disciplines of the physical and engineering sciences in which the Bureau is active. These include physics, chemistry, engineering, mathematics, and computer sciences. Papers cover a broad range of subjects, with major emphasis on measurement methodology and the basic technology underlying standardization. Also included from time to time are survey articles on topics closely related to the Bureau's technical and scientific programs. Issued six times a year.

Nonperiodicals

Monographs—Major contributions to the technical literature on various subjects related to the Bureau's scientific and technical activities.

Handbooks—Recommended codes of engineering and industrial practice (including safety codes) developed in cooperation with interested industries, professional organizations, and regulatory bodies.

Special Publications—Include proceedings of conferences sponsored by NBS, NBS annual reports, and other special publications appropriate to this grouping such as wall charts, pocket cards, and bibliographies.

Applied Mathematics Series—Mathematical tables, manuals, and studies of special interest to physicists, engineers, chemists, biologists, mathematicians, computer programmers, and others engaged in scientific and technical work.

National Standard Reference Data Series—Provides quantitative data on the physical and chemical properties of materials, compiled from the world's literature and critically evaluated. Developed under a worldwide program coordinated by NBS under the authority of the National Standard Data Act (Public Law 90-396).
NOTE: The Journal of Physical and Chemical Reference Data (JPCRD) is published quarterly for NBS by the American Chemical Society (ACS) and the American Institute of Physics (AIP). Subscriptions, reprints, and supplements are available from ACS, 1155 Sixteenth St., NW, Washington, DC 20056.

Building Science Series—Disseminates technical information developed at the Bureau on building materials, components, systems, and whole structures. The series presents research results, test methods, and performance criteria related to the structural and environmental functions and the durability and safety characteristics of building elements and systems.

Technical Notes—Studies or reports which are complete in themselves but restrictive in their treatment of a subject. Analogous to monographs but not so comprehensive in scope or definitive in treatment of the subject area. Often serve as a vehicle for final reports of work performed at NBS under the sponsorship of other government agencies.

Voluntary Product Standards—Developed under procedures published by the Department of Commerce in Part 10, Title 15, of the Code of Federal Regulations. The standards establish nationally recognized requirements for products, and provide all concerned interests with a basis for common understanding of the characteristics of the products. NBS administers this program as a supplement to the activities of the private sector standardizing organizations.

Consumer Information Series—Practical information, based on NBS research and experience, covering areas of interest to the consumer. Easily understandable language and illustrations provide useful background knowledge for shopping in today's technological marketplace.
Order the **above** *NBS publications from: Superintendent of Documents, Government Printing Office, Washington, DC 20402.*
Order the **following** *NBS publications—FIPS and NBSIR's—from the National Technical Information Service, Springfield, VA 22161.*

Federal Information Processing Standards Publications (FIPS PUB)—Publications in this series collectively constitute the Federal Information Processing Standards Register. The Register serves as the official source of information in the Federal Government regarding standards issued by NBS pursuant to the Federal Property and Administrative Services Act of 1949 as amended, Public Law 89-306 (79 Stat. 1127), and as implemented by Executive Order 11717 (38 FR 12315, dated May 11, 1973) and Part 6 of Title 15 CFR (Code of Federal Regulations).

NBS Interagency Reports (NBSIR)—A special series of interim or final reports on work performed by NBS for outside sponsors (both government and non-government). In general, initial distribution is handled by the sponsor; public distribution is by the National Technical Information Service, Springfield, VA 22161, in paper copy or microfiche form.

U.S. Department of Commerce
National Bureau of Standards
Gaithersburg, MD 20899